UNIVERSIDADE DE LISBOA
FACULDADE DE CIÊNCIAS
DEPARTAMENTO DE FÍSICA

Frequency-Dependence Analysis of the Ankle Reflex Dynamics: Narrow Bandwidth vs. Wide Bandwidth

Hayanna Reinskjen Leite do Valle

Mestrado em Engenharia Biomédica e Biofísica

Dissertação orientada por:
Professor Doutor Rui Miguel de Moura Antunes e Valejo Coelho
Professor Doutor Nuno Miguel de Pinto Lobo Matela

2023

Acknowledgments

I would like to express my heartfelt gratitude to several individuals and entities who have played pivotal roles in the successful completion of this dissertation. Their unwavering support, guidance, and encouragement have been instrumental in shaping my academic journey.

First and foremost, I am deeply indebted to my dissertation advisor, Professor Rui Coelho. Your expertise, patience, and commitment to my academic growth have been invaluable. Your guidance not only steered my research in the right direction but also helped me become a better scholar.

I extend my sincere thanks to Professor Jorge Martins for affording me the opportunity to work and conduct my research at Instituto Superior Técnico of the University of Lisbon. Your institution provided an inspiring environment and the necessary resources for the realization of this dissertation.

I am profoundly grateful to my internal dissertation advisor, professor Nuno Matela, whose continuous support and mentorship throughout my college years and dissertation development have been truly remarkable.

I would like to express my appreciation to Professor Robert Kearney not only for his guidance and availability but also for his past work, which laid the foundation for my dissertation. His extensive contributions to the field have been instrumental in shaping my research and helping me develop a deeper understanding of the subject matter. I am grateful for the insights and knowledge gleaned from his previous works, which significantly contributed to the success of my own dissertation.

To my family, particularly my mother, Reinskjen Ribeiro, and my grandparents, Gildásio Leite and Zélia Ribeiro, whose unwavering support, love, and encouragement have been the cornerstone of my academic journey, I am eternally grateful. I want to extend a special note of gratitude to my sisters, Hassana and Hadassa do Valle. Their support, encouragement, and understanding during the ups and downs of this academic endeavour have been a source of strength.

To my friends, Beatriz Rodrigues, Diogo Silva, Diana Aires, Duarte Cunha, Inês Lopes, Laura Martins, Maria Gonçalves and Rafael Marques, who brought light and laughter into the sometimes-challenging world of academia, thank you for showing me the fun side of this process. Your camaraderie has made the journey all the more memorable.

In closing, I extend my gratitude to all the teachers, mentors, and peers from Faculty of Sciences of the University of Lisbon who have contributed, directly or indirectly, to my academic and personal growth. This dissertation stands as a testament to the collective efforts of those who believed in me and supported me along the way.

Thank you all for being a part of this transformative journey.

Resumo

O tornozelo, uma parte multi-funções e fundamental do corpo humano, desempenha um papel crucial na mobilidade, absorvendo impactos e contribuindo significativamente para a estabilidade. Além da sua função primária na locomoção, esta articulação é essencial para minimizar riscos de lesões em atividades diárias, destacando-se também como um componente fundamental para manter o equilíbrio, em conjunto com outros elementos do sistema musculoesquelético.

No contexto abordado, os reflexos no tornozelo se destacam como elementos de interesse, exercendo impacto significativo em várias dimensões. Esses reflexos desempenham um papel crucial ao responder a lesões, agindo de forma instantânea diante de perturbações ou situações de risco para evitar ou minimizar danos físicos. Além disso, sua importância se estende à monitorização da função neuromuscular. Destaca-se, por fim, a valiosa contribuição desses reflexos para a estabilidade postural, manifestando respostas rápidas e precisas diante de mudanças nas condições ou demandas de movimento.

Neste contexto, a presença de reflexos no tornozelo emerge como um elemento de destaque e de interesse. Estes reflexos têm um impacto profundo em várias dimensões. Primeiramente, desempenham um papel crucial nas respostas a lesões. Quando ocorre uma perturbação súbita ou uma situação de risco, os reflexos associados ao tornozelo agem instantaneamente para evitar e/ou minimizar danos físicos. Além disso, é importante realçar o papel primordial dos reflexos na monitorização da função neuromuscular. Por fim, destaca-se a valiosa contribuição dos reflexos no tornozelo para a estabilidade postural. Isto ocorre através de respostas rápidas e precisas às mudanças nas condições ou nas demandas do movimento.

Um dos tipos principais de reflexo que ocorre no tornozelo é conhecido como o reflexo de estiramento, também chamado de reflexo miotático. Este reflexo desempenha um papel crítico na manutenção do equilíbrio e na resposta a perturbações. Quando um indivíduo está em pé e por alguma razão perde o equilíbrio, os reflexos miotáticos são rapidamente acionados para ajudar na recuperação do equilíbrio. Os mecanismos neuromusculares permitem que o corpo responda instantaneamente a alterações nas condições do músculo, contribuindo para a estabilidade e para a coordenação durante o movimento. O reflexo de estiramento do músculo é um componente essencial do sistema de controle neuromuscular que opera em níveis subconscientes para manter a funcionalidade e a segurança do corpo.

Este reflexo desempenha um papel fundamental no controlo neuromuscular e na manutenção do equilíbrio do corpo. Ele entra em ação quando ocorre um rápido estiramento de um músculo e envolve mecanismos neurológicos complexos. Os principais órgãos sensoriais envolvidos neste reflexo são os órgãos tendinosos de Golgi e os fusos musculares, com destaque para estes últimos. Os fusos musculares têm fibras intrafusais que estão conectadas aos neurónios sensoriais aferentes. Quando os fusos musculares detectam um estiramento no músculo, eles geram potenciais de ação. Estes sinais são então transmitidos pelos neurónios sensoriais aferentes até à medula espinal.

Na medula espinal, os neurónios sensoriais aferentes estabelecem sinapses diretas com os neurónios motores α, que são responsáveis por inervar as fibras musculares extrafusais. Estas fibras musculares

extrafusais são aquelas que efetivamente produzem a contração muscular. O processamento do reflexo de estiramento ocorre inteiramente na medula espinal, sem a necessidade de envolvimento direto do cérebro, tornando-o um reflexo monossináptico. Quando os neurónios motores α são ativados, eles enviam sinais para as fibras musculares extrafusais do músculo que está a ser estirado. Este processo desencadeia uma resposta rápida de contração muscular reflexa e involuntária no músculo estirado. O objetivo deste reflexo é restaurar o comprimento original do músculo, prevenindo assim a sobrecarga ou o estiramento excessivo que poderiam levar a lesões musculares.

Estudos anteriores descobriram que entradas de alta frequência inibem os reflexos de estiramento, enquanto que entradas de baixa frequência os realçam devido à ressonância do fuso muscular e à consequente ativação síncrona das unidades motoras. Kearney et al. investigaram o impacto dos reflexos de estiramento na mecânica da articulação do tornozelo, concluindo que os mecanismos reflexos influenciam significativamente o comportamento da articulação, especialmente em condições de frequência específicas. Van der Helm et al. e Schouten et al. estenderam essa pesquisa para o braço humano, confirmando que os ganhos dos reflexos são mais proeminentes em baixas frequências. Estes enfatizaram a importância da eletromiografia (EMG) na avaliação da contração muscular durante tarefas de manutenção da postura. Estas descobertas destacam coletivamente a natureza dependente da frequência dos mecanismos reflexos.

Nesta dissertação de mestrado em questão, o objetivo primordial é explorar minuciosamente de que forma os reflexos do tornozelo se manifestam em resposta a estímulos caracterizados por diferentes bandas de frequência. Para alcançar com sucesso este propósito, procedeu-se à aplicação de perturbações sob a forma de sinais sinusoidais diretamente no tornozelo, sob rigorosas condições que asseguraram um sistema em anel aberto. Estas perturbações foram habilmente administradas em duas faixas de banda de frequência distintas: uma com banda estreita, abrangendo frequências que variam entre 0,12 Hz e 1,80 Hz, e outra com banda larga, compreendendo frequências no intervalo de 0,12 Hz a 20 Hz. O binário (ou torque, τ) foi adotado como o sinal de entrada no sistema experimental, enquanto que o ângulo de deslocamento (α) assumiu a função de sinal de saída. Esta meticulosa abordagem permitiu uma análise detalhada e abrangente das respostas reflexas no contexto dos diferentes regimes de frequência aplicados.

Além dos dados de resposta em frequência, em simultâneo, foram adquiridos dados de electromiografia. Um elétrodo foi posicionado no músculo gastrocnêmio e o outro elétrodo no músculo tibial anterior. Os resultados obtidos foram normalizados. Esta padronização foi feita a partir do máximo obtido através de um ensaio de contração máxima voluntária para cada um dos elétrodos, e teve como objetivo facilitar a comparação de resultados entre sujeitos e entre bandas de largura.

Este estudo envolveu a participação de quatro indivíduos saudáveis, que receberam instruções claras para permanecerem relaxados e para não contrariarem os estímulos recebidos durante as experiências. Dadas as instruções, foi assumido que todas as respostas obtidas a partir destes participantes são indicativas da dinâmica dos reflexos no tornozelo. Os dados obtidos poderão eventualmente ter dinâmicas não-relacionadas com o reflexo, sendo esta uma restrição deste estudo.

Ao longo desta dissertação, as respectivas funções de resposta em frequência também foram obtidas. Os resultados obtidos revelaram diferenças notáveis na dinâmica dos reflexos em relação às diferentes larguras de banda para o estudo da resposta em frequência. No entanto, os resultados da eletromiografia não evidenciaram variações significativas em resposta às diferentes larguras de banda.

Especificamente, foi observado que o ganho da resposta em frequência foi mais acentuado nos resultados de banda larga, sugerindo que a banda estreita exibe uma maior rigidez. Primeiramente, é importante realçar que a rigidez está altamente conectada com o reflexo de estiramento. Como já foi provado por vários estudos, quanto maior a rigidez, mais proeminente também será a dinâmica dos re-

flexos. Por causa desta relação, o ganho do reflexo foi traduzido como a impedância/rigidez durante esta tese. A rigidez é um componente da impedância.

A elevação da rigidez observada nos ensaios com banda estreita pode ser adequadamente elucidada ao considerar a taxa de sincronização dos fusos musculares. Ao introduzir perturbações, verifica-se um aumento na sincronização da atividade dos fusos musculares aferentes, resultando na ativação simultânea das unidades motoras. No entanto, à medida que a frequência das perturbações aumenta, observa-se uma redução na probabilidade de ocorrência desse fenômeno de sincronização. Este fenômeno ressalta a complexidade das interações dinâmicas entre os estímulos aplicados e as respostas neuromusculares.

Assim sendo, a conclusão provenient desta pesquisa reforça de maneira contundente a hipótese inicial que postula uma variação significativa na dinâmica dos reflexos no tornozelo, influenciada de modo preponderante pela amplitude da banda de frequência dos estímulos aplicados. No entanto, é crucial observar que tal constatação foi ratificada exclusivamente mediante a minuciosa análise dos resultados obtidos por meio da resposta em frequência. Nesta análise, tornou-se manifesta a proeminência dos reflexos na faixa de frequência estreita, denotando a peculiar sensibilidade e responsividade do sistema do reflexo do tornozelo frente a variações na largura de banda dos estímulos a que é submetido. Esta constatação, portanto, não apenas valida a conjectura inicial, mas também proporciona uma visão aprofundada sobre a complexidade da interação entre os estímulos aplicados e as respostas reflexas, delineando a relevância de considerações mais pormenorizadas ao abordar a compreensão dos mecanismos subjacentes a tais fenômenos no âmbito experimental.

Em relação aos dados extraídos da electromiografia, é imperativo salientar que as conclusões alcançadas não coincidiram com aquelas derivadas da análise da resposta em frequência. Este desvio de resultados é traduzido através da ausência de variações substanciais nas amplitudes das respostas observadas entre os estímulos caracterizados pela banda larga de frequência e aqueles associados à banda estreita. Esta discrepância entre os desfechos evidencia novamente a intricada natureza das respostas fisiológicas manifestadas pelo tornozelo diante de estímulos distintos, destacando, assim, a premente necessidade de aprofundamento nas investigações neste domínio específico. Este cenário ressalta a complexidade intrínseca dos fenômenos neuromusculares, indicando a viabilidade e relevância de pesquisas mais detalhadas para elucidar as nuances subjacentes a tais respostas e aprimorar a compreensão dos mecanismos envolvidos.

Palavras chave: Reflexo de estiramento, Articulação do tornozelo, Bandas de frequência, Fusos musculares, Electromiografia

Abstract

The ankle is a complex and crucial part of the body movement. It plays a key role in human mobility, impact absorption, and balance. The presence of reflexes in this limb is highly significant in terms of responses to injuries, monitoring neuromuscular function, maintaining stability, among other factors. The current study aims to investigate the presence or absence of reflexes with variations in the frequency bandwidth of the stimuli applied to the system. To achieve this, perturbations of the sum of sinusoids type are applied in open-loop conditions to the ankle for two different frequency bandwidth: narrow band (0.12Hz - 1.80Hz) and wide band (0.12Hz - 20Hz). This study was conducted with four healthy participants in five different trials, and they were told to stay relaxed during the experiments and to not contradict the stimuli. All of the outcome was considered as reflex dynamics. The respective frequency response functions were obtained, along with data from electromyography that was acquired simultaneously. Results showed a difference in the reflex dynamics for different bandwidths when it comes to the frequency response. Electromyography results did not show a significant difference for different bandwidths. The frequency response gain is higher for wide band results, which means that the narrow bandwidth has a higher stiffness. This conclusion can be explained by the synchronized firing rate of afferent muscle spindles that leads to a synchronous motor unit firing. However, when the frequency of perturbations are augmented, the likelihood of synchronized firing decreases. Because of this relation, the reflex gain was traduced by the impedance/stiffness during this dissertation. Because the stretch reflex is also pronounced when the stiffness is also higher, it is coherent for the narrow band to present a lower admittance gain and, consequently, a higher stiffness.

Keywords: Stretch reflex, Ankle joint, Frequency bandwidths, Muscle spindle, Electromyography

Contents

List of Figures

List of Tables

Abbreviations and symbols

Acronyms

ADP: Adenosine Diphosphate
ATP: Adenosine Triphosphate
BD: Bode Diagram CNS: The Central Nervous System
CPG: Central Pattern Generator
DDR: Direct Drive Rotary
EMG: Electromyography
FRF: Frequency Response Function
IMU: Inertial Measurement Unit
MVC: Maximum Voluntary Contraction
m.u.a.p.: Motor Unit Action Potential
NB: Narrow Band
NMJ: Neuromuscular Junction
QQB: Quanser Q8 Board
RF: Radio Frequency
RMS: Root Mean Square
TF: Transfer Function
VAF: Variance Accounted For
WB: Wide Band
3D: Three Dimensions

Greek Symbols

ϕ: Phase
ϕ_k: kth phase
ω: Frequency
ω_k: kth frequency
ω_c: Cutoff frequency
$\dot{\theta}$: Velocity signal
Θ: Angular displacement
τ: Torque
ζ: Damping ratio

Roman Symbols

C: Compliance c: Damper/visco-elastic factor
k_m: Motor stiffness
k_a: Ankle stiffness
k_{am}: System total stiffness
m: System's mass
Y_m: Motor admittance
Y_a: Ankle admittance
Y_{am}: System total admittance
Z_m: Motor impedance
Z_a: Ankle impedance
Z_{am}: System total impedance

Superscripts

$\dot{}$: Derivative

Chapter 1

Introduction

The ankle, a complex joint pivotal to human locomotion, is governed by an intricate interplay of biomechanical structures and neuromuscular processes. Its ability to swiftly respond to external stimuli is a fundamental feature for both stability and efficient human movement. This reflexive response, mediated by specific neural circuits, plays a critical role in injury prevention and adaptation to various physical demands.

This introductory chapter marks the beginning of an exploration into the intricacies of ankle physiology and the reflex phenomena intertwined with it. Understanding the mechanisms underlying these processes is essential to contextualize the subsequent research on the influence of frequency on ankle reflex dynamics. In this chapter, the anatomical structures and neural systems involved in ankle function will be examined, as well as the fundamental principles of reflexes. By providing this solid foundation, it is aimed to establish a comprehensive backdrop for the in-depth analysis of the interactions between frequency and reflex responses, which will be addressed throughout this study.

By the end of this chapter this dissertation motivation, hypothesis, questions and objectives will be described.

1.1 Neuromuscular System

The brain is the origin of voluntary movement. Upper motor neurons in the primary motor cortex provide signals to the brain stem and spinal cord, while lower motor neurons in the spinal cord send signals to the skeletal muscles. The Central Nervous System (CNS), which is composed by the brain, brainstem and spinal cord, is in charge of movement control. (Michael-Titus et al., 2010)

Hence, information is conveyed down a serial line in the nervous system, where the value is encoded using the frequency of electrical impulses. These electrical impulses are known as action potentials and spread throughout the body via neurons. The CNS system is composed by hundreds of millions to billions of neurons, many of which are engaged in movement control. Sensory neurons are often referred to as sensory receptors, they are located in various body tissues and transmit signals to neurons throughout the CNS, which receive and process those signals. (Burdet et al., 2013)

1. INTRODUCTION

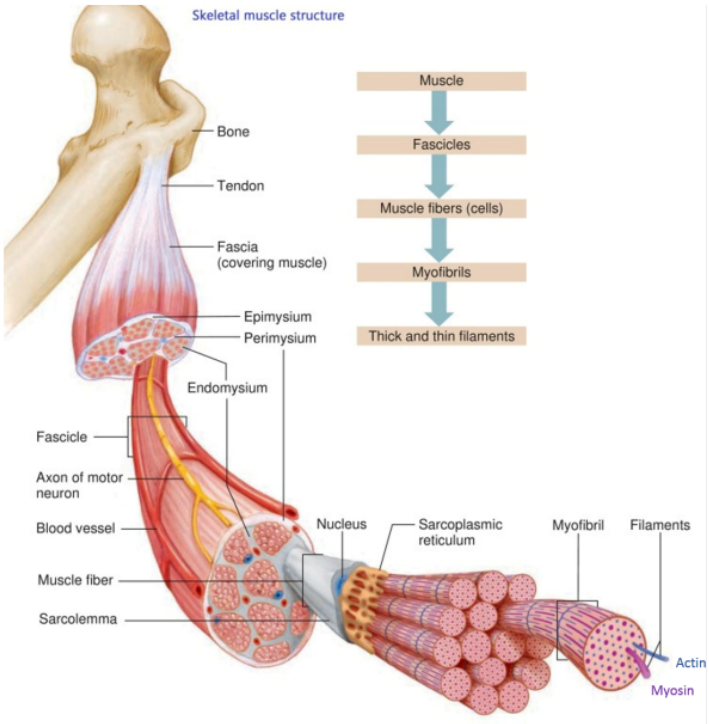

Figure 1.1: Structure of the skeletal muscle. (Coelho, 2021)

The muscle activation happens at the muscle fiber level where acetylcholine binds to neurochemical receptors, released by the α-motoneuron, at the neuromotor junction synapses. There are numerous excitatory and inhibitory synaptic junctions in the neural system. Together their control is summed into a final synaptic junction located in the spinal cord resulting in the control of individual motor units. The sarcomeres, contractile unit that creates force in accordance with the sliding-filament hypothesis, produce an electrical impulse and contraction by repeatedly binding and distancing the myofilaments actin-myosin cross-bridges. A collection of sarcomeres form the myofibril, and a parallel bundle of myofibrils creates the muscle fibre. A group of muscular fibres form a fascicle, and the muscle is ultimately made by a pack of fascicles. The skeletal muscle structure can be visualized in Figure 1.1. Each element of the muscle activation will be discussed with more detailed throughout this section. (Coelho, 2021; Burdet et al., 2013)

The α-motoneuron, a neuron found in the spinal cord, is responsible for controlling large clusters of muscle fibres that are dispersed randomly throughout the muscle. A motor unit is constituted by several muscle fibres and α-motoneurons that regulate them. At various points throughout the body, groups of nerve fibres/axons branch off from the main nerve and travel along predetermined paths to the muscles they regulate. Each axon divides when it enters the muscle, and each branch forms a neuromuscular junction (NMJ) with a single muscle fibre. Each muscle is regulated by a single α-motoneuron. (Burdet et al., 2013)

Numerous additional neurons, including peripheral sensory neurons (excitatory or inhibitory), provide input to the α-motoneurons. The output of the motoneuron, or the control signal for the motor unit, is determined by the integration of these inputs. The control signal is a series of action potentials that measure the force produced by the motor unit's muscle fibres. The higher the firing rate, the more force is produced. (Burdet et al., 2013)

1.1.1 Nerve axons: Afferents and Efferents

The nerves axons can be classified by its direction. If the nerve axon carry information out of the spinal cord, then it is called efferent. If the nerve axon carry information to the spinal cord, then it is called afferent. (McMahon, 1984)

The dorsal root ganglion, a swollen area of the peripheral nerve, contains the nerve cell bodies for the afferent nerve fibres. Based on the diameter of their axons, groups I and II of afferent fibres are distinguished. Information is received via Group I fibres, which have long axons and consequently relatively high conduction velocities, from the Golgi tendon organs (*Ib*), which can be seen in Figure 1.3, or spindle organs (*Ia*). The nuclear bag and nuclear chain fibre centres are encircled by the *Ia* nerve terminals. The nuclear chain fibres found inside the spindle organs are where the majority of Group II afferents, which have smaller axons, terminate. (McMahon, 1984)

On the other hand, efferent motor neurons' nerve cell bodies are all located in the spinal cord, in a specific region of the grey matter (constituted by nerve cells and their dendrites) in the ventral root. (McMahon, 1984)

The long nerve fibers of the white matter are embedded in neuroglial cells, prized for their properties as electrical insulators, and it is these which give the white matter its light colour. Long nerve fibres that run up and down the cord, carrying information to and from the brain, and connecting one level of grey matter in the cord to another, form the majority of the surrounding white matter. While the ventral root only has efferents and the dorsal root only has afferents, both run together in the one peripheral nerve that is a supplier for the muscle. As previously indicated, the efferents that service the intrafusal fibres in spindle organs are referred to as γ-motoneurons and the extrafusal fibres that are used to innervate the primary muscle mass are referred to as α-motoneurons. (McMahon, 1984)

1.1.2 Muscle Receptors

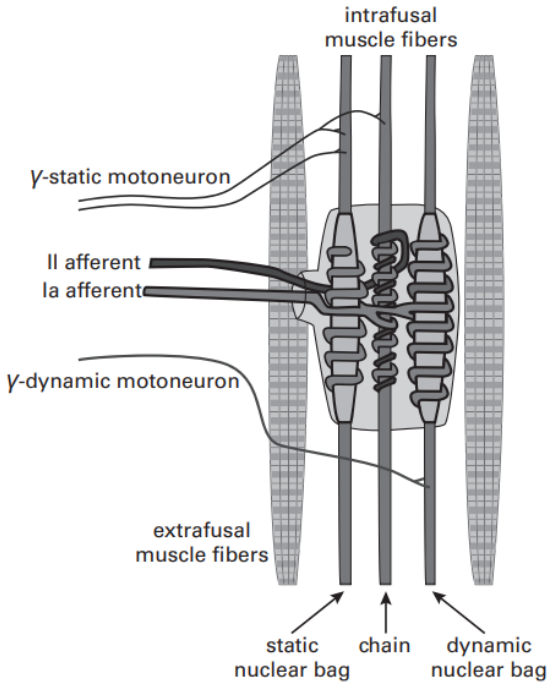

Figure 1.2: Up to three different types of intrafusal muscle fibres that are innervated by various sensory nerve fibres and motoneurons can be found in muscle spindles. The intrafusal fibres' various mechanical characteristics and their innervation by γ-motoneurons give the muscle spindle a diversity of responses to muscle tension. (Burdet et al., 2013)

1. INTRODUCTION

Peripheral sensory receptors activated in the skin, muscles, and joints send synaptic input to α-motoneurons. The majority of these receptors are referred to as mechanoreceptors since they are responsive to mechanical stimuli. They have a major impact in the feedback loop that activates muscle and its state. (Coelho, 2021; Burdet et al., 2013)

There are two types of mechanoreceptors: muscle spindles and Golgi tendon organs. Muscle spindles act in response of the muscle stretch by measuring the muscle length and stretch velocity (rate of change), they transmit this information to the spinal cord through *Ia* and *II* afferent neurons. They are deeply present within practically all the muscles and are located on the muscle belly in intrafusal fibers. They are constituted by small muscle fibres, also known as intrafusal fibres, interlaced by sensory nerve endings compressing it all together into spindle-shaped structures, they layout in parallel to the skeletal muscles fibres (extrafusal fibres) along the muscle. It is possible to observe this description in Figure 1.2. Muscle spindles present a interesting characteristic: at specific amplitudes, reflexes are triggered due to the simultaneous activation of muscle spindle sensory fibers, leading to coordinated firing of motor units. However, when perturbations rate augment, the likelihood of synchronized firing decreases. (Coelho, 2021; Burdet et al., 2013; McMahon, 1984; Schouten et al., 2008a)

The proportion of how an applied stretch that will act on the sensory terminals and, as a result, how the stretch will be converted into action potentials, are determined by the mechanical characteristics of intrafusal fibres. Changes in intrafusal fibre stiffness can affect the sensitivity of primary and secondary sensory terminals, which appears to be directly related to local strain in the fibres. The intrafusal fibres polar zones are much stiffer than the sensory zones, which are located closer to the fibres centre. Consequently, the sensory zone experiences the majority of the length change when a muscle spindle is stretched. (Coelho, 2021; Burdet et al., 2013)

The neurons that innervate intrafusal fibres are normally γ-motoneurons, they control the muscle spindles sensitivity to the stretch. When these motoneurons are stimulated, a constrained contraction of an intrafusal fibre is produced, which normally happens close to the poles. The polar zones become substantially stiffer and more stretch resistant as a result of the contraction, which expands the sensory zone and increases its sensitivity to stretch. There are two types of γ-motoneurons, static and dynamic. These definitions describe how the activation of the γ-motoneurons affects how sensitive the muscle spindle is. (Coelho, 2021; Burdet et al., 2013)

In 2011, Prochazka observed that when there is a rise in the muscle length, firing rate increases for both the primary (*Ia* afferent) and secondary (*II* afferent) endings, which show that muscle spindles are extremely sensitive to detect movement. When there are γ-static motoneurons activated, the sensitivity of the secondary ending to variations in length is slightly increased, while the sensitivity of the primary ending is significantly decreased. When it comes to the γ-dynamic motoneuron activation, the secondary ending remains unchanged and the firing rate and sensitivity to the constant velocity stretch are both increased for the primary ending. (Burdet et al., 2013)

During muscle shortening, the primary endings are present due to γ-motoneuron activation. When there is a coactivation of α-motoneurons and γ-motoneurons, it allows the CNS to obtain information during both muscle lengthening and muscle shortening from the primary endings. (Burdet et al., 2013)

When the muscle suffers large stretches, there is a reduction in the sensory endings' sensitivity, since this sensitivity is considerably larger in the presence of a small stretch. Seconds after this large stretch, the primary endings suffer a reset to its sensitivity. The shift in the stiffness of the polar portions of the intrafusal muscle fibres is responsible for this feature. With small stretches, this stiffness is elevated which increases the stretch quantity transferred to the sensory zone. Whereas with larger stretches, there is a stiffness reduction that causes a sensitivity reduction in the sensory zone. The sensory zone

sensitivity is reestablished once a new length is achieved and upheld. There is an increase in the firing rate of primary endings modulation, when γ-dynamic axons are stimulated during sinusoidal stretching. (Burdet et al., 2013)

The other type of mechanoreceptors are the Golgi tendon organs, they are the kind of mechanoreceptors that react to force by measuring the tension applied in the muscle and send this information to the spinal cord through *Ib* afferent neurons. They usually can be found in the tendon closely to the tendon/muscle fibre junction. They are composed by bundles of collagen strands and sensory nerve endings encased in connective tissue capsules found at junctions between skeletal muscle fibres and a tendon or aponeurosis. (Coelho, 2021; Burdet et al., 2013; McMahon, 1984)

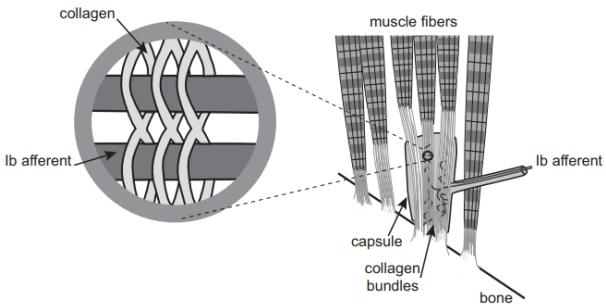

Figure 1.3: *Ib* afferent nerve fibres that terminate among collagen fibres close to the intersection of muscle fibres and tendon form the Golgi tendon organs. Collagen fibre tension increases cause the nerve terminals to deform, which causes depolarization and action potentials triggering. (Burdet et al., 2013)

In Figure 1.3 it is possible to observe the pathway of force transmission, it goes from the tendon and muscle ends of the Golgi tendon organ (*Ib* afferents) to its sensory endings through the collagen bundles and embedded capsules. The group *Ib* afferents is constituted by all of the sensory never fibres innervating tendon organs. When there is an in-series muscle fibres contraction, this *Ib* group fires.(Burdet et al., 2013)

Golgi tendon organs are highly sensitive to forces produced by active contraction of in-series muscle fibres but have a comparatively low sensitivity to tension produced by passive stretching of the tendon. However, even in active muscle, the sensitivity to tension produced by passive stretching of the entire muscle will be lower than that produced by contraction of in-series muscle fibres because the majority of the tension produced by passive stretching will be shunted through the in-parallel muscle fibres and therefore will not be transmitted to the Golgi tendon organ.(Burdet et al., 2013)

In static conditions, individual Golgi tendons are not able to signal whole muscle force due to multiple factors such as reduced firing rate, unloading caused by in-parallel muscle fibres, and better sensitivity to dynamic changes in force. However, the mean firing rate of all Golgi tendon organs in a muscle is less affected by unloading and tracks variations in motor unit force better than absolute levels of force. Golgi tendon organs are better sensors of rate of change of force than force itself. Nevertheless, as Gandevia concluded in 2011 (Walsh et al., 2011), the combined firing rate of an ensemble of Golgi tendon organs varies linearly with force at the tendon. (Burdet et al., 2013)

1.1.3 Functional Control of Movement by the Central Nervous System

Lower motoneurons, located at the spinal cord, are the main output neurons that transmit control signals directly to muscles. The signals originate at sensory receptors, interneurons (local circuit neurons in the spinal cord) and upper motoneurons (neurons in the brainstem and brain). In 2009, Horak (Horak

et al., 1993) concluded that human beings maintain balance through the neural pathways that initiates at the brainstem upper motoneurons and ends at the lower motoneurons. The synaptic targets are the extensor muscles of the lower limbs, proximal muscles of the upper limbs, and trunk muscles. This pathway will command the compensation mechanism of balance disturbances. (Burdet et al., 2013)

Bizzi et al. reached the conclusion that a network of spinal interneurons can regulate the synaptic input to each muscle in a group, creating a relative activation pattern referred to as a synergy. Higher-level control can combine synergies in diverse ways by selecting the timing and strength of each synergy, allowing for a large repertoire of movements for different activities. The cerebellum and other regions involved in higher-level motor control play important roles in this process. (Burdet et al., 2013)

The CNS structures governate the neuromuscular system. For example, the cerebellum plays an important role in motor learning (Galea et al.,2011), the basal ganglia the controls the motor command magnitude and trains the early stages of motor learning (Turner & Desmurget, 2010), the primary motor cortex is the main executor of motor control (Galea et al., 2011), the premotor areas have shown to be part of the selection of actions based on the action' s context (Nachev, Kennard& Husain, 2008), the dorsal premotor integrates information necessary to specify movement parameters (Scangos & Stuphorn, 2010), the primary somatosensory area integrates the received information into body configuration, hand shape, properties of manipulated objects, and so on. (Burdet et al., 2013)

1.2 Muscle Mechanics and Control

Muscles are biological engines that actively produce movement and force through contraction. In 1957, H. E. Huxley and A. F. Huxley (Huxley et al., 1957) presented the sliding filament cross-bridge model of muscle contraction. Along the years, this model has been adjusted, but its basis was maintained. This model is a great tool to understand the muscle viscoelastic properties. (Burdet et al., 2013)

1.2.1 The Motor Unit

The tendon is a passive viscoelastic element that permits the skeletal muscle bone insertion allowing mobility (Burdet et al., 2013). The neuromuscular system controls and generates the patterns of tension at the tendon. This tension will stipulate the physiological characteristics of the muscle and dictate whether it is rested or fatigued (metabolic state). (Winter, 2009)

Motor units are composed by a motor neuron and all of the skeletal muscle fibres. These fibres are innervated by the neuron's axon terminal, which includes the neuromuscular junction formed between the neuron and the fibres (Purves et al., 2001). The number and length of muscle fibres present on motor units can vary: fingers, eyes and face muscles have shorter fibres in small quantities, meanwhile, larger muscles (leg muscles) have longer fibres in a larger score. (Winter, 2009)

A muscle fibre is constituted by fibrils that are constituted by filaments (contractile proteins). There are two principal filaments, actin and myosin, which can be observed in Figure 1.4. The darker structures are myosin (thicker structures), and the lighter bands are actin (thinner structures). Two elongated globular head portions and a tail region form a myosin molecule. The globular proteins known as actin have myosin head-binding sites with strong affinity. Myosin and actin filaments together with adenosine triphosphate (ATP), results in transformation of chemical energy into mechanical work. (Burdet et al., 2013; Winter, 2009)

The noticeable space between myosin and actin filaments is where the tension is created, it is called the cross-bridge structure, a binding between these filaments can occur if an actin molecule is close

enough to a myosin head (cross-bridge attachment). This is the part where shortening (muscle contraction) and lengthening (muscle stretching) occurs. The actin filament is drawn towards the myosin filament during attachment as a result of a change in the molecular conformation of the myosin cross-bridge. This results in the creation of tension. (Burdet et al., 2013; Winter, 2009)

The sarcomere is a repeating pattern along muscle fibres. It is composed by a variation of partly overlapping actin and myosin filaments. At each end of the sarcomere there are *Z*-discs, they connect the actin filaments of each sarcomere to the next one. (Burdet et al., 2013; Winter, 2009)

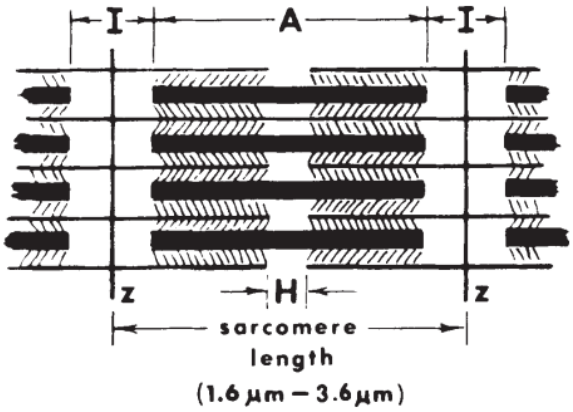

Figure 1.4: Basic components of muscles' contractile element. Through cross-bridges (cross-hatched lines), the thicker, black myosin filament communicates with the thinner, actin filament. (Winter, 2009)

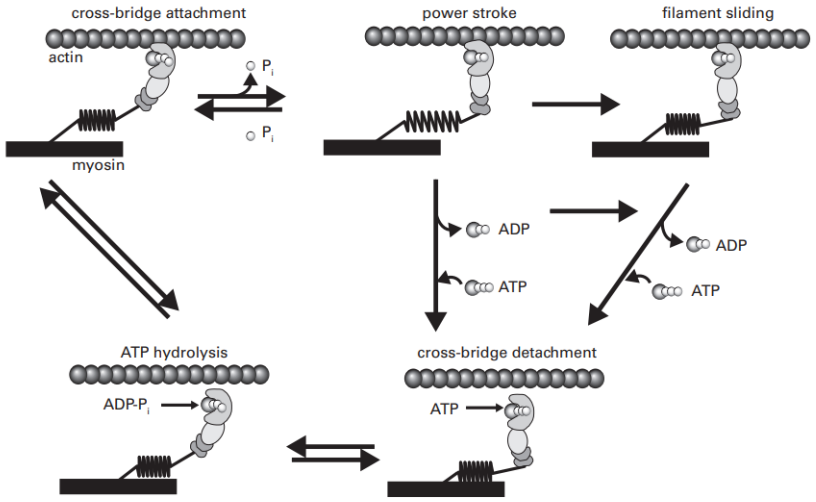

Figure 1.5: In the cross-bridge cycle, the myosin heads connect to specific points on the actin and then undergo a change in shape by using energy released from the breakdown of ATP into ADP. This change in shape creates an increased tension between the actin and myosin filaments, causing them to move closer together. If the tension becomes strong enough to overcome the resistance to movement, the actin filament will slide towards the center of the sarcomere. Once ADP is released, the myosin heads release their grip on the actin and wait for a new ATP molecule to bind, which starts the detachment of the cross-bridge. (Burdet et al., 2013)

Muscles are structured in a way where filaments are in parallel and sarcomere elements are in series (myofibrils - series of sarcomeres together in series) in order to compensate the contractile element. (Winter, 2009)

As Nyitrai and Geeves explained in 2004 (Nyitrai et al., 2004), during the cross-bridge cycle, the myosin heads bind to specific sites on the actin filament and undergo a change in shape using energy

obtained from the hydrolysis of ATP into adenosine diphosphate (ADP). This adjustment in shape results in a tension increase between actin and myosin filaments, leading them to move closer together. If the tension surpasses the force required for movement, the actin filament will slide towards the center of the sarcomere. Following the release of ADP, myosin heads release their grip on the actin, waiting for a new ATP molecule to bind, initiating the detachment of the cross-bridge. This can be observed in Figure 1.5. (Burdet et al., 2013)

The relationship between a single cross-bridge's force and displacement when shifting an elastic load showed that the force-displacement relationship is highly linear, indicating that the release of elastic energy from the cross-bridge is what drives the tension build-up and filament sliding. (Burdet et al., 2013)

The sarcomere length is reduced when myosin heads are at the center of the filament and get attached to the actin binding sites pulling actin filaments from each half of the sarcomere to the filament center. The myosin filaments slide past each other as a result of the successively attaching, pulling, and releasing of cross-bridges in an asynchronous way causing the muscle to shorten (contract). When a muscle fibre is under persistent contraction, this cycle can be repeated numerous times. (Burdet et al., 2013)

In 1966 Gordon, Huxley and Julian (Gordon et al., 2004) presented that the sarcomere force depends on length, the force is proportional to the amount of overlap between myosin and actin filaments. Thus, the number of cross-bridges, or the number of bonds that can form between actin and myosin, reflects in the sarcomere force. When there is no overlap, the sarcomere length is wider. It starts to decrease as the contraction begins leading to a maximum sarcomere force when there is a complete overlap of actin and myosin. In 2010, Herzog, Joumaa and Leonard (Leonard et al., 2010), reinforced that the sarcomere force can suffer alteration considering its prior situation (elongated or reduced). (Burdet et al., 2013)

There is another fibrous structure constituted by connective tissue and contains active contractile elements, this structure is called fascia. The fascia acts like a coating structure that surrounds muscles, it separates them into layers and groups, making the connection between the muscles and the tendons that are placed at each end of them. Some of this connective tissue are in series with the contractile element, whereas some are in parallel. The effect of this connective tissue is sometimes modelled as springs and viscous dampers. (Winter, 2009)

1.2.2 Muscle Viscoelasticity

Cross-bridges behave reminds a small springs: when stretched by pulling there is a tension increase and when shortened there is a tension decrease. The sarcomere has a cross-bridge attached and its length can be changed. The ratio of the force change to the length change is known as the stiffness. The connective tissue elasticity and the sarcomere cross-bridges this elastic (stiffness) component of the muscle force. (Coelho, 2021; Burdet et al., 2013)

The summatory of the individual sarcomere's length changes originates the length change in myofibril if the change in force is the same for each sarcomere. Otherwise, if one sarcomere's force change was larger than that of its neighbour, the neighbouring sarcomere would be pulled resulting in the stretch of the attached cross-bridges until there is a balance in force. When there is a change in force, it happens everywhere in the series sarcomere's chain. Nonetheless, the summatory will be equal to the overall length change since this change is distributed along the components. The stiffness of a myofibril decreases with the number of sarcomeres. It follows that a muscle fibre will be less rigid the longer its myofibrils are. (Burdet et al., 2013)

When a muscle contracts concentrically, it does positive work by applying force in the direction of

the movement. In an eccentric contraction, the muscle lengthens against the force of its contraction and generates negative work. Depending on the contraction of the muscles (active component) and the inherent mechanical characteristics of its constituent parts (passive component), the muscle-tendon unit produces and transfers force. Ligaments, articulating surfaces, and skeletal structure are considered passive anatomical structures and they generate the tendon tension. All of the muscle-tendon unit together will bring the muscle to active. In general, the behaviour of a muscle-tendon unit can be described as that of a nonlinear viscoelastic element with stiffness and viscosity components that depend on both passive and active. (Zajac, 1989)

When there are no muscle activation only passive components are present. Thus, while the muscle is activated it increases the number of parallel cross-bridges that function as elastic components and raise active stiffness, the cross-bridges created in a muscle with no activated fibres will modestly contribute to the passive stiffness. The length and rate of change of a muscle both influence the force it produces, which can be seen in Figure 1.6 and Figure 1.7. (Coelho, 2021)

In Figure 1.6 it is possible to observe that throughout isometric contraction, at the optimal length, l_0, the muscle is exerting its maximum force, $F_{\max}$. For a particular activation level, maximum force can be generated when the cross-bridges overlap, which happens at l_0. When the muscle length exceeds or have a value lower than l_0, the overlap of the cross-bridges is reduced dropping the active component force. When the stretch surpasses l_0, it can be observed that the passive component (mostly tissue elasticity) rises notably, contributing to the total force. (Coelho, 2021)

As a convention, sarcomere lengthening velocity is considered negative work (eccentric) and sarcomere shortening velocity positive work (concentric). It can be observed on Figure 1.7 that in the stretching phase, the force is greater when the velocity is different than zero. For lower velocity values force increases until it becomes constant for higher absolute velocity values. (Burdet et al., 2013)

The stretching of attached cross-bridges is the main cause of the force increase with the increase of muscle lengthening velocity. Stretched cross-bridges generate a higher force than isometric cross-bridges (velocity zero) do during the period of attachment. This happens because more cross-bridges are stretched during higher lengthening velocities. The maximum force is limited in muscle lengthening. The reason behind that is that cross-bridges separates when the lengthening velocity rises since they stretch beyond actin-myosin binding force supports. This causes the muscle to lose its capacity to generate force. (Burdet et al., 2013)

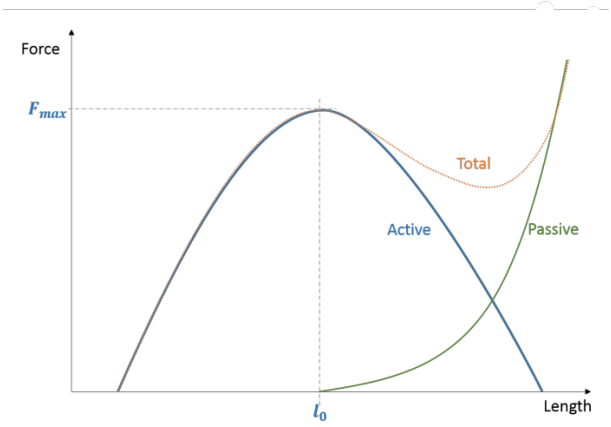

Figure 1.6: Muscle force in function of muscle length. (Coelho, 2021)

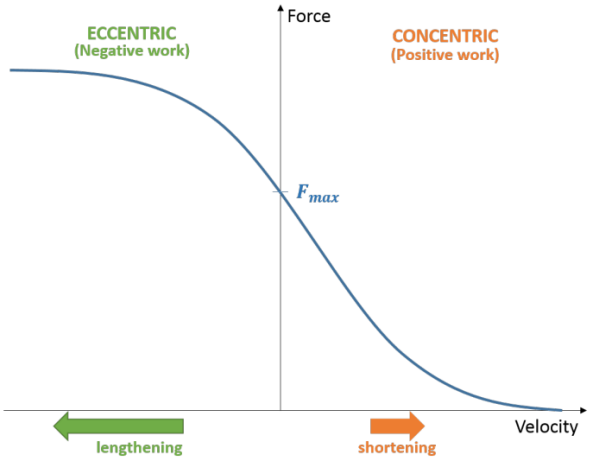

Figure 1.7: A sarcomere's force while it is being stretched is greater than isometric force (zero velocity). A sarcomere's force decreases below the isometric force when it is shortened, decreasing inversely with the shortening velocity. (Coelho, 2021)

In 2010, Edman (Tynelius et al., 2010) colluded to the fact that when the sarcomere shortens against a load, the velocity of shortening spontaneously adapts to its magnitude. The shortening velocity drops as the load rises. As it can be observed in Figure 1.7, there is a hyperbolic decrease in the force while there is an increase in shortening velocity. At maximum shortening velocity, force decreases. In view of the fact that, firstly, during the shortening period there are not a lot of cross-bridges attached, and this quantity decreases even more as the shortening velocity increases (cross-bridge detachment rate increases). Secondly, the attached cross-bridges loses tension in the shortening phase as it can be observed in Figure 1.4.

At higher shortening velocity, those cross-bridges will not be able to generate a good amount of force in comparison to isometric cross-bridges. This happens because the cross-bridges cycle occurs more frequently, which means that the attachment time will have a lower duration, not allowing a proper force production (Coelho, 2021). Thirdly, in the shortening period there may be some cross-bridges compression before their detachment, generating negative forces. This compression reduces the whole sarcomere tension, and it happens more frequently with a higher shortening velocity. (Burdet et al., 2013)

When cross-bridge detachment happens, it will dissipate elastic energy. Considering the mass-spring system and its damping capacities (oscillations will decrease in the amount that energy is dissipated). For the sarcomere, this damping will rely on the velocity. The concept of viscosity is based on a system that alters the resistive force to counteract a change in velocity. In the sarcomere system, the resistive force will withdraw towards its center. (Burdet et al., 2013)

As seen before, sarcomere lengthening velocity is considered to be negative while sarcomere shortening velocity is considered positive. Nevertheless, Newtonian mechanics denotes muscle lengthening velocity as positive whereas muscle shortening velocity is negative. As a result, there is a sarcomere positive force when its ends are pulled towards its center. Sarcomere force increases when there is an increase in sarcomere lengthening velocity, resulting in a positive viscosity coefficient, D. When the sarcomere is at a shortening phase and there is an increase in shortening velocity, there is a decrease in force, resulting in a positive D value as well, since the change in force and the change in velocity are both negative. (Burdet et al., 2013)

The sarcomere viscosity is at its highest point around isometric force (zero velocity) and at its lowest point when both lengthening and shortening velocities are at their highest, resulting in an insufficient change in force. The number of attached cross-bridges affects how much elastic energy can be released.

(Burdet et al., 2013)

As seen before, each myofibril sarcomere that build up the muscle fibre have a change in length when the muscle fibre itself does. All of the sarcomeres in the fibre experience the same force change, which is equal to the force change of the myofibril itself. However, this force change is dependent on the total number of sarcomeres: the more sarcomeres exist in the myofibril, the smaller is the change in length for each sarcomere, which means that the force change resulting from the stiffness of the cross-bridge is smaller. (Burdet et al., 2013)

In 2010, Campbell described that as a muscle fibre is stretched there is an increase in force while stiffness does not show significant changes until the sarcomere length increases by 15 to 20 *nm*. By this time, the actin-myosin link can no longer sustain the elastic strain produced by the stretch of a cross-bridge, if the fibre continues to be stretched the actin-myosin bond breaks. This defines the threshold of the short-range stiffness zone. (Burdet et al., 2013)

Muscle fiber length, rate of change of length and length change are factors that influences viscoelasticity. However, as Kirsch, Boscov and Rymer pointed in 1994, viscoelasticity is also a function of the activation level. Both viscosity and stiffness grow linearly with muscle force, which can be expected from the linear relationship between sarcomere force and the number of attached cross-bridges. (Burdet et al., 2013)

The results indicate that stiffness decreases as the amplitude of the pulses increases. Furthermore, viscosity decreases for higher frequency bands, which can be attributed to higher average rates of muscle length change. According to the findings, stiffness reduces as pulse amplitude increases. Additionally, viscosity decreases with increasing frequency bands, which is explained by a greater average rate of changes in muscle length. (Burdet et al., 2013)

1.2.3 Control of Muscle Force

Muscles have a determinate number of motor units, each one of them is controlled by a separate nerve ending. Excitation of each unit is an event that occurs completely or does not occur at all. This is electrically indicated by an action potential and mechanically indicated by a twitch of tension, which is a short muscular contraction. The type of muscle fibre affects how long a twitch lasts. Slow-twitch (type I) fibres take longer to contract and relax than fast-twitch (type II) fibres do during a twitch. (Burdet et al., 2013)

Tension can vary positively by a stimulation rate raise for the motor unit or by excitation of an additional motor unit, also called as recruitment. The CNS regulates tension by dictating the quantity of active motor units and the pace at which they fire (firing rate). Due to the build-up of intracellular Ca^{2+}, the force generated by each muscle fibre of the motor unit increases with its firing rate. (Burdet et al., 2013)

Figure 1.8 represents an electromyogram of a muscle that is suffering the tension rise. In the first trace it is possible to see the arousal of only one motor unit, in the middle trace there is an arousal of two motor units, and in the last trace there are three motor units that get excited.(Burdet et al., 2013)

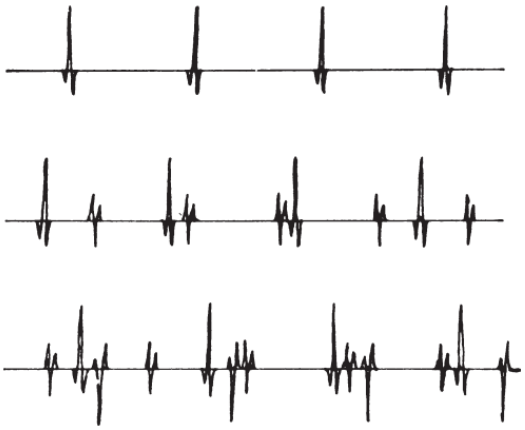

Figure 1.8: Electromyogram that results from a needle electrode muscle placement that develops tension. In the first trace there's the recruitment of one motor unit. In the second trace there's enough tension for the recruitment of two motor units. In the third trace there's enough tension for the recruitment of three motor units. (Winter, 2009)

In Figure 1.8 it is possible to observe that the smallest motor unit is first recruited and by its rate arises, it allows the recruitment of more motor units. Each action potential depolarizes the muscular membrane, releasing more Ca^{2+} into the intracellular region where it diffuses and activates additional actin-binding sites. The motor action potential characteristics depends on the size of the motor unit and the distance from the electrode to the fibres of the motor unit. (Burdet et al., 2013; Winter, 2009)

In the beginning, muscle tension raises with the increase of the firing rate for the first motor unit. Nevertheless, every unit has a maximum firing rate, which is achieved as soon as the next unit is recruited. These rates are high enough so that a number of action potentials can happen before the first action potential from the first twitch force reaches zero. When there is a tension reduction the process occurs in reverse, meaning that the firing rates will decrease until the last-recruited unit firing rate reduces sufficiently. (Burdet et al., 2013; Winter, 2009)

There is a Ca^{2+} build up in the muscle fibre as a result of repeated action potentials that happen at intervals that are shorter than the twitch duration. The force increases with the quantity of Ca^{2+} accumulated since the number of cross-bridges that can form depends on this substance availability. As the force increases, the firing rate also increases monotonically. Though, when the force increases too rapidly to a maximum voluntary contraction (from 0 to 100%), the firing rates will increase nonlinearly. (Burdet et al., 2013; Winter, 2009)

In 1974, Henneman (Henneman et al., 1974) introduced the size principle. This principle declares that the magnitude of a recently recruited motor unit grows as the amount of force required for its recruitment increases. Essentially, the smallest units are called upon first and the largest units are called upon last. Which means that precise incremented steps will result from low-tension movements and the recruitment of lager motor units will result in high forces with no fine control movements. (Winter, 2009)

There are frequency thresholds that will define how much tension it is necessary to recruit the next larger motor unit. The progression of tension escalation, crossing of new thresholds, and recruiting of larger motor units persists until the maximum voluntary contraction is achieved, which corresponds to the point where all motor units are firing their maximum frequencies. The reverse process to the one described before will lower the tension. In 1982, DeLuca et al. (DeLuca et al., 1982) wrote that there will be a continuous decrease of the firing rates and the first ones to cease will be the larger units. (Winter, 2009)

Larger motor units have larger motoneurons innervating them, this results in a greater depolarization

potential at the motor end plate (connects the motor unit feature to the skeletal muscle fibres). Also, in larger motor units there will be greater electrode voltage oscillations. Hence, in 1975, Milner-Brown and Stein (Milner-Brown et al., 1975) reached the conclusion that larger motor units will have increased action potentials and smaller motor units will have lower action potentials. Nevertheless, it is important to refer that it is not possible to foresee motor unit sizes from an electromyogram recording, since the motor unit's action potential also decreases with the distance between the recording location and the electrode position. (Winter, 2009)

The voluntary tension also depends on the individual muscle twitches profile, which means that if a maximum contraction is made by a certain muscle, the rate of tension increase depends on the individual motor units and how they are recruited, it can take hundreds of milliseconds for maximum tension to be achieved. There is also a delay for voluntary relaxation, and in this case the delay is more noticeable. Besides that, there is the contribution of the delay in the motor units drop out (size principle). Therefore, the muscle takes longer to shut off than to shut on. (Winter, 2009)

1.2.4 Muscle Frequency Bandwidth

In 1965, Partridge (Partridge, 1965) described the conversion of action potentials into muscle force as a low-pass filters: because the muscle fibre does not completely relax between successive action potentials, the amplitude of the force control decreases as the motor unit firing frequency rises and the mean force intensifies. The force reaches its maximum magnitude and can no longer be modulated at firing rates that are sufficiently high. (Burdet et al., 2013)

It is possible to specify the control bandwidth by modulating the firing rate in different sets of frequencies. The effective cut-off frequency for limb muscles is 2 to 3 Hz, which is the frequency response threshold of a system where energy going into the system starts to be diminished (attenuated or reflected) instead of passing through (Carr, 2000). Therefore, a single muscle has very limited capacity to regulate force at higher frequencies. The delay between the electrical input and mechanical output grows as the electrical input frequency lowers due to the lag between the release of Ca^{2+} and the beginning of cross-bridge production. There is also the low pass filtering process to consider. (Burdet et al., 2013)

The fatigue, drop in the muscle fiber force supplying capacity due to an extended muscle activation, causes the peak twitch amplitude to decrease and the twitch duration to increase. Thus, the response becomes slower since muscle force reduces, meaning that the control bandwidth is diminished by fatigue. (Burdet et al., 2013)

Muscles operate in an agonist-antagonist dynamic, which enables the realization of higher bandwidths. Because muscle force can be increased more quickly than it can be decreased, this occurs. Strong antagonist muscle group activation creates a rapid rise in opposing joint torque, which causes the net joint torque to fall more quickly than it would with just agonist muscle group relaxation. (Burdet et al., 2013)

1.2.5 Muscles force-length characteristics

The muscle is composed by an active (contractile element) and a passive element (connective tissue). These elements force-length characteristics combined results on the net force-length of the muscle. Changes at a sarcomere level can provide the force-length curve (Figure 1.9). (Winter, 2009)

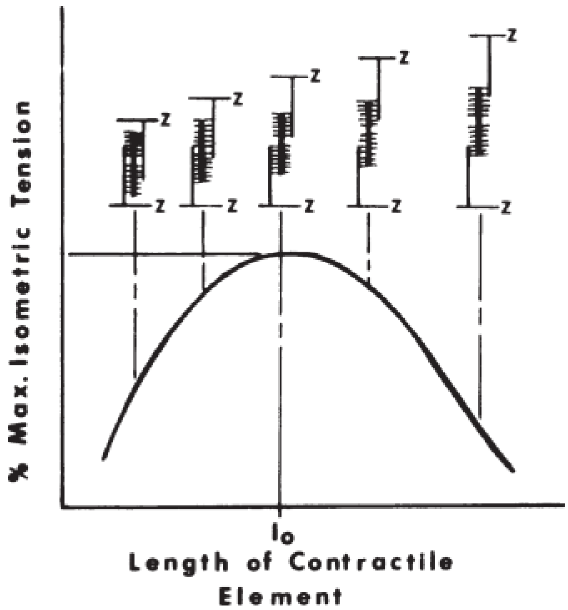

Figure 1.9: Tension generated by the muscle in function its variation from the resting length, l0. The decrease in tension that occurs on both sides of the maximum point can be accounted for by the interactions among cross-bridge attachments in the contractile components. (Winter, 2009)

In Figure 1.9 it is possible to observe that at resting length, l_0, the number of cross-bridges between the filaments is at its maximum, resulting in a maximum isometric tension. When the muscle elongates, the filaments get separated from each other, which leads to a decrease in cross-bridges and, ultimately, a reduction in tension. When the muscle is fully extended, there are no cross-bridges present, which is when the tension ceases completely. Before l_0 there is an interference caused by the cross-bridge overlap, which results in a tension decrease that is prolonged until the occurrence of a complete overlap. In these values of contractile element length, the tension does not fall until it reaches a null value, but the interfering elements causes it to reduce significantly. (Winter, 2009)

The connective tissue adjacent to the contractile element that acts like an elastic band is called the parallel elastic component. The parallel elastic component is at a resting and loose state and without tension when the muscle is also at its resting length or less. When the muscle starts to lengthen, this parallel element strengths as well, building tension up. This starts to happen very slowly but then it happens in a quick way. In opposition to a spring (linear force-length relation), this element is nonlinear. (Winter, 2009)

There are also connective tissue that are in series with the contractile component, those are called the series elastic element. Tendons are included in this category. In isometric contractions, when tension increases, series elastic elements will lengthen to some degree, which happens because they are under tension. When it comes to a dynamic contraction, these elements, along with viscous components, will affect the time taken by the muscle tension to develop tension. (Winter, 2009)

In general, the external muscle length is constant, thereby the series elastic element can only stretch if there is an equal shortening of the contractile element itself, an internal shortening. As it can be observed in Figure 1.10, the series elastic element will lengthen in the same quantity that the contractile element will shorten internally, which is caused by the increased tension from the contractile element.

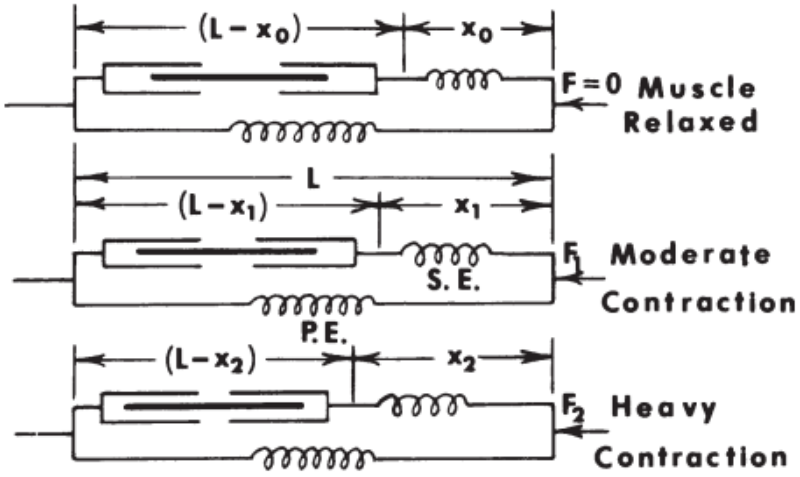

Figure 1.10: Actuation of series elastic (S.E.) elements. The tendon tension changes as the series element lengthens and the contractile element internally shortens during isometric contractions. The presence of the series elastic element is not very significant during normal human movement, but during high-performance movements, like jumping, it is in charge of storing energy as a muscle lengthens just before rapidly shortening. (Winter, 2009)

1.2.6 Muscles force-velocity characteristics

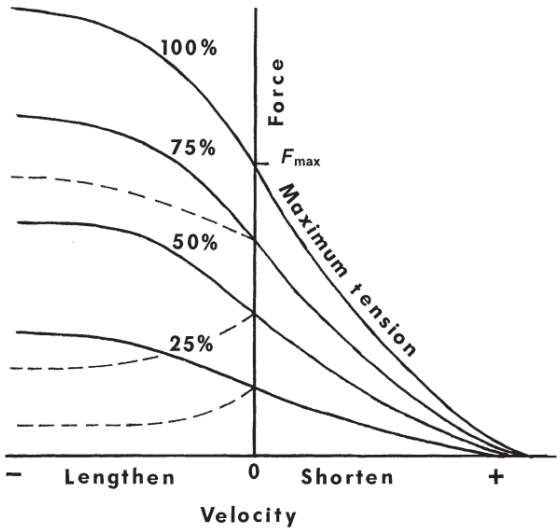

Figure 1.11: Different levels of muscular activation are represented by the force-velocity properties of the skeletal muscle; these levels are 25%, 50%, 75%, and 100%. The length of the muscle must be recorded, and all such actions must be taken as the muscle shortens or lengthens at a specific length. The solid lines represent isotonic activity, while the dashed lines represent isovelocity activity; during shortening, the curves adhere to the hyperbolic Hill model, while during lengthening, the curves depend on the experimental technique. (Winter, 2009)

Muscle shortening and lengthening occurs alternatively and regularly, because movement would not be achieved without muscle length changes. As a muscle shortens in response to a load, its tension reduces, this characteristic can be observed in a muscle force-velocity curve (Figure 1.11). Maximum contraction is at 100%, but it is rare to see this kind of performance even in professional athletes. (Winter, 2009)

In Figure 1.11 it is possible to observe a tension decrease as the shortening velocity increases. As the cross-bridges in the contractile element break and then rebuild in a shorter condition, tension is lost,

which is why this occurs. Moreover, the fluid viscosity in the connective tissue and contractile element appears to be a contributing factor as well. As a viscosity result, there is friction. To overcome this friction, it is necessary an internal force, and as a consequence there is a decreased tendon force.

1.2.7 Kinematics and Kinetics

Kinematic variables will describe the movement and they do that independently of external or internal forces. These can be linear and angular displacements, velocities, and accelerations. (Winter, 2009)

Kinetics is the term that describes the movement causing forces (internal and external). Internal forces refer to the ones that come from muscles and joints friction, ligaments, and muscle activity. External forces refer can have origin in different scenarios, they can come from the ground, from external loads, from active bodies, or from passive sources. A diversity of approaches can be used to analyse the movements kinetic, the one used in the present work relies on the moments of force produced by muscles crossing a joint, which was mentioned earlier. Yet, other approaches using power flowing can be used. (Winter, 2009)

1.3 Biomechanical Modelling

In biomechanical modelling it is common to resource to the use of the inverse problem in order to predict variables. In this case, the causes are identified from the effect. The alternative to this type of analysis would be the forward solution or direct problem, which it is based on assumptions. (Winter, 2009)

The direct problem predicts the kinematics using assumed moments of force as forcing functions, so the effect is identified from the causes. After there is a valid model, it is possible to start the modelling process to predict the results that are impossible to measure directly. (Winter, 2009)

1.3.1 Synthesis of the Human Movement

A movement begins with the varying neural drive to the muscles which leads to a variation in the recruitment's levels of agonist and antagonist muscles. Then, the summation of all muscle forces actuating at each joint generates a moment that varies in time. This variation will cause acceleration or deceleration of the adjacent segments directing to a displacement. (Winter, 2009)

The inverse problem mentioned before enables the estimation of internal reaction forces and moments (originated in the joint) by combining the kinematic measures with the measured external forces. With the outcome measures and an estimated model, it is possible to predict the forces that caused the movement. By doing this, it is possible to model this approach allowing a forward solution. (Winter, 2009)

Nevertheless, the forward solution has substantial constrains compared to the inverse solution. For the forward solution, it is necessary to model and validate the entire body before starting. Evidently, this approach is easier when there is a pre validated model ready to use. (Winter, 2009)

A joint acts upon two adjacent segments causing reaction forces on segments further away from the origin. Thus, the acceleration of all body segments can be affected by one origin point. If the model have errors, the prediction will also present errors that were accumulated with time. (Winter, 2009)

Forward solution models come with assumptions and constrains, some of them can be (Winter, 2009):

- No kinematic constrains whatsoever;

- The model must be allowed to fall over, jump, or collapse as dictated by the motor inputs;
- The only inputs to the model are externally applied forces and internally generated muscle forces or moments;
- The model must incorporate all important degrees of freedom and constraints;
- External reaction forces must be calculated.

In order for the validity of the model be assessed, there is a necessary but not sufficient condition that can be evaluated. It compels for an inverse solution in order to calculate the moments at each of the joints in every essential plane. A forward solution should be successfully obtained with the assistance of the motor patterns as inputs and the measured initial conditions, which should reproduce the kinematics measured originally. In case the model does not pass this test, it will result in an inaccurate set of motor patterns based on an incorrect biomechanical model. (Winter, 2009)

It is common to recur to the link-segment model to describe the human locomotion (Winter, 2009). The link-segment model is used in the inverse dynamics study, it represents the mechanical characteristics of coupled segments. Considering the kinematics of the distinct parts, this dynamic will derivate the minimum forces and moments that causes movement. From the external forces and limbs motion measurements, the inverse dynamics computes the internal moments and forces, respecting a collection of assumptions (Nicholas et al., 1998).

Because of the complexity of the movement and the model, it was common to either make oversimplifications, or the simulation was done in a brief period movement. This oversimplifications would normally result an inaccurate model that produced incorrect results. This is a problem that used to occur with complex movements studies, simple motions were able to be modelled correctly. (Winter, 2009)

Unfortunately, this accumulating errors are a forward solution characteristic. Therefore, sometimes some of the constraints must be violated in the forward solution. (Winter, 2009)

Other successful attempt to model the movement is the Mass-Spring-Damper-System model. The muscle is normally described as a second order model: the muscle or articulation as a mass (m), the tendons behaviour as springs (k), the damper symbolizes the visco-elastic term (c). The illustration of this model can be seen in Figure 1.12. (Winter, 2009)

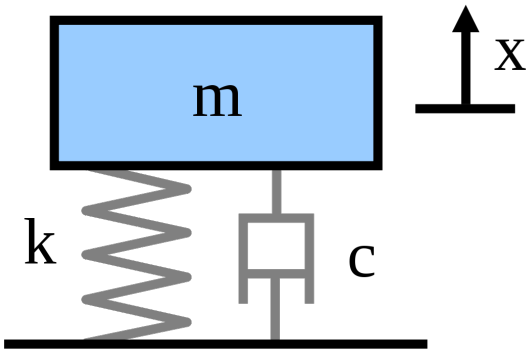

Figure 1.12: Mass-Spring-Damper Model illustration: m is the mass term, k is the viscoelastic term and c is the damper term.

1.4 Kinesiological Electromyography

The information obtained by performing an electromyography (EMG) is concerning the final control signal of each muscle, and it can be considered the primary input signal of the muscular system. The information received allows the identification of the muscles responsible for generating movement. EMG also offers information about diverse types of muscle fibres recruit and the muscle fatigue condition. (Winter, 2009)

The electromyogram is produced as a result of muscle contractions, and its magnitude rises as tension does. The speed at which the muscle contracts or relaxes, the pace at which tension accumulates, exhaustion, and reflex activity are just a few of the many factors that might impact the signal at any moment. (Winter, 2009)

It is crucial to understand that muscle tissue transmits electrical potentials somewhat similarly to how axons do so when sending action potentials. A motor unit action potential (m.u.a.p.) is the name given to this electrical signal produced in the muscle fibres as a result of the recruitment of motor units. The algebraic total of all m.u.a.p.s being conveyed along the muscle fibres at that moment is recorded by electrodes inserted on the surface of a muscle or inside the muscular tissue (indwelling electrodes). As smaller m.u.a.p will be produced by motor units' distance from the electrode site than by motor units of an equivalent size close to the electrode. (Winter, 2009)

There may be a variable number of motor units for a given muscle, and each one is regulated by a motor neuron through unique synaptic connections known as motor end plates. A series of electrochemical events are started when an action potential that was conveyed down the motoneuron (also known as the last common pathway) reaches the motor end plate. A quantum of acetylcholine is released, crosses the synaptic gap, and results in the postsynaptic membrane becoming depolarized. When the end plate potential reaches a certain threshold, an action potential starts to develop in the muscle fibre membrane next to it. (Winter, 2009)

By spreading the stimulus inward along the transverse tubular system, the m.u.a.p. starts at the Z line of the contractile element (Figure 1.4), and as a results the sarcoplasmic reticulum releases Ca^{2+}. This product diffuses quickly to the actin and myosin contractile filaments, where ATP is digested to create ADP along with heat and mechanical energy (tension). The mechanical energy appears as an impulsive force at the contractile element's cross-bridges. The sarcoplasmic reticulum and transverse tubular system depolarize, causes a depolarization "wave" to move in the direction of the muscle fibres. The repolarization wave is what the electrodes record. (Winter, 2009)

This signal, which is the summation of m.u.a.ps, must be clean and devoid of noise or artefacts. The muscle is not the only place where noise can be produced. It can also come from biological or synthetic sources. Artefacts are false signals produced by the electrodes or the cable system. Additionally, there are movement artefacts that are caused by the wires movement and touching of the electrodes. (Winter, 2009)

Hence, the signal must be amplified in order for it to be valid. A comparison or correlation with other physiological or biomechanical signals can then be made using the processing done after that. Because the raw EMG may not be acceptable for recording or correlation, the EMG must be converted into another processed form. (Winter, 2009)

EMG can be used to observe the relationship between its amplitude and muscle tension (Figure 1.13). It can also be used to enumerate the number of action potentials that happen progressively over time. (Winter, 2009)

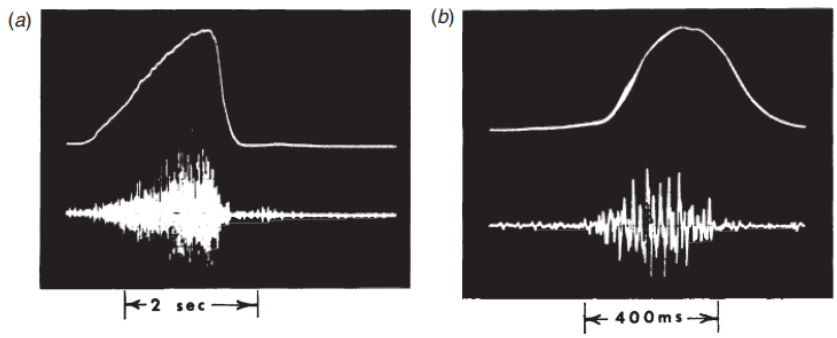

Figure 1.13: EMG and muscle tension were captured on a storage oscilloscope as the bicep's muscles underwent various isometric contractions It takes time for the tension to build up initially, it reaches its peak, and then decreases when the EMG stops. (A) During a slow build-up and quick release. (b) Throughout a brief 400ms contraction. (Winter, 2009)

A muscle must alter in length when under tension in order to perform. Therefore, it is crucial to assess how effectively the EMG can forecast tension in these circumstances. In 1973, Komi observation was that, despite decreasing tension during shortening and increasing tension during eccentric contractions, the EMG amplitude remained mostly constant. These findings support the hypothesis that, in contrast to the tension measured at the tendon, the EMG amplitude represents the state of activation of the contractile element. In 1987 Komi et al. reported that for the same amount of negative work, the EMG amplitude is significantly lower than for the equivalent amount of positive activity. Since negative effort has a somewhat lower metabolic cost than positive labour, if the EMG amplitude is a relative measure of muscle metabolism, this conclusion confirms those experiments. (Winter, 2009)

Muscle fatigue shows its effects when the muscle tissue is unable to provide metabolism for the contractile element due to ischemia or localised depletion of any of the metabolic substrates. In 1973, Vredenbregt and Rau (Nicholas et al., 2009) made the observation that mechanical fatigue represents a drop in tension when the muscle activation, as shown by a constant surface EMG or stimulation rate, is assumed to remain constant. In contrast, to account for a decline in the firing rate of the rest of the units, maintaining a steady tension following the onset of fatigue necessitates a higher motor unit recruitment of new units. These results also suggest that all or some of the motor units are increasing their contraction times while decreasing their peak twitch tensions. These modifications lead to a general reduction in tension. (Winter, 2009)

1.5 Reflexes and Motor Control

The impulses in the spinal cord segment that are almost immediately returned to the muscles, without having a considerable delay for being sent to higher levels of the CNS, provide the fastest feedback loops. These rapid feedback loops in the spinal cord segment are known as reflexes. Reflexes are instantaneous actions potentials that does not require brain interference. They are essential to protect the body from injuries. (Coelho, 2021)

The central pattern generators (CPGs) are controlled in part by reflexes, which also play a significant role in postural and gait stability. The muscle spindles identify the lengthening and communicate it to the spinal cord via *Ia*-afferent neurons. At the spinal cord, α-motoneurons that innervating muscle fibres that contain the muscle spindles and *Ia*-afferent neurons that operate synergistically with the muscle form excitatory monosynaptic connections. In a process known as reciprocal innervation, the *Ia*-afferent neurons also form excitatory connections with interneurons that, in turn, have an inhibitory effect on the α-motoneurons of antagonist muscles. An inhibitory signal is sent to relax antagonist muscles when

agonist muscles contract. (Coelho, 2021)

Reflexes can be categorized by the stimulus that triggers it and the resulting response. In this dissertation, it is only relevant to mention more profoundly the stretch reflex, which has an appropriated section below. Thus, it can be mentioned that there are other types of reflexes, such as the withdrawal reflex, which is a response to noxious stimulus (e.g.: touching a hot surface or accidentally needling the finger) and it entails the rapid body withdrawal from the stimulus source (Derderian et al., 2023). Other example is the crossed extensor reflex, it happens when a withdrawal reflex initiates in one limb, causing it to withdraw from the stimulus, while at the same time, the opposite limb extends to maintain balance and support the body (Eccles et al., 1929). The tendon reflex, also known as the Golgi tendon reflex, begins when the tendon feels tension and as a protective response it prevents the exertion of an excessive force on the muscle, inhibiting the muscle contraction leading it to a relaxation mode (Lyle et al., 2019). These were just a few examples of reflexes in the human body.

1.5.1 Muscle Proprioceptors

There are diverse types of sensory receptors, each of them reply to a distinct set of stimulus: light, sound, odor, heat, touch, pain, acceleration, etc. Exteroceptors are receptors that conduct to a conscious sensation. Proprioceptors are receptors that conduct to a non-conscious sensation, they have mainly motor functions. (McMahon, 1984)

Sensory receptors in the skin and subcutaneous tissues are responsible for many reflex motions. Sensory receptors also exist in and around joints, essentially in the ligaments that stabilize it. These kind of receptors answer to changes in the joint angle. Because some reflexes, such as the withdrawal reflex, mentioned before, are immediately reversed when a limb is fully extended as opposed to slightly flexed, it is believed that the joint receptors play a significant role in locomotion. (McMahon, 1984)

Golgi tendon organs and stretch receptors (muscle spindles) are the muscle associated proprioceptors. As it was said before, these receptors alter and sometimes even control many aspects of muscle behaviour. (McMahon, 1984)

1.5.2 The Stretch Reflex

When an outside agent activates a muscle, it feels like an additional effort is made in order for it to get back to its original length, since the contraction is more powerful than it would normally be from a voluntary contraction. Thus, there is an unexpected lengthening of the muscle which causes the muscle to contract to keep its length constant. This is called the stretch reflex or the myotatic reflex. (Coelho, 2021; McMahon, 1984)

What happens in the stretch reflex is that since the spindle organs are mechanically parallel to the muscle, they are stretched by the same relative amount as the muscle as a whole. The type *Ia* afferents perceive the stretch of the spindles, which increases the firing rate of the motoneurons that regulate muscle force. Hence, the muscle spindles notice the lengthening and communicate this information to the spinal cord via *Ia* afferent neurons. At the spinal cord, *Ia* afferent neurons transmit this information to α-motoneurons that innervate muscle fibres containing muscle spindles. This is what happens when a doctor strikes the patellar tendon above the knee. (Coelho, 2021; McMahon, 1984)

The stretch reflex happens in only one synapse, which means it happens rapidly and it has a monosynaptic reflex circuit. This synapse occurs between the *Ia* afferent axon and the motor neuron. Polysynaptic reflex circuits demand target motor neurons and one or more spinal cord interneurons. (McMahon, 1984)

For example, the crossed extension reflex, mentioned before, has a polysynaptic reflex circuit. Consequentially, it has a long latency period in comparison to the stretch reflex because the synapses between many interneurons must be traversed by the incoming information before arriving at the proper motor neurons on both sides of the spinal cord. (McMahon, 1984)

The stretch reflex has the ability to automatically adjust muscle tone to counteract the effects of external disturbances to a muscle's length. Nonetheless, if voluntary movement were simply prompted by a change in α-motor activity from higher brain centres, the stretch reflex would also make locomotion challenging. For example, an increase in α-motoneuron activity would force the extrafusal muscle fibres to contract, shortening the muscle and causing the spindles intrafusal fibres to relax. When the *1a* afferent activity decreased, the motor activity would also decrease, cutting off the muscular force, triggering the stretch reflex. If both α and γ activity increases simultaneously (coactivation) to the signal muscle commands, the issue is avoided since a contraction of the major muscle mass is not accompanied by a slackening of the spindles. (McMahon, 1984)

1.5.2.1 Reflex Stiffness

The monosynaptic reflex arc, which contains the spindle organ, is traditionally used to explain the stretch reflex. However, recent research suggests that tendon organs may also play a role in the regulation of muscle reflex stiffness. (McMahon, 1984)

The diagram present in (Figure 1.14), was suggested by Nichols and Houk (Houk, 1979) to illustrate the regulation of stiffness in the stretch reflex. Because of the way that the stretch reflex appears to be fixed at a value that is nearly constant, neither muscle force nor muscle length should be thought of as controlled quantities. Instead, it is their ratio, the change in force per change in length. In this approach, it has been proposed that skeletal muscles can exhibit a constant stiffness to the outside world despite having significantly variable intrinsic mechanical properties as a result of functioning on various length-tension curve segments. When muscles contract on flat or falling stretches of their tension-length curves, the risk of instability and collapse that might otherwise be possible may be reduced by the consistent stiffness. (McMahon, 1984)

Additionally, the stretch reflex automatically makes up for tired muscles. The α-motoneuron activity of the muscle is automatically increased (recruiting additional motor units) when fatigue renders, the initial number of motor units is incapable of delivering the necessary force increase for a given length increase. This is because the increase in force accompanying an increase in length is fixed by the reflex. (McMahon, 1984)

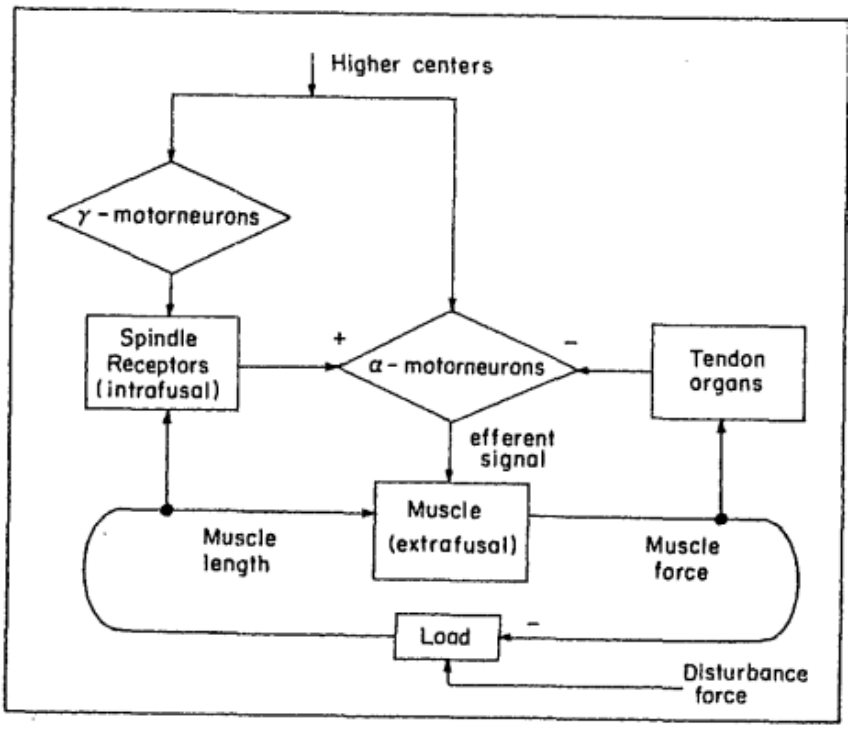

Figure 1.14: Diagrammatic illustration of the stretch reflex's stiffness regulation. Movement causes the signal both $\alpha$and motor neurons to fire more often all at once, keeping the length of the extrafusal and intrafusal muscle fibres about constant. Afferent input from both spindle receptors and tendon organs influences the shift in the efferent signal to the muscle when a disturbance force occurs. When a muscle is stretched, the spindles create an increase in activity, but when a muscle is forced harder, the tendon organs cause a decrease in activity. In order to control the reflex stiffness in response to external disturbances, the two must be in balance. Based on Houk (1979), modified. (McMahon, 1984)

In 1978 and 1981 Hoffer and Andreassen (Hoffer et al., 1981) performed an experiment that supported the hypothesis that muscle stiffness is controlled quantity in the stretch reflex. This experiment was done by holding firmly decerebrated cats and measuring force increment in as the soleus muscle was forcibly lengthened by a small stretch. As it can be seen in (Figure 1.15), reflex stiffness was found to grow with force at low force levels, but quickly hit a stage, so that stiffness was practically constant at moderate and high force levels when the experiment was repeated over a wide range of various initial levels of force. The stiffness was shown to be lower in the isolated muscle at all force levels and highly dependent on the force when the muscle was isolated by severing the soleus nerve and different force levels were created by stimulating the cut nerve end over a range of stable frequencies. Concluding that the effective reflex stiffness is significantly higher than the stiffness of the muscle alone when the stretch reflex is intact. In addition, the reflex compensates for the variable stiffness of the muscle by maintaining a relatively constant stiffness property at moderate and high force levels. (McMahon, 1984)

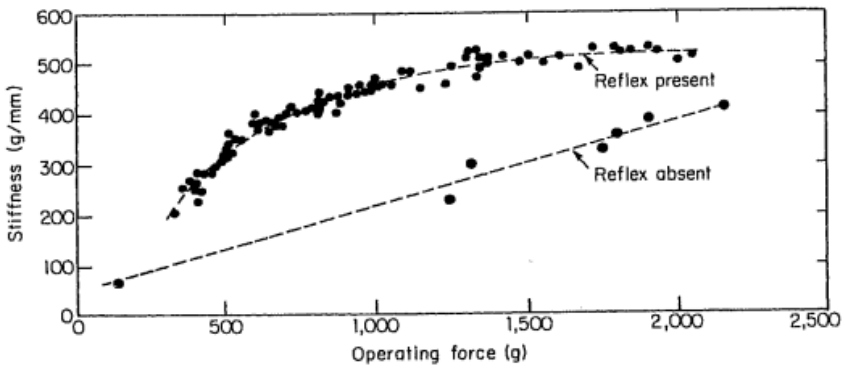

Figure 1.15: In the cat soleus, force versus muscle stiffness. When the stretch reflex is intact, the stiffness, measured as the increase in force for a mild stretch, is a drastically rising function of force at the low end of the force range but nearly constant at moderate and high forces. In contrast, when the reflex is eliminated by severing the efferent soleus nerve and electronically stimulating the severed end at 10–50 Hz to maintain tension, the isolated muscle displays a lower stiffness that is a continuously rising function of force (lower curve). (McMahon, 1984)

In 1979, Greene and McMahon (McMahon, 1984) performed another experiment that also supported the hypothesis that muscle stiffness is controlled quantity in the stretch reflex. This experiment consisted of a series of male volunteers carrying weights on their shoulders and standing on a springboard with their knees flexed at a constant angle. The weights on their shoulders had the intuit to subject the legs antigravity muscle to a steady force levels scope as the subject performed low-amplitude up and down bouncing movements. It was found that, as long as the springboard was waved at a specific frequency, even a tiny effort like waving a hand or an elbow caused resonant bouncing deflections of several inches amplitude. Waving at other frequencies had minimal impact. As a result, the "tuning curve" for the resonant system composed by the weights' mass, the man's mass, his stiffness, and the mass and stiffness of the board (very small). Given that all other parameters were known, and the system is assumed to be a second order coupled linear system, the stiffness of the man could be determined from the measured (lowest mode) natural frequency. It was shown that as the weight on his shoulder climbed from zero to more than twice his body weight, his stiffness increased by less than 10%. The result is that the legs muscles respond to a wide range of moderate and strong stimuli like a linear spring with roughly constant stiffness.

In summary, the ankle reflex is closely related to the system's stiffness because it is a reflexive response that involves the sensory detection of muscle stretch (which is, once again, related to stiffness) and a subsequent motor response to regulate muscle length and prevent overstretching. Variations in muscle stiffness can affect the strength and characteristics of the ankle reflex, making it an important clinical tool for assessing neuromuscular function.

1.5.3 Reflex Identification: EMG

The most used method for gathering data on reflex activity is electromyography. A variety of studies, Crago et al. in 1976 (P. E. Crago et al., 1976), Lacquaniti et al. in 1982 (Lacquaniti et al., 1982) and Carter et al. in 1990 and 1993 (Carter, P. Crago, and Keith, 1990; Carter, P. Crago, and Gorman, 1993), associated step-like disturbances to a considerable EMG activity, this can be connected to the stretch reflex mechanisms. Nevertheless, it is important to consider that EMG is a combination of reflex and other muscular activities, such as voluntary movements as seen in 1976 by Crago et al. This means that using only EMG as method to measure the reflex activity is complicated. (Helm et al., 2002)

In 1993, Toft and Skinkjaer (Toft and Sinkjaer, 1993) introduced the use of H-reflexes to measure the

reflex activity. This consist in a nerve stimulation. The resulting EMG, both direct and indirect responses, are assumed to indicate the loop gain of the reflexive pathways. Nonetheless, numerous afferent routes, some with excitatory connections and some with inhibitory connections, are expected to project on the α-motoneurons, from Golgi tendon organs and muscle spindles. Numerous of these routes are stimulated with the nerve stimulation, and the EMG response that results is a summation of all of the stimulated afferent pathways. Which means that the results from the H-reflex response is unclear. (Helm et al., 2002)

In 1995, Stein and Kearney (Stein et al., 1995) studied the ankle joint to identify different reflex torque contributions for several types of disturbances. They used other technique to measure the reflex activity by determining stiffness and viscosity changes to calculate the reflexive contribution. Other researchers suppressed the reflex system using ischaemia, Allum and Mauritz in 1984 (Allum et al., 1984), Sinkjaer and Hayashi in 1989 (Sinkjaer et al., 1989), and Sinkjaer et al. in 1988, and electrical stimulation, Sinkjaer et al. in 1988 (Toft, Sinkjaer, et al., 1988).Or both of these methods were used and then the reflex contributions were assessed from data with and without the suppressing agent. Yet, one cannot be certain that the stretch reflex is the sole one impacted by ischaemia or to what degree. Most likely, the muscle's motor control is also impacted. Because the recruitment order is different and not all motor units are activated, electrical stimulation does not stimulate a muscle in the same way that natural stimulation does. It is challenging to solely credit reflex contributions for the differences between electrical and natural stimulus. (Helm et al., 2002)

It can be concluded that using EMG as the only method to identify and quantify the reflex dynamics is not the best alternative (Helm et al., 2002). In this study in particular, the EMG will be used to ascertain the presence of muscle contraction.

1.6 Biomechanics of the ankle: control and function

The interaction between the lower limb and the environment is controlled by the ankle joint complex. This complex is made by 26-foot-bones and by the two long lower legs bones, the tibia and the fibula. The lower limb stabilizers and propulsors are the numerous ligaments connecting the bones, and various muscles and tendons. (Coelho, 2021)

The main ankle joint actuating muscles are the Tibialis Anterior, Gastrocnemius, Soleus and Peroneus Longus. The Tibialis Anterior is the principal dorsiflexor muscle, which means that it allows the foot to lift and pull in the leg direction, positive rotation around the ankle, and it also promotes foot inversion as well. The Gastrocnemius and the Soleus together enable energized plantarflexion. The Soleus alone maintains posture steadiness. The Gastrocnemius while promoting energized ankle plantarflexion it also promotes knee flexion during propulsion. The Peroneus Longus enables foot eversion. It must be kept in mind that multiple other muscles contribute to the ankle joint function, only a few were referenced. (Mendez-Rebolledo et al., 2021)

The muscles are innervated by nerves. Some of them include the superficial and deep peroneal (fibular) nerves of the common peroneal (fibular) nerve, which originates from the lumbar spine (L4, L5) and the sacral area (S1, S2) of the spine. The anterior lower leg muscles, including the Tibialis Anterior, are supplied by the deep peroneal nerve. The lateral lower leg muscles, including Peroneus Longus, are innervated by the superficial peroneal nerve. The Soleus and Gastrocnemius are both innervated by the tibial nerve, which arises from L4, L5, S1, S2, and S3. (Coelho, 2021)

Joints contraction enables the muscles to activate. For example, it is important to contract the Tibialis Anterior, a dorsiflexor muscle, as well as to block plantarflexion muscles in order to enhance dorsiflexion.

Agonists act on the muscles direction, while antagonists act against the muscles direction. The CNS's neuromotor control allows for the simultaneous contraction of the agonist muscles and inhibition of the antagonist muscles. Co-contraction, or the simultaneous contraction of both agonist and antagonist muscles, is another option that can be used to slow down or stabilise movement around a joint. (Coelho, 2021)

As such, to promote dorsiflexion, for instance, it is necessary to contract the Tibialis Anterior, a dorsiflexor muscle, but also to inhibit plantarflexion muscles. The muscles that act on the direction of joint movement are called agonists, while the ones that act against are named antagonists. This simultaneous contraction of the agonist muscles and inhibition of antagonist muscles is achieved through the neuromotor control by the CNS, as explained in the next section. It is also possible to simultaneously contract both agonist and antagonist muscles, or co-contraction, which is achieved when there is the need to decelerate or stabilize movement about a joint. (Coelho, 2021)

1.7 Motivation

The human neuromuscular system is a remarkable and intricate network of sensory receptors, neurons, and muscles that work in unison to enable precise motor control and reflex responses, as it could be seen from the previous sections. Among the various reflexes that play a crucial role in maintaining postural stability and facilitating coordinated movement, the ankle reflex stands out as a fundamental component. Understanding the dynamics of the ankle reflex is not only a subject of scientific curiosity but also holds significant implications for clinical applications, sports science, and rehabilitation.

The ankle reflex serves as a vital protective mechanism, helping humans maintain balance and avoid injury during sudden perturbations to the ankle joint. However, despite its fundamental importance, the precise mechanisms governing the ankle reflex's behavior under varying perturbation conditions remain a subject of ongoing investigation.

This dissertation aims to explore a specific aspect of ankle reflex dynamics that has garnered limited attention in the existing body of research – the influence of different frequency bandwidth perturbations on the ankle reflex response. The hypothesis posits that altering the frequency characteristics of the stimulus applied to perturb the ankle system will lead to measurable changes in the dynamics of the ankle reflex.

It is believed that variations in the frequency of the perturbation stimulus will affect the neuromuscular system's response. As a consequence, the observation of differences in electromyography data and reflex parameters when subjecting individuals to perturbations with distinct frequency bandwidths is anticipated .

This research seeks to achieve several key objectives. It aims to investigate the influence of different frequency bands in stimuli on the gain of the ankle reflex response. Additionally, it strives to examine whether variations in stimulus frequency influence motor unit recruitment patterns and muscle activation during the ankle reflex, which can be quantified by the electromyography amplitude. These objectives collectively contribute to a comprehensive understanding of how changes in stimulus frequency affect the dynamics of the ankle reflex.

This research not only delves into the basic science of neuromuscular control but also carries practical significance. Understanding how the ankle reflex responds to different frequency bandwidths can have implications in fields such as sports science, where optimizing athletes' balance and stability is paramount. Additionally, in the realm of clinical rehabilitation, this knowledge may inform the development of tailored interventions for patients recovering from ankle-related injuries or neurological conditions affecting reflexes. Besides, all of the findings can be applied to the design of more realistic prosthetics for amputees patients.

It is expected that these findings will contribute to a deeper understanding of the neuromuscular system's adaptability and provide valuable insights for both scientific and practical applications.

The main question to this dissertation is: "How does varying the frequency of stimuli affecting the ankle system impact the dynamics of the ankle reflex?". It is hoped that this question is well answered and this dissertation objectives are well accomplished.

Chapter 2

State of the Art

In the realm of biomechanics and neural control, ankle reflex dynamics represent a key convergence of physiology, neuroscience, and motor control. This chapter serves as a comprehensive review of existing research, synthesizing important findings, methodologies, and theoretical frameworks that have shaped the understanding of ankle reflexes.

The anatomical and physiological aspects of the ankle, neural pathways governing reflex responses, and the factors influencing these responses are explored. Additionally, clinical applications, neurorehabilitation, and implications for motor disorders are explored. This chapter lays the foundation for this study on the influence of frequency on ankle reflexes, contributing to this dynamic field of research.

This dissertation had an limited amount of papers to resort. Mainly because this kind of research have not been done that frequently. Kearney was the pioneer starting his research in the 80s. Most of the existing studies about the ankle's reflex dynamics are not from recent studies.

In 1984, Kearney et al. studied the stretch reflexes in the ankle flexor, also known as the tibialis anterior muscle. Subjects maintained a tonic contraction of the tibialis anterior muscle while perturbations were applied to the ankle. To reduce the impact of nonlinearities and eliminate contributions from voluntary mechanisms, small amplitude, stochastic perturbations of ankle position were applied. An method created in their 1982 research was then used to establish the linear dynamic impulse response function relation between ankle velocity (obtained by numerically differentiating the position record) and the tibialis anterior EMG. According to this study's findings, a linear dynamic model accurately captures the stretch reflexes that stochastic perturbations at a constant tonic activity level elicit in the human tibialis anterior. (Kearney and Hunter, 1984)

In 1997, Kearney et al. continued his work by using perturbations that were created to offer a wide-bandwidth input with a low average velocity to explore the dynamic stiffness at the human ankle. The overall stiffness was divided into intrinsic and reflex components using a parallel-cascade, nonlinear system identification technique. A linear second order system described intrinsic stiffness. Reflex stiffness dynamics included a delay, a single rate-sensitive element, and low-pass dynamics, making them more complicated. (Kearney, Stein, et al., 1997)

In previous studies it was concluded that stretch reflexes are inhibited by high frequency, vibratory inputs, both by blocking the firing of muscle spindle afferents and by presynaptic blocking of transmission from the afferents to the motoneurons. In light of these discoveries, Kearney etc. al set out to determine how the stretch reflex affects joint mechanics using experimental and analytical techniques designed to account for the nonlinear, velocity-dependent nature of the stretch reflex. In order to do this, the position perturbations utilised were chosen to have the low average velocity necessary to prevent suppressing the reflex reaction, as well as the wide bandwidth necessary to detect the dynamics. Additionally, approaches

that were specifically tailored to the nonlinear behaviour of stretch reflexes were used for identification. (Kearney, Stein, et al., 1997)

The findings of this work show that these experimental and analysis methodologies can be used to accurately identify the dynamics of the intrinsic and reflex contributions to joint mechanics. Also, a small frequency range (5–10 Hz) was shown to have strong reflex torques, with other frequencies seeing a dominance of intrinsic torques. Gain and reflex stiffness dynamics changed significantly with the perturbation's parameters. Under certain circumstances, torques produced by reflex mechanisms were of a similar magnitude to those produced by intrinsic processes. In this study they highlighted how difficult it is to separate the mechanical effects of reflex action from those resulting from the inherent characteristics of the joint and muscle. They also tried to characterize the stretch reflex dynamics by modulating EMG activity. Nonetheless, they were not very successful. The overall conclusion of this study was that the reflex mechanisms may play a considerable role in the mechanical behaviour of the ankle, but the exact nature of that role will be greatly influenced by the functional circumstances. (Kearney, Stein, et al., 1997)

In 2002, van der Helm et al. proposed a study to "quantify reflexive feedback gains from the mechanical behavior of the human arm during posture maintenance is proposed" (Helm et al., 2002). The subjects were told to reduce the deviation brought on by random force disturbances as they were continuously applied at the hand. Frequency response functions were used to conduct a frequency domain analysis of the results. The mechanical admittance and reflexive impedance, which express the dynamic relationship between position and muscle activity (measured using electromyography, or EMG), were both tested. Equally as it happened in this dissertation experimental work, the input is the disturbance signal and the output is the hand position deviations. The experiment functioned in closed-loop conditions. Subjects had two tasks: stiff and slack. In the stiff task the subject was asked to "minimize displacements" and in the slack task the subject was asked to "relax arm muscles and do not react to the disturbances". van der Helm et al. considered that the stiff task could be used to describe both intrinsic and reflexive dynamics and the slack task to describe the intrinsic dynamics alone. They used narrow band frequency ranges for the stiff task only and wide band for both of the tasks. (Helm et al., 2002)

van der Helm et al. used a mass-spring-damper system to describe the visco-elasticity of the system. The reflex dynamics are represented by the reflexive position and velocity feedback gains, which was estimated from the estimated frequency response functions. They considered the reflex component negligible for the wide band conditions. For the narrow band conditions they assumed that the intrinsic contribution was constant, the same as the contribution for the wide band conditions. To estimate intrinsic parameters in the wide band conditions, the intrinsic model was fitted on the estimated frequency response function and reflexive parameters were set to zero. For the narrow band conditions intrinsic parameters were fixed and the reflexive parameters were estimated. The Variance Accounted For (VAF) percentage was calculated to validate the models and values were normally greater than 85%. van der Helm et al. concluded that the NB estimated frequency response functions show clear differences to the WB conditions and the results indicate that the intrinsic dynamics are constant (this was also supported by EMG recordings) and the reflexive dynamics decrease and increase depending on the input bandwidth. (Helm et al., 2002)

Overall, van der Helm et al.'s findings suggest that it is probable that high reflex gains are most efficient at low frequencies. (Helm et al., 2002)

In 2008, Schouten et al. performed a study to "identify the functional contribution of reflexes to human motor control during posture maintenance" (Schouten et al., 2008b). This study was a continuation of Helm et al., 2002. They supported the findings in Kearney, Stein, et al., 1997 that the frequency range

between 5 and 10 Hz was where reflex mechanisms were most significant, and the amplitude of the reflex torque was of the same order of magnitude to that of intrinsic processes. From previous study results, Schouten et. al. also concluded that by including EMG to measure muscle contraction, procedures could show improvements. The goal of asking the subjects to "minimize displacements" was so that the muscle activation due to reflexes would be small. Since EMG normally has significant noise, these small variations are not easily identified. In Schouten et al., 2008b, the goal was to "redesign the continuous signals used as force disturbances such that the dynamic relation between position and EMG can be estimated reliably in addition to the mechanical admittance during active postural control tasks" (Schouten et al., 2008b).

Schouten et al. created optimized inputs signals. These signals were created with a certain frequency content and with a reduced the crest factor (the signal's compression or compactness). Similarly to their previous study, they opt to use closed-loop conditions to estimate the frequency response functions of the mechanical admittance and reflexive impedance. They considered that the mechanical admittance involved both the visco-elastic and reflexive feedback. However, the reflexive impedance was a result of reflexes mechanism only. In this papper they successfully estimated the mechanical and reflexive admittance using the optimally designed input signal. Previous studies always had to rely on estimated mechanical admittance with fixed parameters from additional experiments. This paper resulted in more information about the underlying neuromuscular system that are of interest and that will allow precise measurement of neuromuscular properties.(Schouten et al., 2008b)

The overall conclusion for the papers mentioned is that there is a reflex gain augmentation for lower frequencies, and the opposite occur for a higher frequency bandwidth. In the [5-10]Hz bandwidth, reflex torque gains are predominant. All of these studies also agree on the reason behind this conclusion. Muscle spindles resonance frequency must be framed in the low frequency range. When low frequency stimuli are applied, afferent muscle spindles amplify its synchronous rate (also concluded by Kearney, Stein, et al., 1997) which leads to the augmentation of the synchrony of motor units firing as well. When the stimuli rises its frequency, the synchronized firing rate starts to decrease.

It is also important to highlight that most of the studies mentioned and others, such as Lee et al., 2014, show that the ankle joint's response frequency function can be described as a second-order-system. In Caires, 2022, Caires had the same result for all of the four subjects of his studies. Caires concluded that, a second order system with a rotational inertial, visco-elastic properties and stiffness represents nicely the relaxed ankle dynamics.

As it could be seen in this chapter, most of the studies in this area have the limb under contraction during the experiments. Nevertheless, as it will be seen later on this dissertation, there were no muscle contraction to contradict the perturbations in this study.

Chapter 3

Methods

In this chapter, it is provided a clear and systematic account of the procedures and techniques employed in this study investigating the influence of frequency on ankle reflex dynamics. A robust methodology is essential for ensuring the rigor and reliability of the research findings. The experimental design, data collection methods, and analytical approaches used to address this research objectives will be outlined.

The tests were carried out on four healthy subjects. Subject 2 and 3 are females while subject 1 and 4 are males. Subject 2 performed the trial twice in two different dates. Resulting in five trials in total. All of the subjects have similar age but different heights and weights. Through the experiments subjects stood in an structure while stimuli were applied. They were told to **relax** and to **not counteract the perturbations**.

The *apparatus* and, consequently, communication network used were analogous to the one used by Vera Dias in Dias, 2022 and by Nivaldo Caires in Caires, 2022. However, in Dias, 2022 and in Caires, 2022, EMG was not used. The *apparatus* development was not part of this dissertation' work.

3.1 *Apparatus*

The ankle was provided with perturbations driven by a Housed Direct Drive Rotary (DDR) Motor (Figure 3.1). A conventional servo system frequently contains a mechanical gearbox to connect the motor and the load using gears, gearboxes, belts/pulleys or cams. The mechanical design of DDR motors directly links the load to the motor with no need for a gearbox. This design allows for an increased accuracy which results in a higher product quality. The DDR advantages are:

- It allows for a higher bandwidth to be implemented;
- It has improved reliability and zero maintenance;
- Fewer parts are needed for the assembly;
- It has reduced audible noise;
- It does not require inertia matching.

Figure 3.1: Kollmorgen DDR Motor. (*Housed Direct Drive Rotary (DDR) Motors: Selection Guide* 2017)

The Advanced Kollmorgen Drive (AKD), which features an analogue input for the current reference, feeds the motor with current. Throughout the motor position feedback, the AKD emulates and outputs an incremental sine-encoder. The software used by the AKD is the Workbench. (Dias, 2022)

In Figure 3.2 it is possible to observe the structure used to cause perturbations. There it can be observed the motor (1), aluminium structures (2), a load cell (3), a green strap (4), a circular rubber (5) and weights (6). The aluminium structures attaches the foot to the motor and secure the whole *apparatus*. The foot is secured to the load cell by the green strap. It fixes the feet to a 3D printed plate that is on top of the load cell. The foot rests in such a way that the ankle dorsiflexion-plantarflexion (sagittal) rotation axis is aligned with the motor rotation axis. When perturbations are applied, the resultant movement is comparable to a pendulum. The load cell then measures the forces applied on the foot. The motor is secured by an aluminium structure with rubber legs, minimising any kind of vibrations. The motor also has a gravity and friction compensation and an impedance controller.

The ankle impedance identification experiment was performed on four healthy individuals. These volunteered to participate in this study with prior consent. The left foot of the subjects was strapped, and the experimental procedure was followed as mentioned before. Care was taken to make the foot placement as correct as possible, aligning the virtual sagittal rotation axis of the ankle with the motor rotation axis.

In the initial stages of each trial, the subjects were asked to stay in a dorsiflexion position until the controller were initiated. This was done in order for the structure to be at angle zero at the beginning of each experiment. Once the controller were initiated, the subject would go into a neutral and relaxed position.

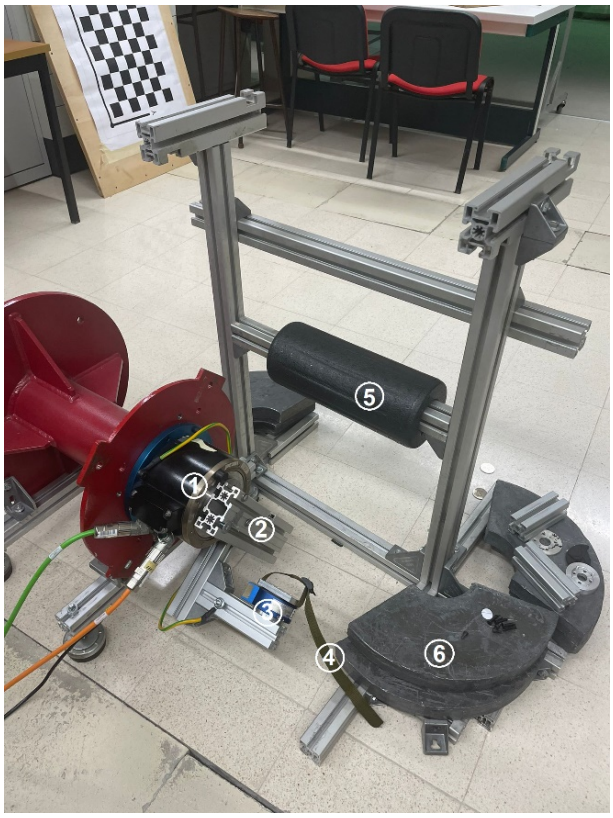

Figure 3.2: The *apparatus*: (1) motor; (2) aluminium structure; (3) load cell; (4) strap; (5) circular rubber; (6) weights.

The subjects support themselves by placing their left knee in the circular rubber area and their arms are leaning into the big aluminium structure that holds the circular rubber (Figure 3.3 and Figure 3.8). The knee must be kept unmovable. There are six weights (25kg each) to help the whole structure to stay unaffected alongside with discs that are placed below the whole structure preventing vibrations.

The subjects positioning can be observed in Figure 3.3.

Figure 3.3: Subject positioning: (1) lateral view (2) posterior view.

This system also has a safety mechanisms in order for the experiment to be safe: an emergency

button held by the experiment responsible; a mechanical restriction on the motor shell that also controls the displacement of the rotor; SIMULINK's rotor displacement and torque control.

3.1.1 Communication Network

For the system connection there is a communication network. This system is represented in Figure 3.4. A grid and a 24V power source provide current to the AKD, which then sends it to the motor. Then, an emulated encoder signal (θ) along with an analogue velocity signal ($\dot{\theta}$) are transmitted to a Quanser Q8 Board (QQB) installed within the target computer. The target computer transmits the received data to the host computer using a TCP/IP protocol. This protocol consists of the compilation of the responsive control algorithm into a C language. This allows its transmission to the x86-based system running MATLAB 2014 and the real-time kernel on the target computer, which happens via the SIMULINK real-time package present in the host computer.

Consequently, control inputs are transmitted from the host computer to the target computer. The QQB converts this data into an analogue signal for the AKD. The current constant, K_i, converts this signal into current, which is transmitted to the motor where it is converted into torque by K_{torque}, the motor torque constant. The JR3 load cell gathers the torque data, transmits it to the JR3 board, and then inserts it into the target computer. The motor transmits feedback to the AKD encoder.

The MATLAB version used was the one able to support the QQB blocks. These blocks are used to enable the communication between the Workbench software and other computer through a TCP/IP protocol. Setting the encoder resolution, the AKD inputs and outputs, the filters, and allowing current to flow to the motor are essential.

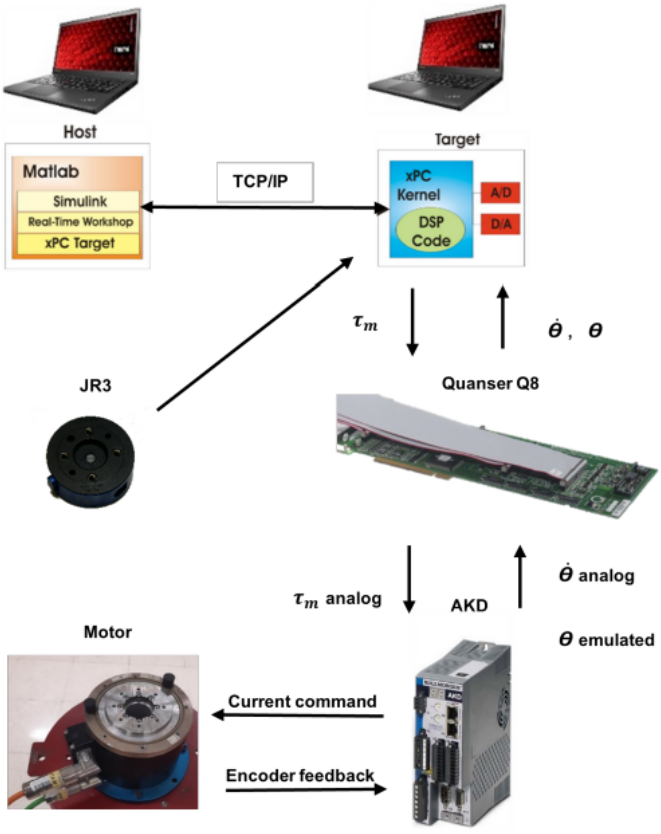

Figure 3.4: Schematic representation of the communication network. (Caires, 2022)

There is a filtering process applied to some signals. Figure 3.6 displays the sampling frequencies that were initially established for the primary components of the communication devices. Figure 3.5 lists the cut-off frequencies that were settled initially to each filter. The filtered signals are: the SIMULINK torque product; the AKD analogue input, filtered with the current analogue command; the designated output ($\dot{\theta}$ ou i), filtered in the AKD at the analogue output, from the AKD to the QQB; and the torque feedback, which is controlled by the SIMULINK JR3 block.

Signals	Cut-off frequency [Hz]
Torque derivative	100
AKD analog input	200
AKD analog output	1000
Torque measurements	500

Figure 3.5: Cut-off frequencies used on each filtered signal. (Dias, 2022)

Instruments	Sampling frequency [kHz]
Motor current controller	10
AKD input (τ_m)	40
AKD output ($\dot{\theta}$)	4
JR3 sensor	8
Controller in Targuet Computer	2
QQB (A/D)	100

Figure 3.6: Initially established frequencies for the primary components of the communication devices. (Dias, 2022)

3.1.2 EMG

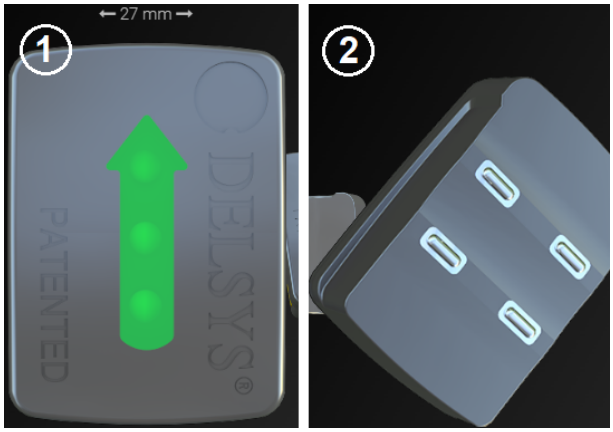

Figure 3.7: Trigno Avanti Sensor: (1) anterior view; (2) posterior view. (Delsys, 2023)

This experiment also counted with EMG assistance. The EMG equipment used was Trigno Research System, an intuitive device from Delsys. It works throughout a software called Trigno Discover. This device is a ”Smart Module for Wireless Physiological Monitoring” (Delsys, 2023). Two Trigno Avanti Sensors (Figure 3.7) were used as wireless electrodes. One of them was placed on the gastrocnemius muscle (agonist muscle) [18] and the other one was placed on the tibialis anterior muscle (antagonist muscle) (Kearney and Hunter, 1984) as it can be seen in Figure 3.9 and Figure 3.8. The placements were

done by the help of an appropriate double sided adhesive tape. This tape adheres to the sensor's posterior part (Figure 3.7.2) so that the electrode can be placed on top of the muscle. The placement must have the arrow presented in Figure 3.7.1 pointing upwards.

The Trigno Discover software allows a real-time EMG streaming. It has multiple collection options: 'EMG Only,' 'EMG & IMU,' 'EMG & Orientation,' 'RMS & IMU,' 'IMU & Orientation' and 'IMU Only'. RMS stands for Root Mean Square and IMU for Inertial Measurement Unit. The data is acquired by the electrodes that send the collected biofeedback to the software via a wireless protocol.

Figure 3.8: Electrodes muscle positioning: (1) Gastrocnemius electrode; (2) Tibialis Anterior electrode.

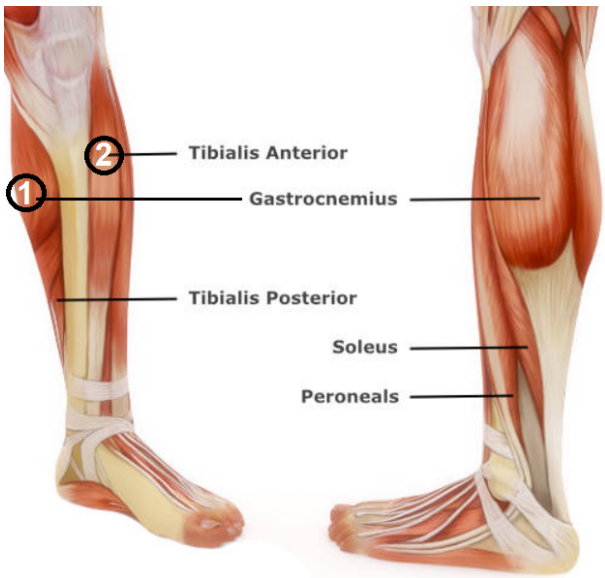

Figure 3.9: Electrodes muscle positioning: (1) Gastrocnemius electrode; (2) Tibialis Anterior electrode. (CENTRAL HEALTH: physiotherapy, 2023)

This system is "specifically designed for a range of human movement studies" (Delsys, 2023). It can stream up to thirty-two sensors of EMG, it has a patented parallel bar technology (inter-electrode distance), it acquires high fidelity data, and it has an on-board IMU. (Delsys, 2023)

The Trigno Avanti Sensor is a superior EMG and IMU technology. It is a compact and durable

device able to acquire precise and insightful measurements and it has an improved Radio Frequency-performance.

EMG data was collected with the intention of assuring the occurrence of muscle contraction. For this research, the Maximum Voluntary Contractio (MVC) test performed initially is crucial to establish baseline data for the studied muscle. It provides a reference point for muscle activity and strength, which can be useful for interpreting the EMG results. The MVC test also allows the data standardization, which helps ensure consistency in the data collection across subjects. This test can also help identify any potential issues or contraindications and is also a great calibration method.

For the gastrocnemius muscle, the subjects provoked this contraction by slightly "jumping" on their toes. For the tibialis anterior muscle, the subjects were asked to singularly step on their heel with their maximum strength. The subjects performed these movements three times. This was done outside the aluminium structure showed before.

3.1.3 Input signal: Sum of Sinusoids

Multisine waves are stochastic signals frequently used both in the research laboratory and in the field. They offer "a periodic, well-characterized waveform that can simulate complex modulated radio frequency (RF) signals" (Carvalho et al., 2008). In Carvalho et al., 2008, they were able to show that the use of multisine signals is very adequate for assessing a nonlinear system activated by real communication signals. (Carvalho et al., 2008)

In the field this type of signals can be used for calibration, wireless communication and device system modelling. In a research scenario, the best signals are those that closely resemble the signal that will be the system's input or those that put the system into a variety of operational states. Although, the Gaussian Noise have both of these advantages, it is very hard to implement due to its continuous spectrum. The sum of sinusoids is simple to produce and to record. Therefore, it is often chosen over Gaussian Noise signals. (Carvalho et al., 2008)

The generated sines throughout a frequency range that was predetermined during signal production originate the sum of sinusoids. This signal can be described by Equation 3.1. (Carvalho et al., 2008)

The input signal is then discriminated in two different trials. One where a narrow frequency bandwidth is used and another where it is used a wide band frequency bandwidth. In simple terms, narrow band systems usually send data at slower speeds, while wide band systems can transmit data much faster. In this case, the frequency range chosen for the narrow band was [0.12 1.8]s. For the wide band was [0.12 20]s. These bandwidths were inspired in the ones used in Helm et al., 2002.

$$x(t) = \sum_{k=1}^{S} A_k \cdot \cos(\omega_k t + \phi_k) \tag{3.1}$$

In the equation, S are the sinusoids signals that are summated in the summatory. The A_k stands for the kth amplitude, the ω_k is the kth frequency and the ϕ_k is the kth phase. The frequency dependency on the order k is a consequence of the following relation $\omega_k = \omega_0 + (k-1)\Delta\omega$, where ω_0 is the first frequency and $\Delta\omega$ is the frequency separation, which is constant. (Carvalho et al., 2008)

In this dissertation, the algorithm used to produce the random sum of sinusoids was provided from (Caires, 2022).

3.2 Experimental Protocol

As mentioned before, this dissertation aims to study the differences in the ankle's reflex dynamics when the external stimuli varies its frequency bandwidth. When different frequency bands are applied as stimuli to perturb the ankle system, it is hypothesized that these variations in the stimulus frequency will lead to observable alterations in the characteristics of the ankle reflex response.

The experimental work involved all of the *apparatus* described previously. Five trials were performed with four different subjects. For every subject EMG/Accelerometerion data and input(τ)/output(Θ) data were acquired. All of the data was analysed on MATLAB.

To achieve this study's objectives, torque, τ, is applied as the input stimuli and the respective angular displacement, Θ, is read as the output. Firstly, it is important to mention that all of the experiments were done in an open-loop condition. An open loop system (Figure 3.10 (b)) refers to a control system in which the output or behavior of the system is not directly influenced or regulated by the system's own output. In other words, in an open-loop system, the input to the system is determined without considering the system's current state or the output it produces.A closed-loop system (Figure 3.10 (a)), often referred to as a feedback control system, is a type of system where the output or behavior of the system is regulated and controlled by continuously monitoring and adjusting it based on feedback information. In a closed-loop system, there is a feedback loop that allows the system to respond to changes and maintain a desired or specified performance (Aeyels et al., 1995). In Dias, 2022, Dias concluded that closed-loop conditions lead to better coherence results with less noise. Nonetheless, open-loop conditions, where human aid is required in order for system regulation, are simpler and easier to apply in comparison to closed-loop conditions. For this dissertation, it was concluded that the best option was to use a open-loop system, which means that the torque was directed to the motor without the position's feedback. The only part of the system that uses closed-loop conditions is the gravity and friction compensation systems.

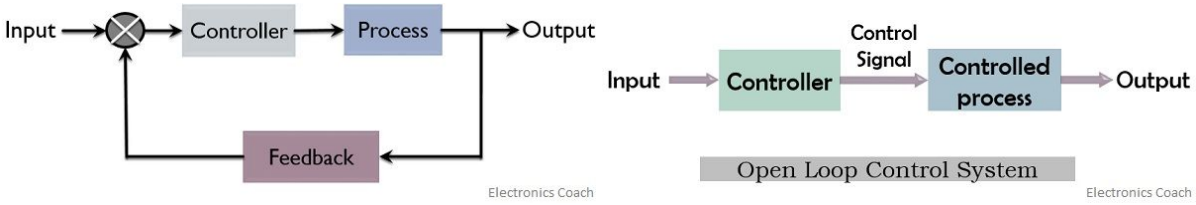

(a) Closed-loop system.

(b) Open-loop system.

Figure 3.10: Different conditions systems. (Aeyels et al., 1995)

For each subject, the experiment was done twice, each time for different bandwidths: narrow band (NB: [0.12 1.8] Hz) and wide band (WB: [0.12 20] Hz).

3.2.1 Procedures Summary

Before moving forward, a step-by-step of what this dissertation practical work consisted of will be done in this section.

Firstly the electrode positioning is done. Then, the subject proceeds to do the MVC test. After receiving the MVC results, the subject places himself at the aluminium structure as showed before (Figure 3.3). Before applying perturbations, it is confirmed that the gravity compensation initialisation makers are aligned. Then, the subject is asked to relax. The perturbations (sum of sinusoids) are applied. The input is the torque and the output (τ) is the displacement angle (Θ). Lastly, the results are exported to MATLAB and analysed.

3.3 Data Analysis

In this section, the methodologies employed within the MATLAB environment to unveil the system frequency response characteristics are described.

The experimental work derived results files were loaded on MATLAB where they were carefully analysed. Firstly, a time window frame was chosen from the output signal. For that time frame, the functions `mean` and `std` were used to calculate the mean and respective standard deviation for the input and output signals.

Afterwards the MATLAB `detrend` function was applied. This function is used to remove a linear trend from a *dataset*, when applied it subtracts the best-fit linear trend from the data. In this case, it was helpful to focus on the underlying fluctuations and patterns in the data without the influence of a simple linear increase or decrease over time. (Ljung, 1999)

The next step was to calculate the coherence for the results. The function `mscohere` was used for this effect. This function was used to estimate the magnitude-squared coherence between the input and output. The magnitude-squared coherence is a measure of the correlation between two signals in the frequency domain. It values range from 0 to 1, where 0 indicates no coherence (signals are unrelated) and 1 indicates perfect coherence (signals are identical) at a specific frequency. Then, the `pwelch` function was used to obtain a estimate of the power spectral density plot. This to estimate the cross-power spectral density (correlation between two signals as a function of frequency and time) and the power spectral density (power content of a signal as a function of frequency) using Welch's method. The Welch's method is a widely used technique for estimating spectral content in a signal. (Ljung, 1999)

Subsequently, the frequency response function (FRF) was computed by using the function `tfestimate`. The frequency response is evaluated in this dissertation by studying the relationship between the input (torque, τ) and the respective output (angular displacement, Θ) at the ankle joint. This results in the total system's dynamics (ankle+motor).

The cutoff frequency was estimated by doing the square root of the independent term of the FRF's denominator. The cutoff frequency refers to the frequency at which the system's response starts to significantly attenuate or reduce the amplitude of the input signals or perturbations applied to the system. Specifically, it represents the point at which the system's output magnitude begins to decrease noticeably as the frequency of the input signal increases.

The `tfest` function was applied in order to approximate the FRF results to a second order system (Equation 3.2). This function is used for estimating linear transfer functions from input-output data using a parametric approach. It is primarily used for modeling dynamic systems. It fits the resulting FRF from `tfestimate` and estimates a transfer function (TF) that describes the system's behavior (Ljung, 1999).

$$H(s) = K \times \frac{\omega_c^2}{s^2 + 2\zeta\omega_c s + \omega_c^2} \tag{3.2}$$

It was also possible to calculate the damping ratio (ζ), $\zeta = \frac{c}{2\omega_c}$ (c: damping factor). It characterizes how the system responds to external forces or disturbances and how quickly it returns to equilibrium after being disturbed, it takes values between 0 and 1. When $\zeta = 0$, the system is said to be undamped, which means that it has no internal resistance to motion, so it oscillates indefinitely when disturbed. It results in a pure sinusoidal oscillation with no exponential decay. When $0 < \zeta < 1$, the system is considered underdamped, which means that it exhibits oscillatory behavior in their response to a disturbance. When $\zeta = 1$, it is called a critical damping and it represents a special case where the system returns to equilibrium as quickly as possible without oscillating. And finally, when $\zeta > 1$, the system is termed

overdamped, meaning that it returns to equilibrium without oscillations, but it takes longer to do so compared to critically damped systems. The damping ratio depends on the function poles (Ogata, 1970). In a study about the ankle's reflex, it is expected for the stiffness to be the prominent factor. Since the damping ratio is related to non-reflexive properties, an underdamped response is expected for the system. (Zhang et al., 2013)

To facilitate a more comprehensive evaluation of the system, a mass-spring-damp second order model is utilized as a representation of the ankle impedance ($Z_a = I_a s^2 + B_a s + K_a$) and the motor impedance ($Z_m = I_m s^2 + B_m s + K_m$). The second order mass-spring-damper system parameters are: the ankle+motor as the a mass/inertia (I or m), the damper symbolizes the visco-elasticity term (B or c), and the tendons are represented by the stiffness term (K or k).

By recognizing that the motor and ankle are interconnected, they can be treated as a combined inertia unit, as illustrated in Figure 3.11. The dynamic equations corresponding to this diagram are detailed in Equation 3.3. This equation involves the application of the Laplace transform ($\mathscr{L}$) and assumes zero initial conditions (Coelho, 2021).

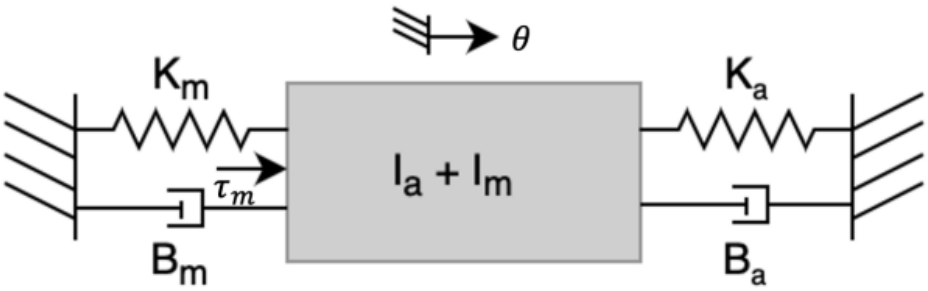

Figure 3.11: Analogous linear depiction of estimating ankle impedance. A representation of the ankle (Z_a) impedance and the motor impedance (Z_m) is made by a second order mass-spring-damper system. (Coelho, 2021)

$$\begin{aligned}
&\tau_m = (I_a + I_m)\ddot{\Theta} + (B_a + B_m)\dot{\Theta} + (K_a + K_m)\Theta \\
&\overset{L}{\Rightarrow} \tau_m(s) = (I_a + I_m)s^2\Theta(s) + (B_a + B_m)s\Theta(s) + (K_a + K_m)\Theta(s) \\
&= (I_a s^2 + B_a s + K_a)\Theta(s) + (I_m s^2 + B_m s + K_m)\Theta(s) \\
&= (Z_a(s) + Z_m(s))\Theta(s)
\end{aligned} \tag{3.3}$$

By analysing Figure 3.11, it can be concluded that Z_a and Z_m are in parallel and the resulting impedance is $Z_{am} = Z_a + Z_m$, which corresponds to the total system impedance. Hence, the resulting total admittance is $Y_{am} = Z_{am}^{-1}$. Which means that when a perturbance is applied to the system, the output depends on both the motor's and the ankle's impedance.

In Equation 3.4, it can be seen that by obtaining the system's FRF, which is the division of the input by the output, it is also obtained the system's admittance, Y_{am}. The system's impedance, Z_{am}, is simply obtained by inverting the resulting FRF. Since the aim is to obtain the ankle's dynamics, the motor impedance has to be removed. With that purpose and as it happened in Dias, 2022, a frequency response subtraction method was used: $Z_a = Z_{am} - Z_m$.

$$H(s) = \frac{\Theta(s)}{\tau_m} = Y_{am}(s) = \frac{1}{Z_a(s) + Z_m(s)} \tag{3.4}$$

That being said, a solo motor trial had to be done in order to obtain the motor's dynamics. All of the procedure described above were repeated for the motor alone and the motor's FRF was obtained. By inverting its FRF, the motor's impedance was acquired. By subtracting the motor's impedance from the total system's impedance, the ankle's impedance is obtained.

The described procedure above was all done for the WB data. For the NB trials, the frequency range maximum is 1.8 Hz, where the system dynamics is practically only influenced by the stiffness. Hence, there is not enough spectral content in the data to accurately do a second order fit, it would not have a meaning. Which is why, for the NB trials, the MATLAB function `tfest` to approximate the FRF to a second order system is only applied with the intention of just contemplating the stiffness. This is done by considering $s = 0$ and by inverting this result to obtain the system's stiffness, k_{am}. This also means that it does not make sense to estimate the damping factor for the NB trials.

To isolate the ankle's stiffness for the NB trials, the motor's stiffness has to be removed as well. However, the motor does not have any mass with elasticity, in reality, it does not have a stiffness factor either. This factor appears because of the pendulum effect. In Caires, 2022, Caires showed that when the motor is free (without any masses attached), it behaves like a pendulum when exposed to perturbances. This attributes to the motor a "stiffness" factor. In summary, Caires concluded that even though the motor itself may not have elasticity, several factors such as inertia, coupling with the structure, and control can contribute to the presence of an apparent stiffness component when disturbances are applied, even if they are low frequency perturbances.

It was not possible to perform a NB trial for the motor alone. The reason for that is because in that bandwidth the motor seems to have a blockage system. The mass does not seem to be enough to surpass the friction and the structure is released in an unwanted range. This causes the system to stop, making the data acquisition impossible for this frequency range. Thus, the WB motor trial was used to obtain the stiffness. This was done by simply considering $s = 0$ in the WB TF, and then inverting the result.

However, it was necessary to validate if this could be done. This is validated by confirming that the motor does not have any influence in the difference between the NB's and WB's FRFs. For that purpose, a NB trial was done with 2 masses of 0.260 kg each. The masses were attached to the green strap as it can be seen in Figure 3.12. This process was repeated for the WB frequency range and the results were then compared. If results present any difference between NB and WB dynamics in this trial, this means that the same frequency response can not be used for both of the frequency bandwidths.

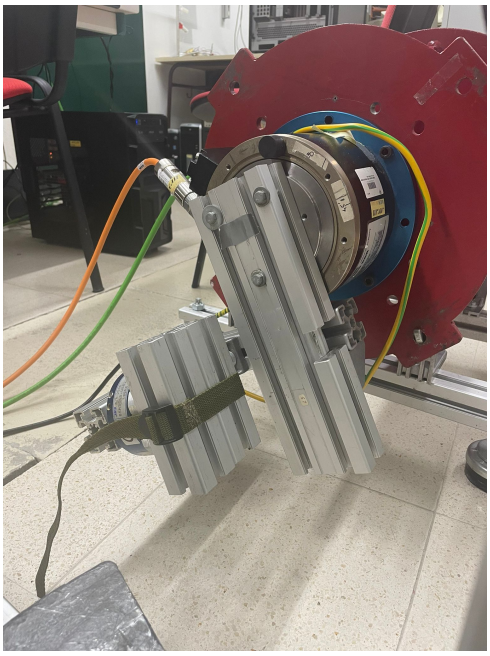

Figure 3.12: Motor+weights trial.

3.3.1 Electromyography

In addition to the frequency response data, EMG and accelerometer data were also acquired to identify muscle contraction. EMG is a specialized tool for the precise identification and characterization of muscular contractions within the ankle region. As it was mentioned before, the EMG system used two electrodes: electrode 1 was placed on top of the gastronemius muscle, and electrode 2 was placed on top of the tibialis anterior muscle.

Data was received through the Trigno Discover software and it was then exported as a *.csv* file. This *.csv* file was later imported to MATLAB. The function `dsp.MovingRMS` was used for computing the moving root mean square (RMS) of the signal. The RMS value is a measure of the magnitude or amplitude of a signal and is often used to quantify the overall "energy" of the signal. This function processes the input signal by sliding the specified window through the data, computing the RMS value within the window at each step, and producing an output signal containing the moving RMS values.

The EMG data was also adjusted to the window chosen for the frequency response data. The mean and standard deviation was also calculated for the EMG data using the functions `mean` and `std`, respectively.

For a better comparison between subjects, the EMG data was also normalized. Normalization allows for the removal of absolute differences in muscle contraction intensity and focuses on the relative proportion of muscle activation relative to MVC. This is valuable when the goal is to understand differences in relative muscle activation among subjects. Furthermore, normalizing the data facilitates standardization and comparison of results between experiments, as it places all data on the same scale from 0 to 1 relative to the maximum MVC.

The MVC maximum value was discovered for each subject and for each electrode. Then, the EMG data for each subject was all divided by this value and the normalized data was estimated. The mean and standard deviation were also calculated for the normalized data.

3.3.2 Reflex dynamics

In most of the studies mentioned throughout this dissertation, subjects were asked to contract the muscles or to even contradict the perturbations. In this study, the difference was that the subjects were only asked to relax and to try not to contradict any disturbance.

This kind of procedure lead to the presumption that any outcome detected is a result of reflex dynamics, since subjects were told not to contract any muscle on purpose.

It is, of course, important to allude to the fact that human behavior and decision-making are complex and can be influenced by a combination of factors. This factors are: reflexes, learned behaviors, cognitive processes, and conscious choices. Therefore, the outcome can be a mixture of all of these factors, even though the subjects were asked only to relax. This procedure can be a limitation of this study. However, in 2002 van der Helm et al. (Helm et al., 2002), among with others researches cited in this dissertation, concluded that intrinsic muscle dynamics does not change when the frequency bandwidth of the applied signal changes. Thus, the EMG is used to verify muscle activation and any difference between the NB and WB results should be attributed to the reflex's dynamics.

Chapter 4

Results

This chapter presents the results of this research study, providing a comprehensive overview of the data collected and analysed. The primary goal of this study was to investigate the effect of the frequency bandwidth on the ankle's reflex dynamics.

In the following sections, the findings will be presented in a structured manner, beginning with an overview of the data and followed by an interpretation of these findings. These results are presented in alignment with the research questions discussed in the context of existing literature.

The results presented in this chapter serve as a critical foundation for their subsequent discussion, where the implications of these findings, their theoretical and practical significance, and their contribution to the overarching objectives of this dissertation will be discussed.

4.1 Trials

As said before, five trials were performed with four different subjects. The results are presented in this section.

4.1.1 Motor's Dynamics

As mentioned before, the ankle joint's center is aligned with the motor's rotation center, so that it can be assumed that the angular displacement measured by the motor's encoder is the same as the ankle. The reason behind a solo motor trial, is so that its dynamics can be removed from every subject's trial. This results can be seen in Figure 4.1.

The time window chosen for the signal was [10 209]s (Figure 4.1 (b)). Figure 4.1 (d) represents the motor's results for the continuous-time identified transfer function and the respective fit. The TF is represented by Equation 4.1. It resembles a second order system and it has the following parameterization: 2 poles and 0 zeros. The percentage of the TF fit is 74.67%. This trial was done under WB conditions.

$$\mathrm{TF}_{\mathrm{motor}}(\mathrm{s}) = \frac{19.92}{s^2 + 5.778s + 45.73} \tag{4.1}$$

4. RESULTS

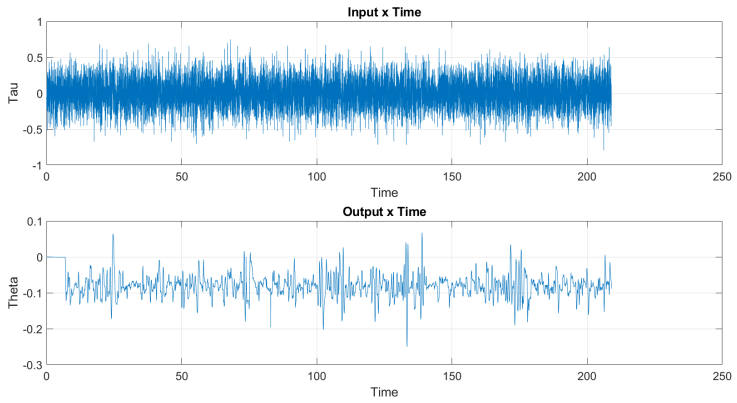

(a) Motor's input, τ (*Nm*), and output, Θ (*rad*).

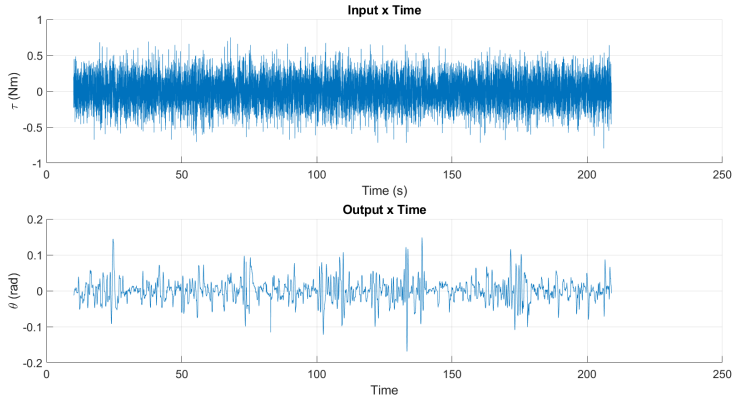

(b) Motor's `detrended` chosen window input (τ (*Nm*)) and output (Θ (*rad*)).

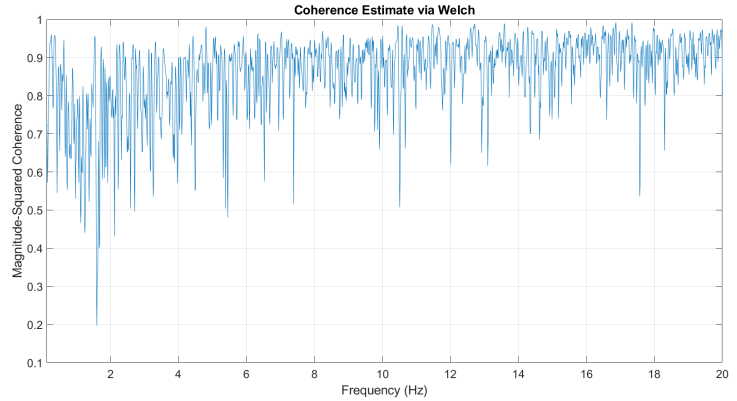

(c) Motor's Coherence.

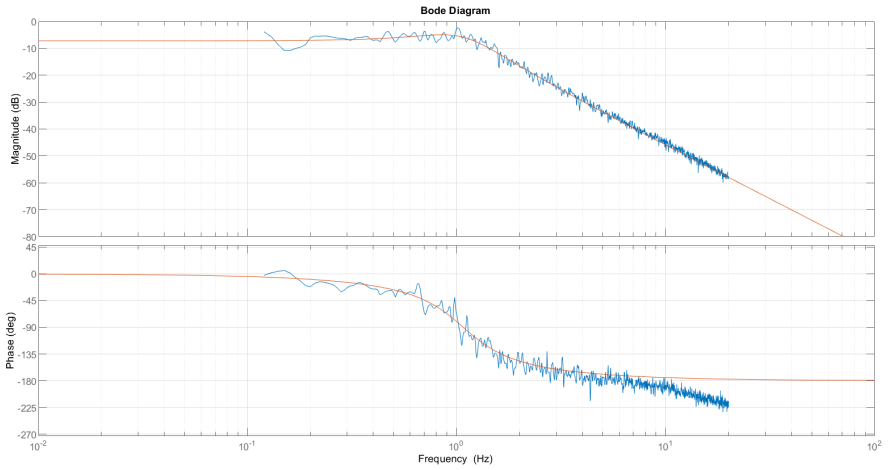

(d) Motor's Bode Diagram: FRF and TF.

Figure 4.1: Motor's dynamics.

The resultant cutoff frequency for the motor's WB trial was $\omega_c = 1.075$ Hz. By knowing the motor's admittance (equivalent to the $TF_{motor}(s)$), it is possible to discover the motor's impedance: $Z_m = \frac{s^2+5.778s+45.73}{19.92}$.

As mentioned before, it does not make much sense to estimate a TF for the NB trials, since the frequency range for this condition is quite small. Thus, it is assumed that for the narrow frequency bandwidth, the only element to consider is the stiffness. This is done by assuming $s = 0$ in the obtained TF for the WB trial. The resultant stiffness is achieved by inverting the TF in that conditions: $k_m = \frac{45.73}{19.92} = 2.2957 Nm/rad$. Consequently, the motor's compliance is: $C_m = 0.4356 rad/Nm$

The summary of the impedance and stiffness acquired is presented in Table 4.3 by the end of the Trials section.

A trial for each of the bandwidths were performed in order to confirm that the motor's dynamics is not affecting any possible differences between NB and WB results. This trial was done by attaching two masses to the motor as showed in Figure 3.12 and applying NB and WB perturbances. The results for these trials can be seen in Figure 4.2 and its respective coherences (for each bandwidth) are in Figure 4.3.

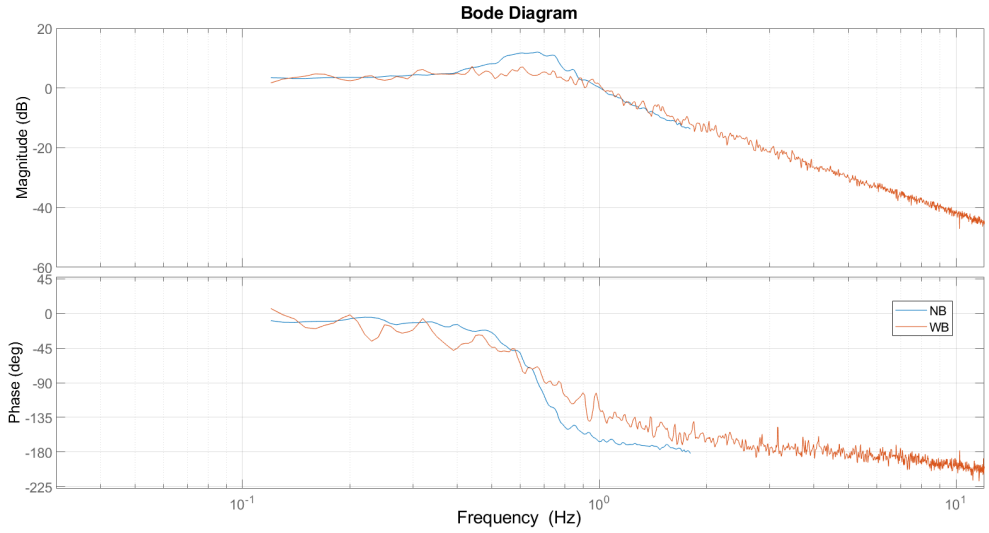

Figure 4.2: Motor+weights trial results: superposition of NB and WB FRFs.

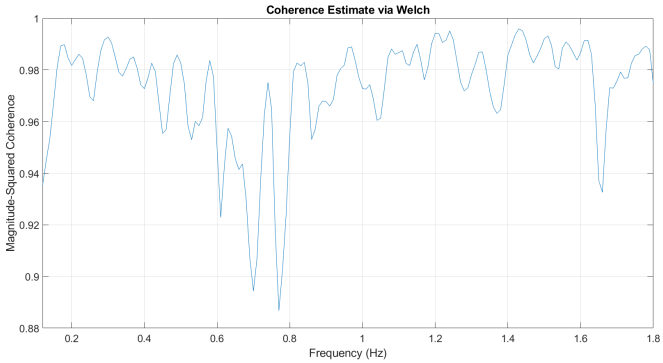

(a) Motor+weights coherence for the NB trial.

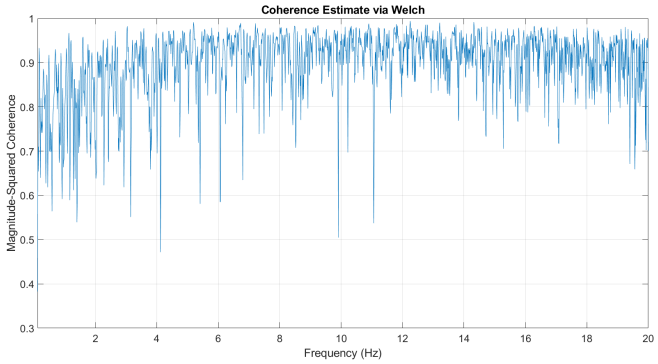

(b) Motor+weights coherence for the WB trial.

Figure 4.3: Motor+weights coherence for NB (a) and WB (b) trials.

4.1.2 Subject 1

Results from the first experiment carried out with subject 1 are represented on this section. Firstly, Figure 4.4 constitutes results from the MVC trial. Then, NB (Figures 4.5 and4.6) and WB (Figures 4.7 and 4.8) results are introduced. The power/frequency spectrum is presented in the Appendix in Figures 6.1 and 6.2. Lastly, FRF comparison results (Figure 4.9) are presented. The summary of the impedance and stiffness acquired is presented in Table 4.3 by the end of the Trials section.

4.1.2.1 Maximum Voluntary Contraction

In order to normalize EMG data, the MVC data presented below was collected for subject 1.

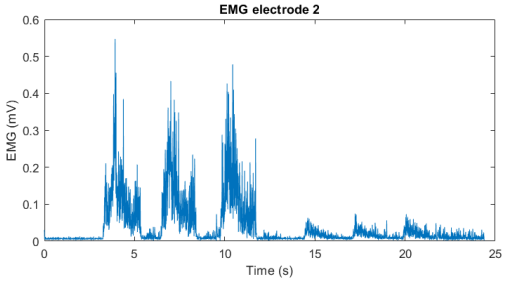

(a) Subject 1 MVC results for electrode 1 (gastronemius muscle).

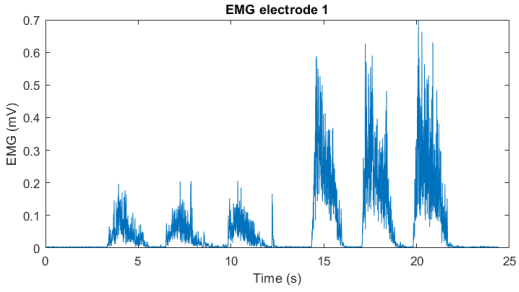

(b) Subject 1 MVC results for electrode 2 (tibialis anterior muscle).

Figure 4.4: MVC EMG results for subject 1.

4.1.2.2 Narrow band

The chosen time window for the signal was [50 120]s, it can be seen in Figure 4.5 (b). The input and output's statistical parameters for the chosen time window (without `detrend`) are presented in Table 4.1. In Figure 4.5 (d) the resulting TF is presented for the NB trial. The red constant horizontal graphic represents the mean for this trial's gain at the chosen time window, which is the inverse of the stiffness.

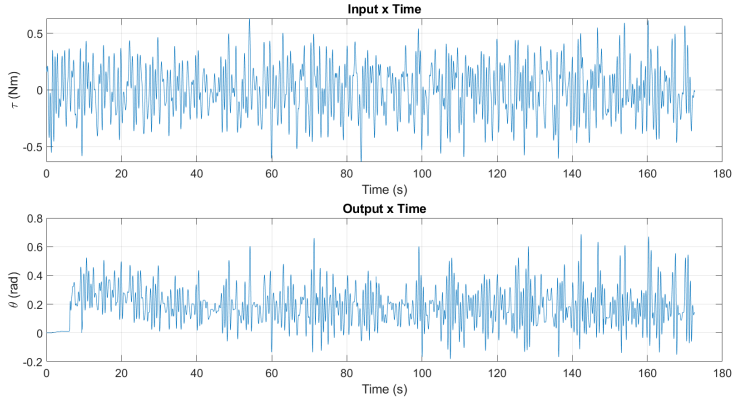

(a) Subject 1 NB input and output.

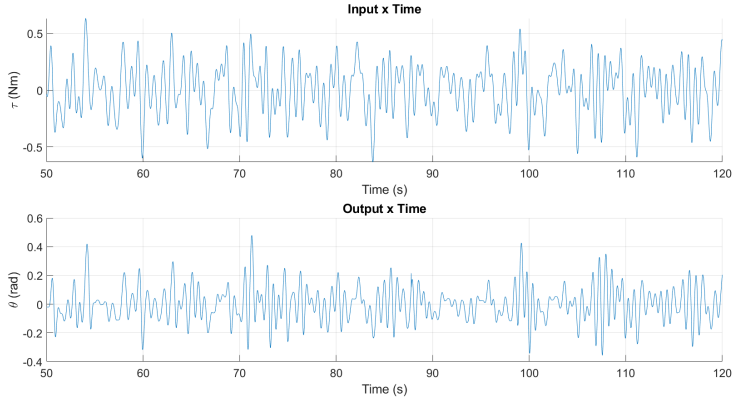

(b) Subject 1 NB `detrended` input and output, for the chosen time window.

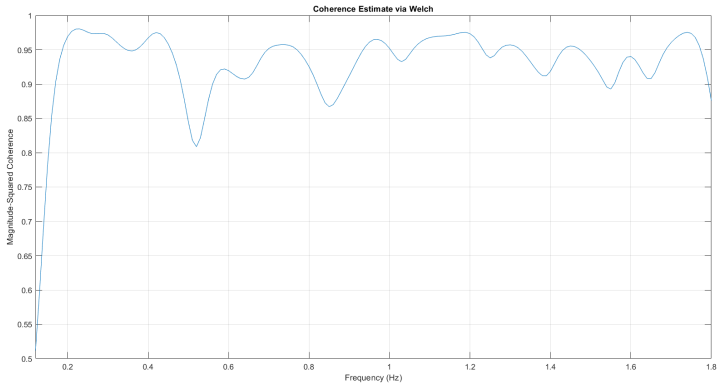

(c) Subject 1 NB Coherence.

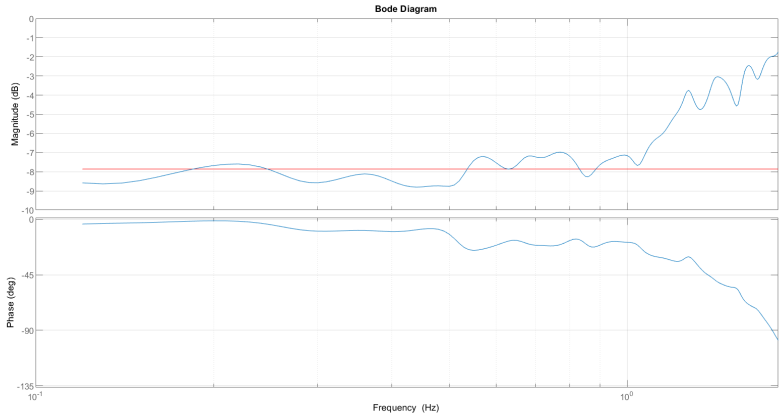

(d) Subject 1 NB FRF and respective gain mean (horizontal line) for the chosen time window.

Figure 4.5: NB results for subject 1.

From the NB FRF fitting, which, once again, will not be presented and it is only done for stiffness estimation. The compliance is acquired. The compliance, visually, is the "constant" part of the FRF, which ends close to the cutoff frequency. In this trial, the cutoff frequency was $\omega_{c,NB1} = 1.755$ Hz. By inverting the compliance, the system's stiffness is obtained. Once the motor's stiffness is subtracted, the resultant ankle's stiffness is: $k_{a,NB1} = 0.5309$ *Nm/rad*.

The normalized EMG for both electrodes for subject 1 are presented in Figure 4.6. By the end of the results section, Table 4.2 presents the mean and standard deviation for the normalized EMG. Data for the non-normalized EMG and Accelerometer are presented in Figure 6.11 and Table 6.1 in the Appendix.

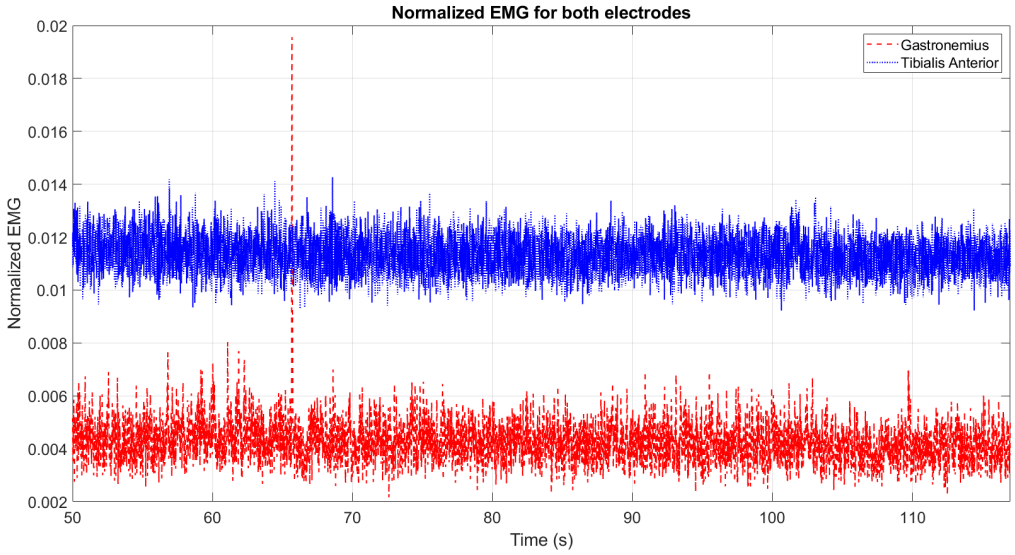

Figure 4.6: Normalized EMG NB trial for the gastronemius and tibialis anterior muscles for subject 1.

4.1.2.3 Wide band

The chosen time window for the signal was [60 130]s, it can be seen in Figure 4.7 (b). The input and output's statistical parameters for the chosen time window (without `detrend`) are presented in Table 4.1. In Figure 4.7 (d), FRF and TF results are presented for the WB trial. The TF can be represented by Equation 4.2 (d). The FRF resembles a second order system and it has the following parameterization: 2 poles and 0 zeros. The FRF fit has a percentage of 87.78%.

$$\mathrm{TF}_{1,\mathrm{WB}}(\mathrm{s}) = \frac{102.2}{s^2 + 5.156s + 148} \tag{4.2}$$

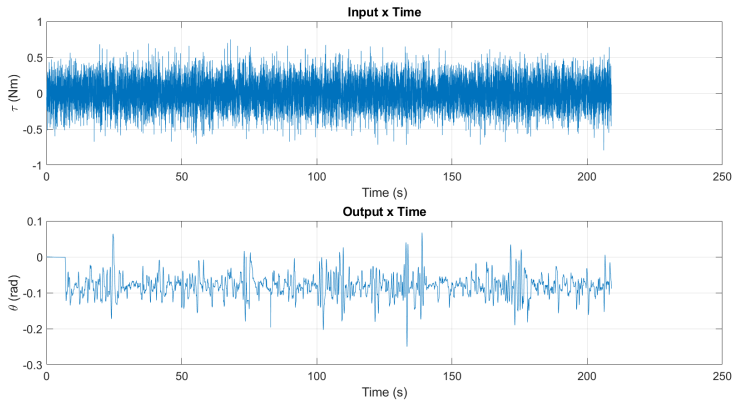

(a) Subject 1 WB input and output.

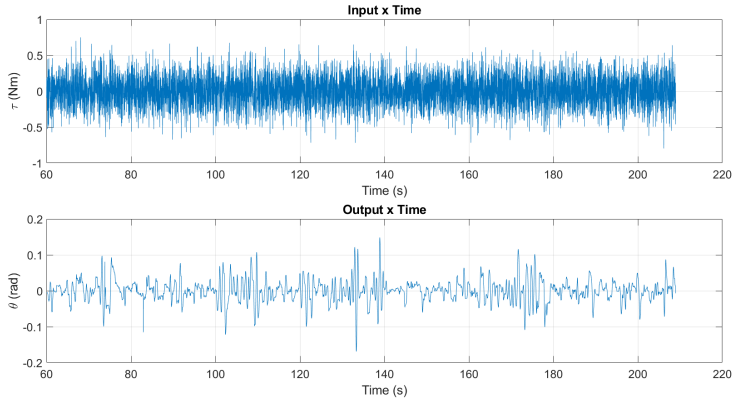

(b) Subject 1 WB `detrended` input and output, for the chosen window.

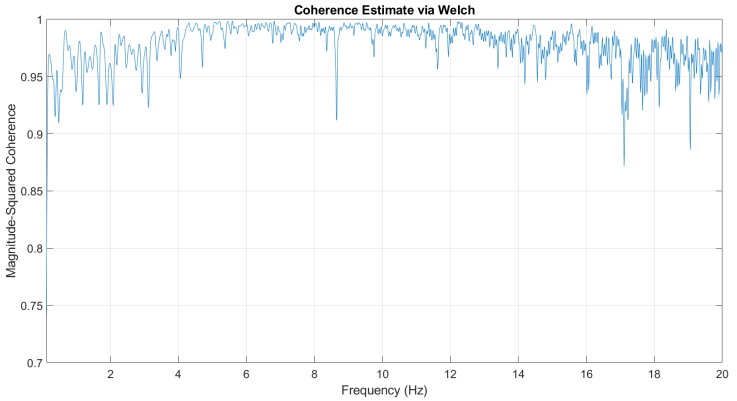

(c) Subject 1 WB Coherence.

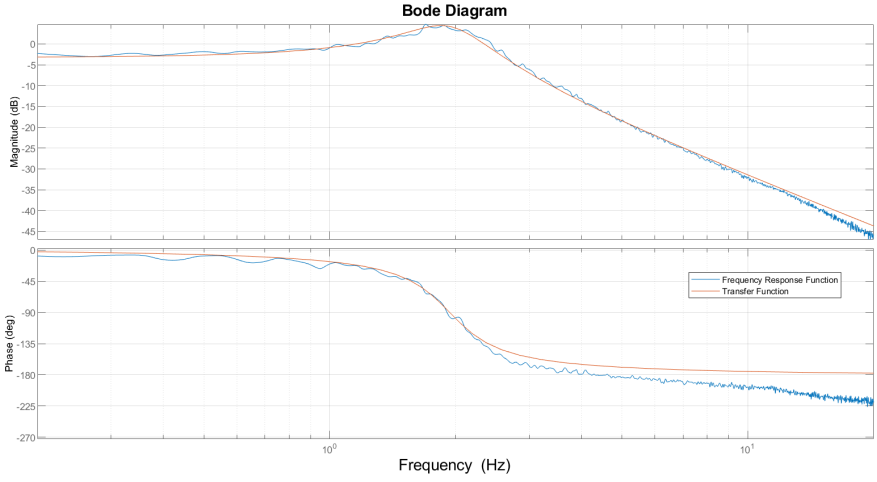

(d) Subject 1 WB fit.

Figure 4.7: WB results for subject 1.

4. RESULTS

The resulting impedance for this test was derived of the subtraction of the system total impedance and the motor impedance: $Z_{a,WB1} = Z_{am} - Z_m = \frac{s^2+5.156s+148}{102.2} - \frac{s^2+5.778s+45.73}{19.92} = \frac{-82.27s^2-487.7s-1724}{2036}$. By inverting the impedance, the admittance is obtained: $Y_{a,WB1} = \frac{1}{Z_{a,WB1}} = \frac{-2036}{82.27s^2+487.7s+1724}$. The system's cutoff frequency is $\omega_{c,WB1} = 0.9228$ Hz and the damping ratio is $\zeta_{WB1} = 0.3162$. The damping ratio is between 0 and 1. Hence, this is an underdamped system.

The normalized EMG for both electrodes for subject 1 are presented in Figure 4.8. By the end of the results section, Table 4.2 presents the mean and standard deviation for the normalized EMG. Data for the non-normalized EMG and Accelerometer are presented in Figure 6.12 and Table 6.1 in the Appendix.

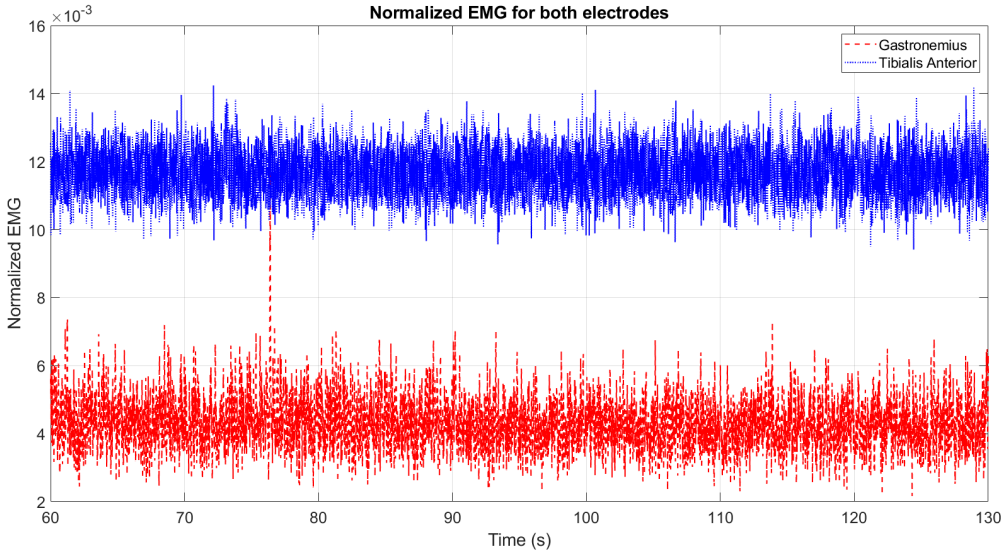

Figure 4.8: Normalized EMG WB trial for the gastronemius and tibialis anterior muscles for subject 1.

4.1.2.4 FRFs comparison between NB and WB

The FRFs comparison is presented in Figure 4.9. The difference between the WB and NB stiffness for the ankle isolated dynamics is 1.3784 *Nm/rad*.

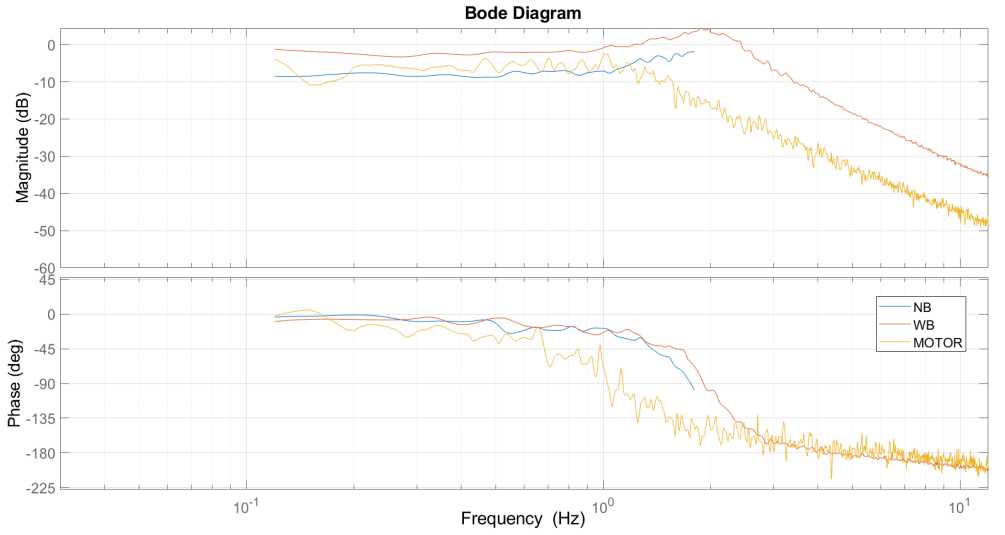

Figure 4.9: FRF overlap of the motor and NB, WB results for subject 1.

4.1.3 Subject 2

Results from the second experiment carried out with subject 2 are presented on this section. As mentioned before, subject 2 went trough 2 trials. Firstly, Figures 4.10 and 4.16 constitutes results from the MVC trials. Then, NB (Figures 4.11, 4.12, 4.17 and 4.18) and WB (Figures 4.13, 4.14,4.19, and 4.20) results are introduced. The power/frequency spectrum is presented in the Appendix in Figures 6.3, 6.4, 6.5 and 6.6. Lastly, FRF comparison results (Figures 4.15 and 4.21) are presented. The summary of the impedance and stiffness acquired is presented in Table 4.3 by the end of the Trials section.

4.1.3.1 Trial 1

4.1.3.1.1 Maximum Voluntary Contraction

In order to normalize EMG data, the MVC data presented below was collected for subject 2 in trial 1.

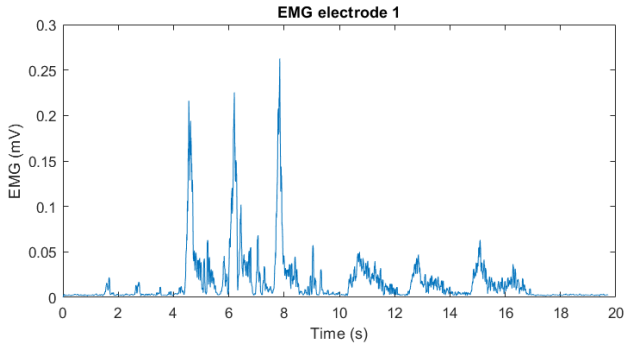

(a) Subject 2 MVC results for electrode 1 (gastronemius muscle).

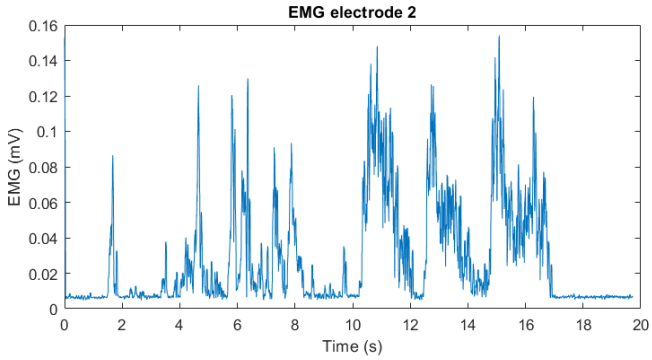

(b) Subject 2 MVC results for electrode 2 (tibialis anterior muscle).

Figure 4.10: MVC EMG results for subject 2, trial 1.

4.1.3.1.2 Narrow band

The chosen time window for the signal was [40 120]s, it can be seen in Figure 4.11. The input and output's statistical parameters for the chosen time window (without `detrend`) are presented in Table 4.1. In Figure 4.11 (d) the resulting FRF is presented for the NB trial. The red constant horizontal graphic represents the mean for this trial's gain at the chosen time window, which is the inverse of the stiffness.

From Figure 4.11 (d), it is possible to see the compliance part of this trial. It ends close to the cutoff frequency, and for this trial this value is $\omega_{c,NB2.1} = 2.094$ Hz. The resultant ankle's stiffness is: $k_{a,NB2.1} = 2.0210$ *Nm/rad*.

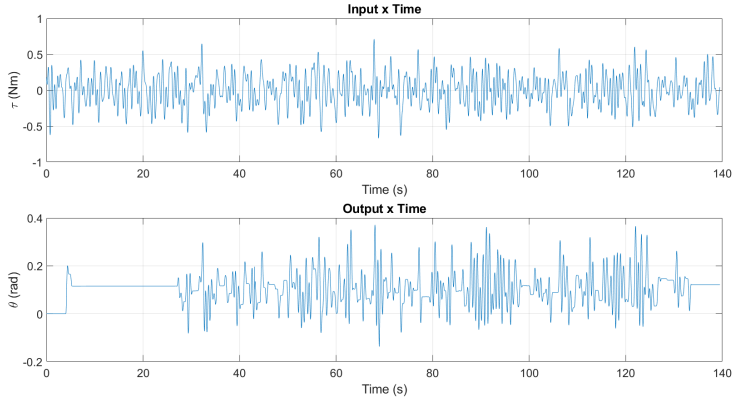

(a) Subject 2, trial 1, NB input and output.

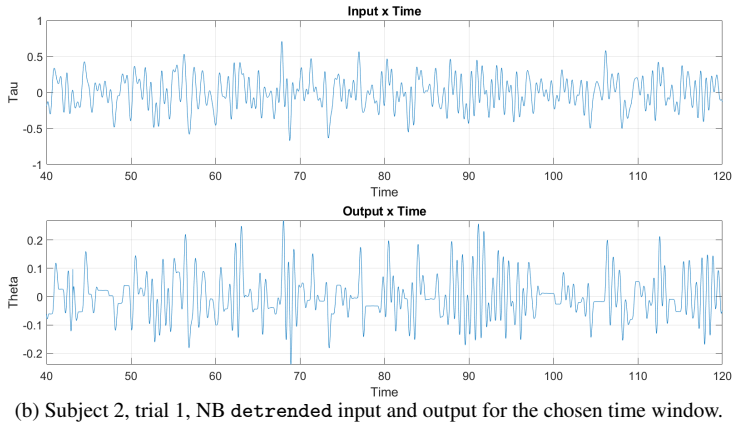

(b) Subject 2, trial 1, NB `detrended` input and output for the chosen time window.

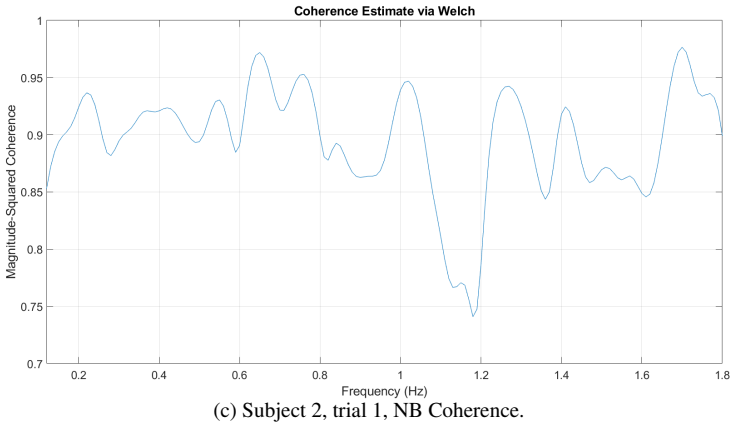

(c) Subject 2, trial 1, NB Coherence.

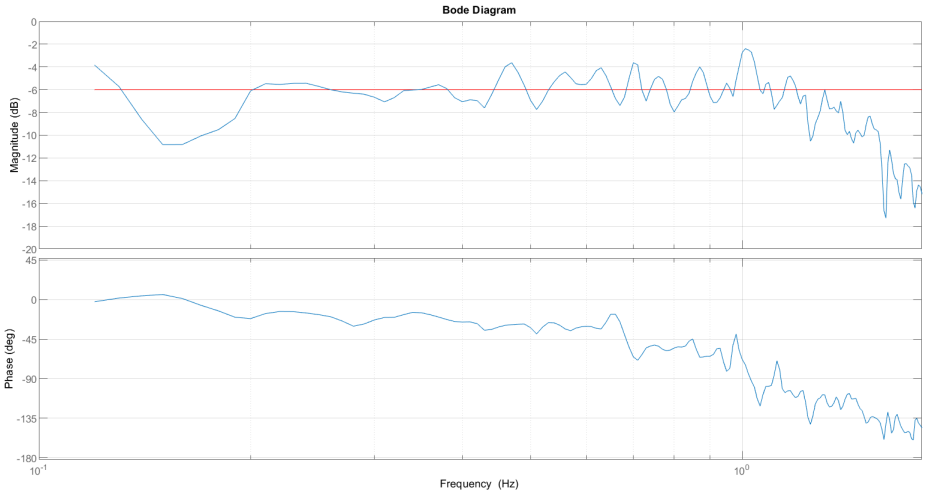

(d) Subject 2, trial 1, NB FRF and respective gain mean (horizontal line) for the chosen time window.

Figure 4.11: NB results for subject 2 trial 1.

The normalized EMG for both electrodes for subject 2, trial 1, are presented in Figure 4.12. By the end of the results section, Table 4.2 presents the mean and standard deviation for the normalized EMG. Data for the non-normalized EMG and Accelerometer are presented in Figure 6.13 and Table 6.2 in the Appendix.

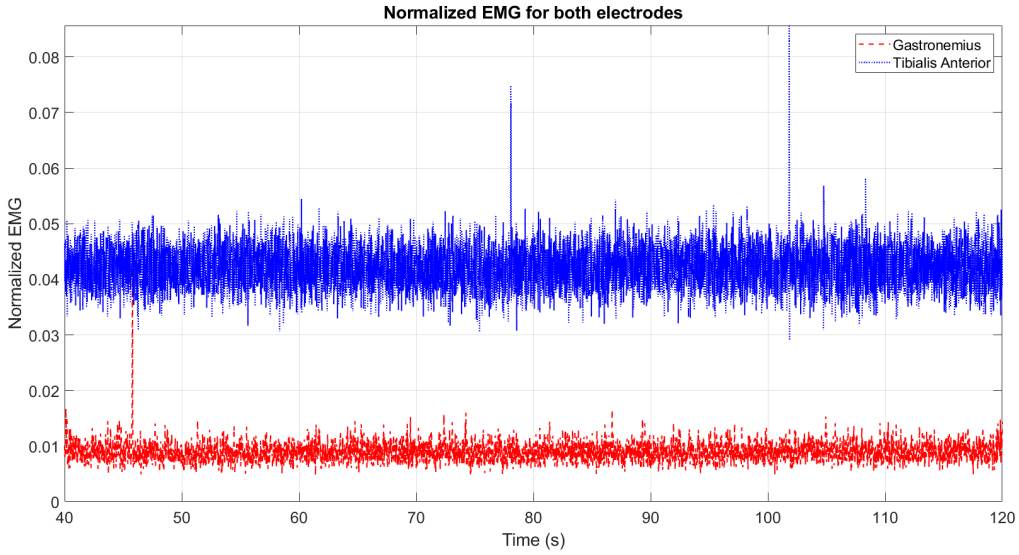

Figure 4.12: Normalized EMG NB trial for the gastronemius and tibialis anterior muscles for subject 2, trial 1.

4.1.3.1.3 Wide band

The chosen time window for the signal was [50 120]s, it can be seen in Figure 4.13 (b). The input and output's statistical parameter for the chosen time window (without `detrend`) are presented in Table 4.1. In Figure 4.13 (d) the resulting FRF is presented for the WB trial. The FRF resembles a second order system. The TF can be represented by Equation 4.3. The FRF has the following parameterization: 2 poles and 0 zeros. The percentage of the FRF fit is 83.47%.

$$\mathrm{TF}_{2.1,\mathrm{WB}}(\mathrm{s}) = \frac{47.22}{s^2 + 7.507s + 99.89} \tag{4.3}$$

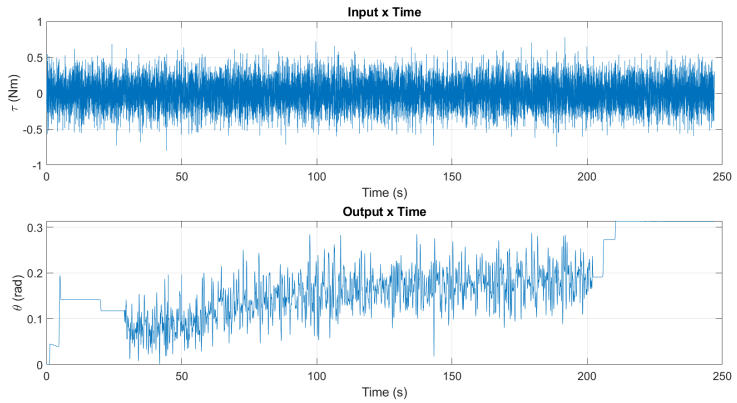

(a) Subject 2, trial 1, WB input and output.

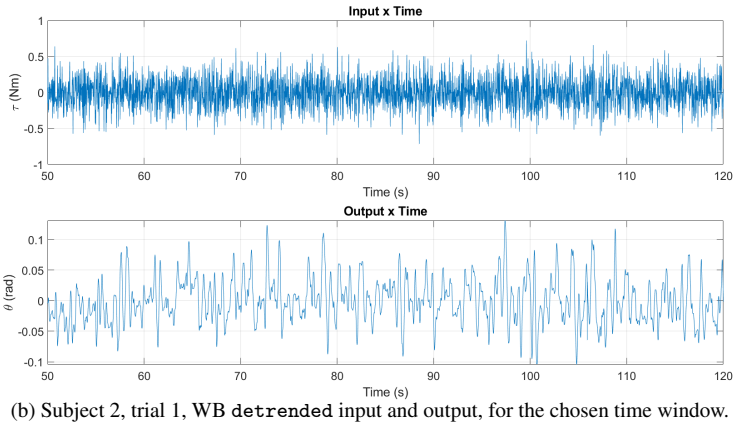

(b) Subject 2, trial 1, WB `detrended` input and output, for the chosen time window.

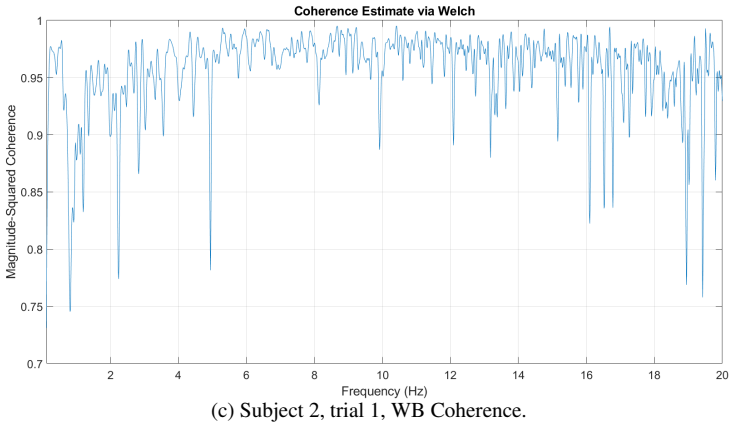

(c) Subject 2, trial 1, WB Coherence.

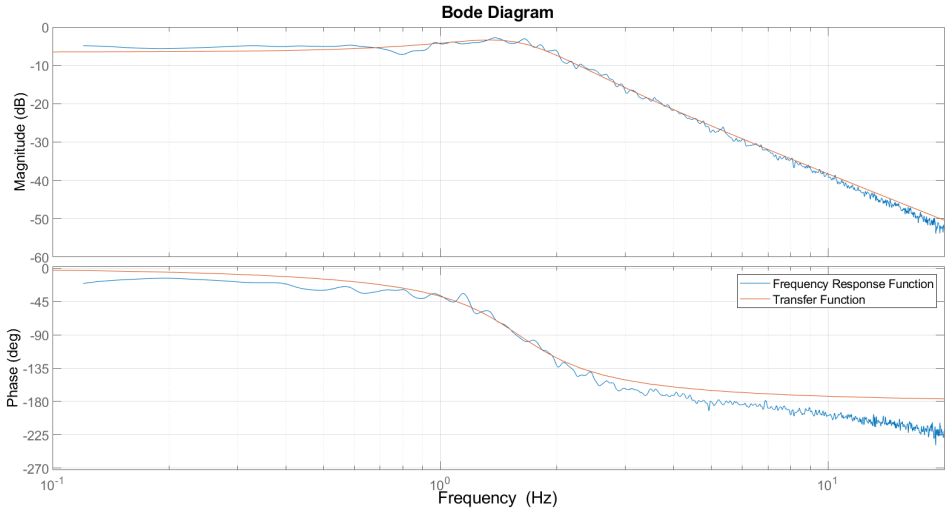

(d) Subject 2, trial 1, WB fit.

Figure 4.13: WB results for subject 2 trial 1.

The resulting impedance for this test was derived of the subtraction of the system total impedance and the motor impedance: $Z_{a,WB2.1} = Z_{am} - Z_m = \frac{s^2+7.507s+99.89}{47.22} - \frac{s^2+5.778s+45.73}{19.92} = \frac{-27.3s^2-123.3s-169.1}{940.9}$. By inverting the impedance, the admittance is obtained: $Y_{a,WB2.1} = \frac{1}{Z_{a,WB2}} = \frac{-940.9}{27.3s^2+123.3s+169.1}$. The system's cutoff frequency is $\omega_{c,WB2.1} = 0.9376$ Hz and the damping ratio is $\zeta_{WB2.1} = 0.3604$. The damping ratio is between 0 and 1. Hence, this is an underdamped system.

The normalized EMG for both electrodes for subject 1 are presented in Figure 4.14. By the end of the results section, Table 4.2 presents the mean and standard deviation for the normalized EMG. Data for the non-normalized EMG and Accelerometer are presented in Figure 6.14 and Table 6.2 in the Appendix.

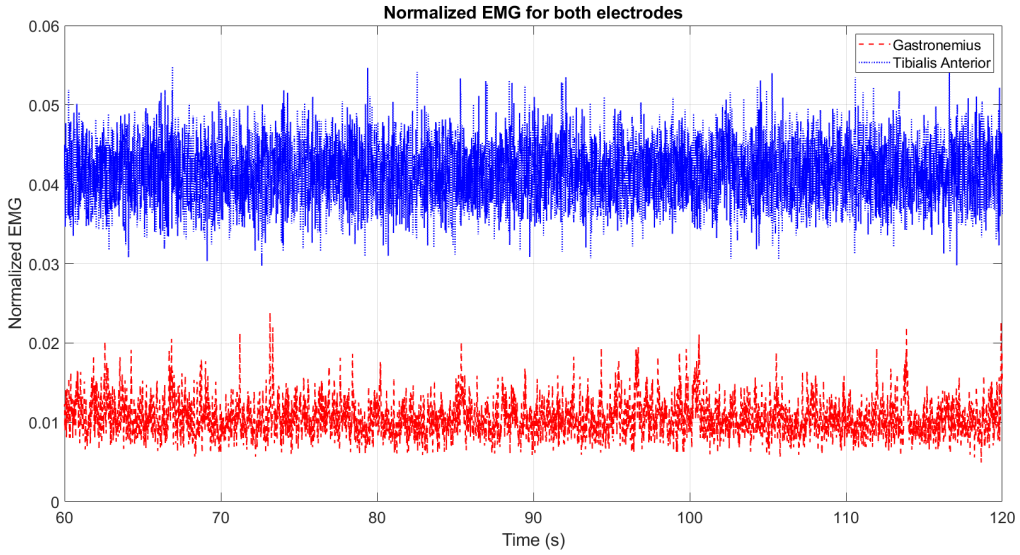

Figure 4.14: Normalized EMG WB trial for the gastronemius and tibialis anterior muscles for subject 2, trial 1.

4.1.3.1.4 FRFs comparison between NB and WB

The FRFs comparison is presented in Figure 4.15. The difference between the WB and NB stiffness for the ankle isolated dynamics is 2.2013 *Nm/rad*.

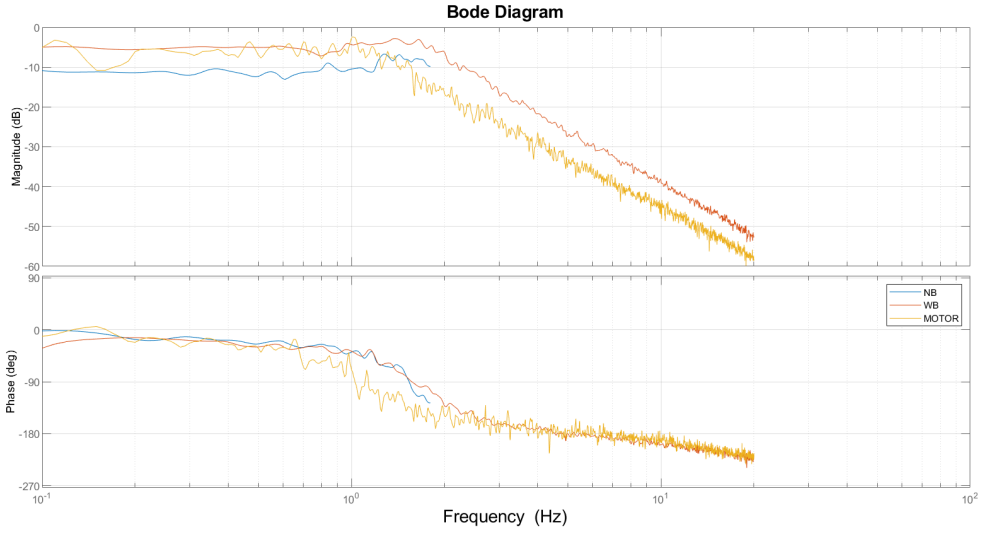

Figure 4.15: FRF overlap of the motor and NB, WB results for subject 2, trial 1.

4.1.3.2 Trial 2

4.1.3.2.1 Maximum Voluntary Contraction

In order to normalize EMG data, the MVC data presented below was collected for subject 2 in trial 2.

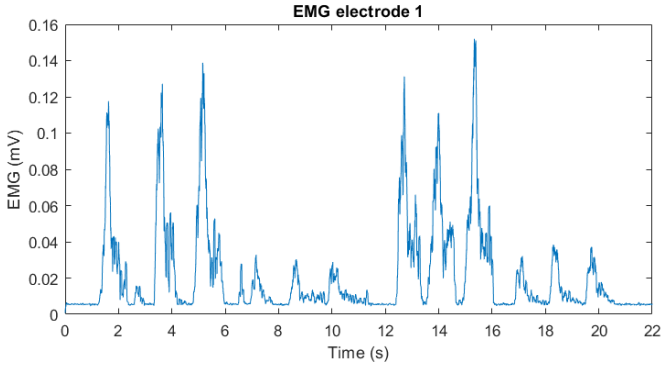

(a) Subject 2, trial 2, MVC results for electrode 1 (gastronemius muscle).

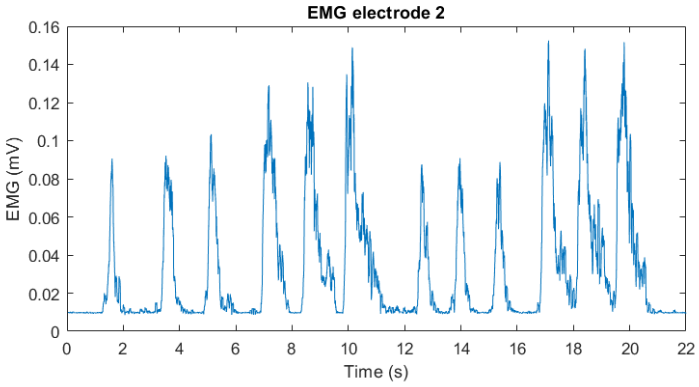

(b) Subject 2, trial 2,MVC results for electrode 2 (tibialis anterior muscle).

Figure 4.16: MVC EMG results for subject 2, trial 2.

4.1.3.2.1 Narrow band

The chosen time window for the signal was [50 150]s, it can be seen in Figure 4.17. The input and output's statistical parameters for the chosen time window (without `detrend`) are presented in Table 4.1. In Figure 4.17 (d) the resulting FRF is presented for the NB trial. The red constant horizontal graphic represents the mean for this trial's gain at the chosen time window, which is the inverse of the stiffness.

From Figure 4.17 (d), it is possible to see the compliance part of this trial. It ends close to the cutoff frequency, and for this trial this value is $\omega_{c,NB2.2} = 1.448$ Hz. By inverting the compliance, the stiffness is obtained. Once the motor's stiffness is subtracted, the resultant ankle's stiffness is: $k_{a,NB2.2} = 3.2745$ *Nm/rad*.

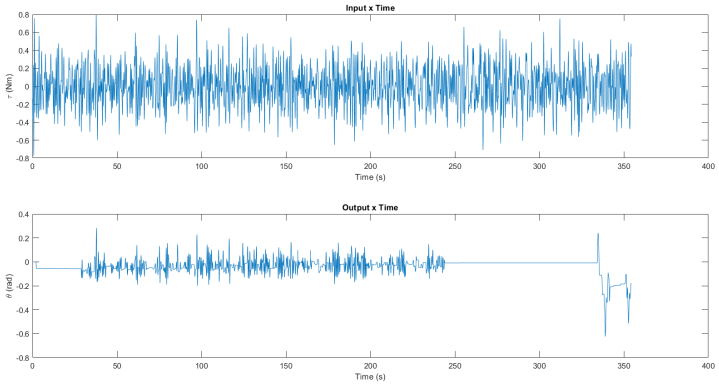

(a) Subject 2, trial 2,NB input and output.

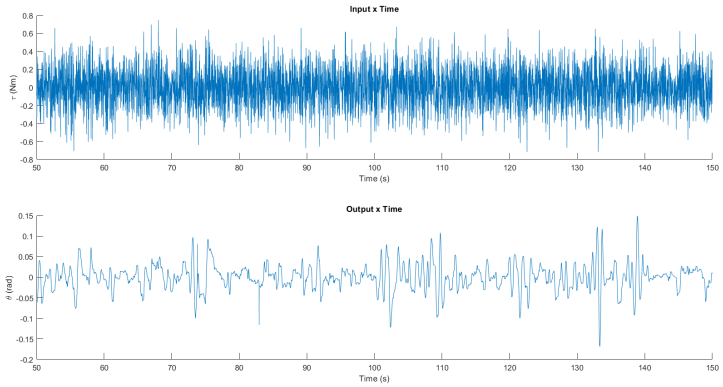

(b) Subject 2, trial 2,NB `detrended` input and output, for the chosen time window.

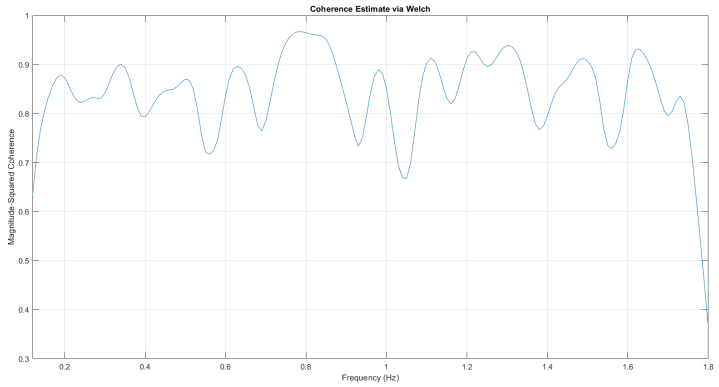

(c) Subject 2, trial 2,NB Coherence.

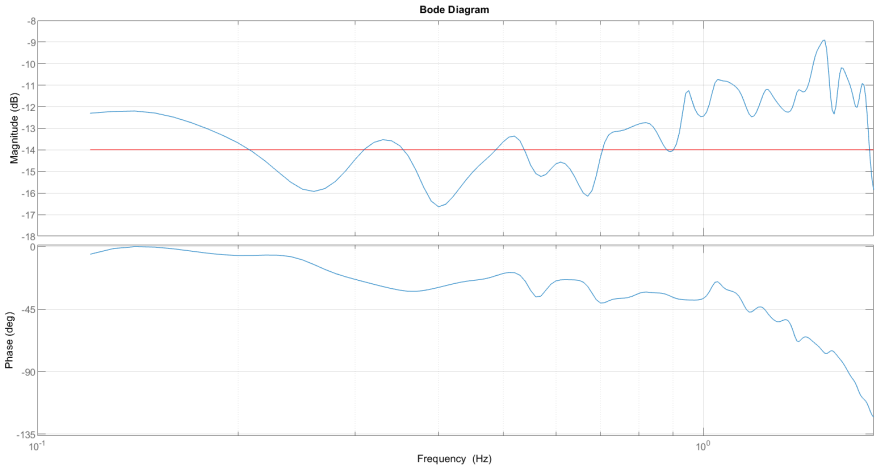

(d) Subject 2, trial 2, NB FRF and respective gain mean (horizontal line) for the chosen time window.

Figure 4.17: NB results for subject 2, trial 2.

The normalized EMG for both electrodes for subject 2, trial 2, are presented in Figure 4.18. By the end of the results section, Table 4.2 presents the mean and standard deviation for the normalized EMG. Data for the non-normalized EMG and Accelerometer are presented in Figure 6.15 and Table 6.3 in the Appendix.

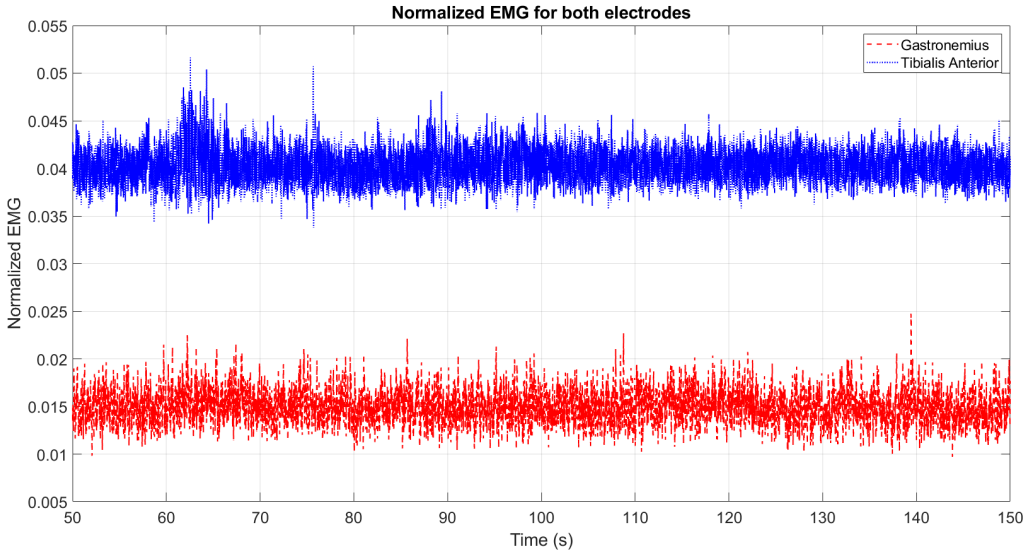

Figure 4.18: Normalized EMG NB trial for the gastronemius and tibialis anterior muscles for subject 2, trial 2.

4.1.3.2.2 Wide band

The chosen time window for the signal was [100 200]s, it can be seen in Figure 4.19 (b). The input and output's statistical parameter for the chosen time window (without `detrend`) are presented in Table 4.1. In Figure 4.19 (d) the resulting FRF is presented for the WB trial. The FRF resembles a second order system. The TF can be represented by Equation 4.4 and it has the following parameterization: 2 poles and 0 zeros. The percentage of the FRF fit is 79.86%.

$$\mathrm{TF}_{3,\mathrm{WB}}(\mathrm{s}) = \frac{34.46}{s^2 + 10.18s + 152.9} \tag{4.4}$$

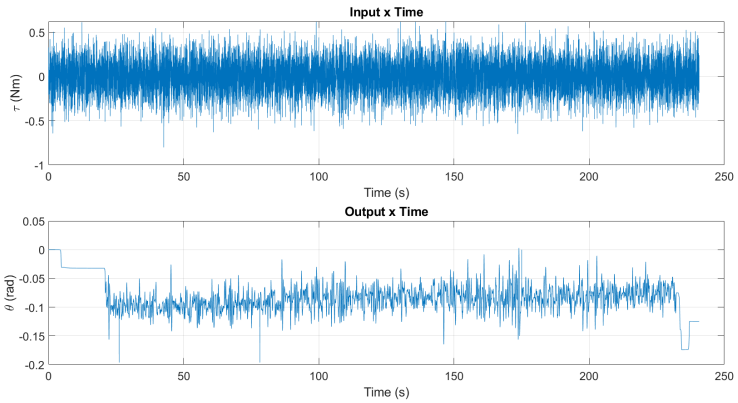

(a) Subject 2, trial 2, WB input and output.

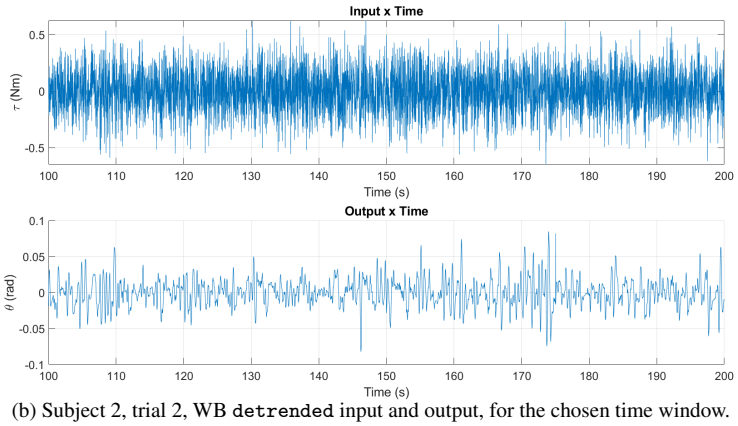

(b) Subject 2, trial 2, WB `detrended` input and output, for the chosen time window.

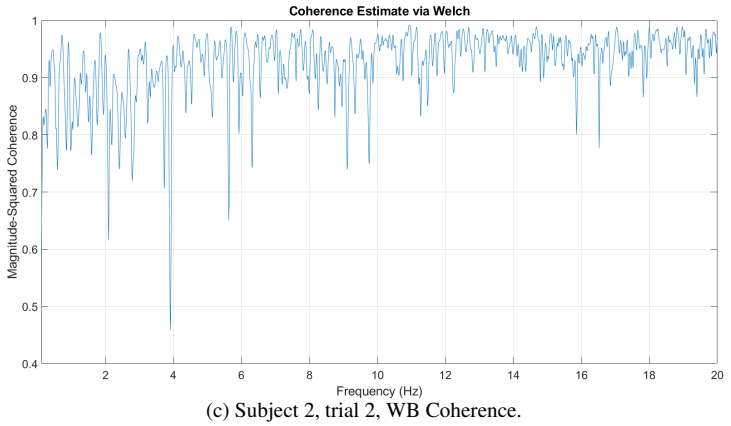

(c) Subject 2, trial 2, WB Coherence.

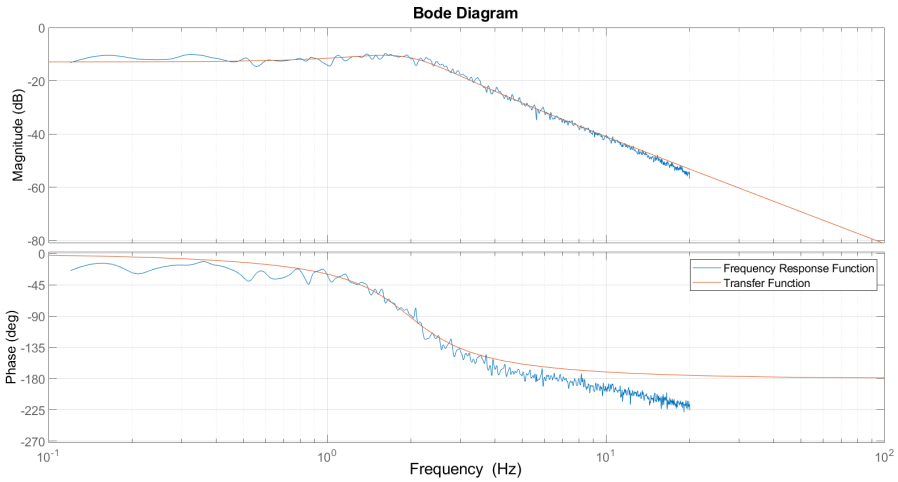

(d) Subject 2, trial 2, WB fit.

Figure 4.19: WB results for subject 2, trial 2.

The resulting impedance for this test was derived of the subtraction of the system total impedance and the motor impedance: $Z_{a,WB2.2} = Z_{am} - Z_m = \frac{s^2+10.18s+152.9}{34.46} - \frac{s^2+5.778s+45.73}{19.92} = \frac{-14.53s^2+3.652s+1470}{686.6}$. By inverting the impedance, the admittance is obtained: $Y_{a,WB2.2} = \frac{1}{Z_{a,WB2.2}} = \frac{-686.6}{14.53s^2-3.652s-1470}$. The system's cutoff frequency is $\omega_{c,WB2.2} = 1.2471$ Hz and the damping ratio is $\zeta_{WB2.2} = 0.1226$. The damping ratio is between 0 and 1. Hence, this is an underdamped system.

The normalized EMG for both electrodes for subject 2, trial 2, are presented in Figure 4.20. By the end of the results section, Table 4.2 presents the mean and standard deviation for the normalized EMG. Data for the non-normalized EMG and Accelerometer are presented in Figure 6.16 and Table 6.3 in the Appendix.

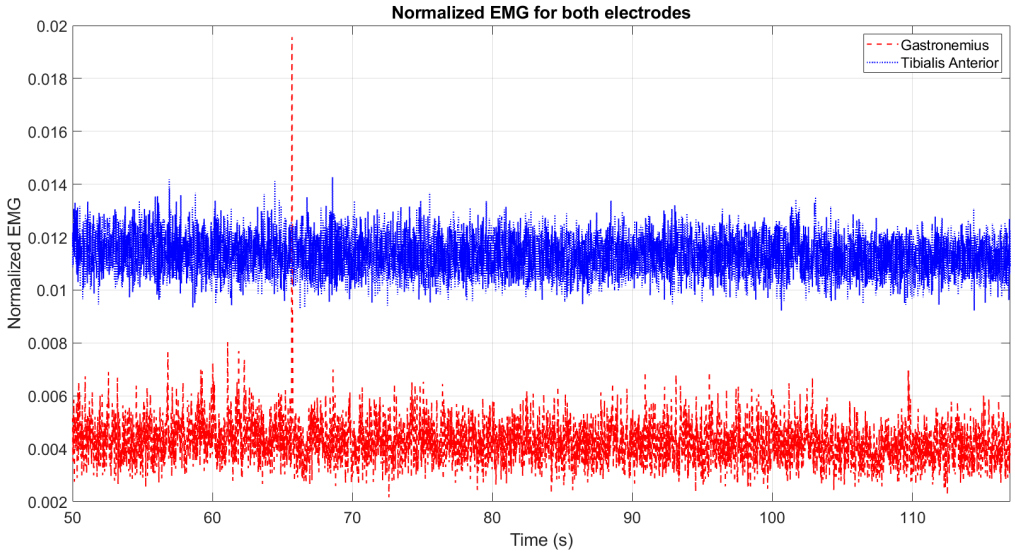

Figure 4.20: Normalized EMG WB trial for the gastronemius and tibialis anterior muscles for subject 2, trial 2.

4.1.3.2.3 FRFs comparison between NB and WB

The FRFs comparison is presented in Figure 4.21. The difference between the WB and NB stiffness for the ankle isolated dynamics is 1.1332 *Nm/rad*.

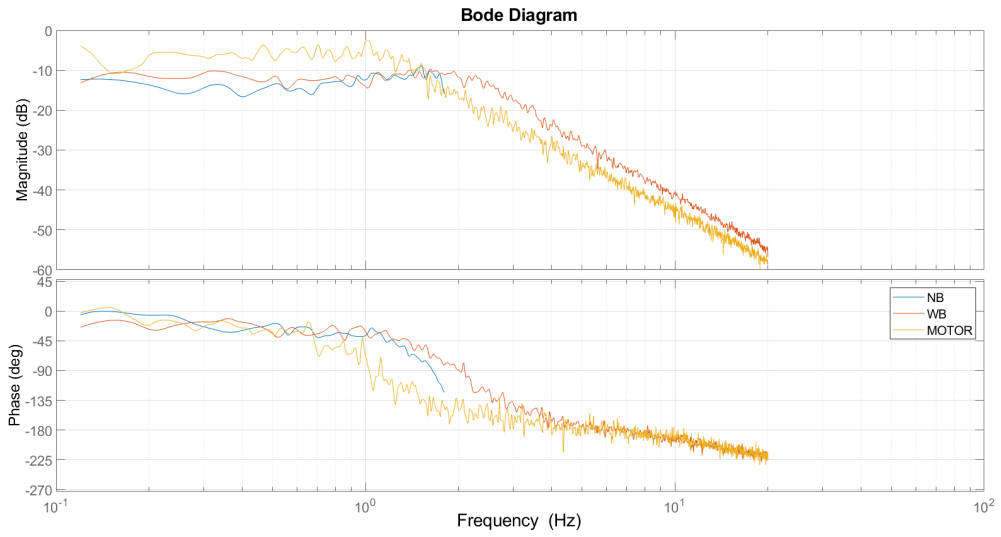

Figure 4.21: FRF overlap of the motor and NB, WB results for subject 2, trial 2.

4.1.4 Subject 3

Results from the third experiment carried out with subject 3 are represented on this section. Firstly, Figure 4.22 constitutes results from the MVC trial. Then, NB (Figures 4.23 and 4.24) and WB (Figures 4.25 and 4.26) results are introduced. The power/frequency spectrum is presented in the Appendix in Figures 6.7 and 6.8. Lastly, FRF comparison results (Figure 4.27) are presented. The summary of the impedance and stiffness acquired is presented in Table 4.3 by the end of the Trials section.

4.1.4.1 Maximum Voluntary Contraction

In order to normalize EMG data, the MVC data presented below was collected for subject 3.

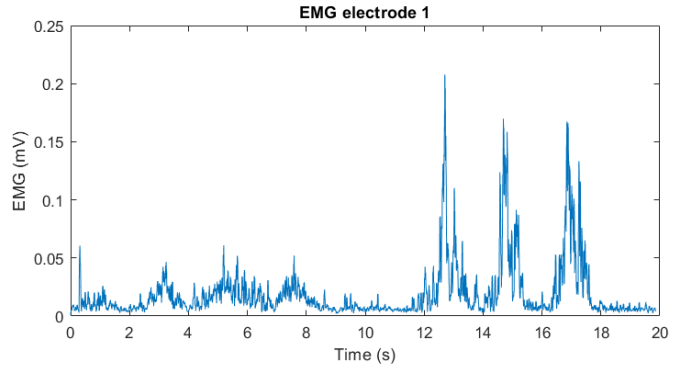

(a) Subject 3 MVC results for electrode 1 (gastronemius muscle).

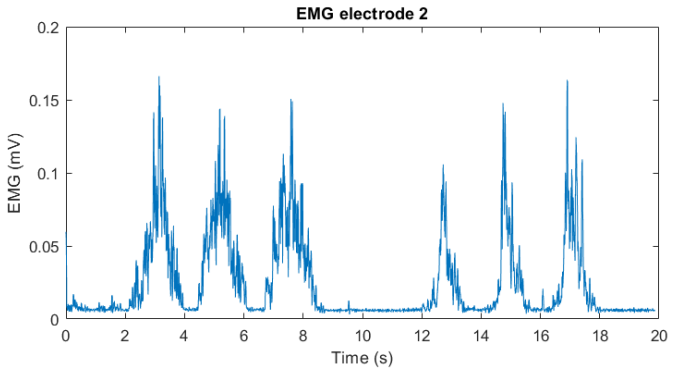

(b) Subject 3 MVC results for electrode 2 (tibialis anterior muscle).

Figure 4.22: MVC EMG results for subject 3.

4.1.4.2 Narrow band

The chosen time window for the signal was [10 60]s, it can be seen in Figure 4.23 (b). The output's statistical parameter for The chosen time window (without `detrend`) are in Table 4.1. In Figure 4.23 (d) the resulting FRF is presented for the NB trial. The red constant horizontal graphic represents the mean for this trial's gain at the chosen time window, which is the inverse of the stiffness.

From Figure 4.23 (d), it is possible to see the compliance part of this trial. It ends close to the cutoff frequency, and for this trial this value is $\omega_{c,NB3} = 1.719$ Hz. By inverting the compliance, the stiffness is obtained. Once the motor's stiffness is subtracted, the resultant ankle's stiffness is: $k_{a,NB3} = 5.6019$ *Nm/rad*.

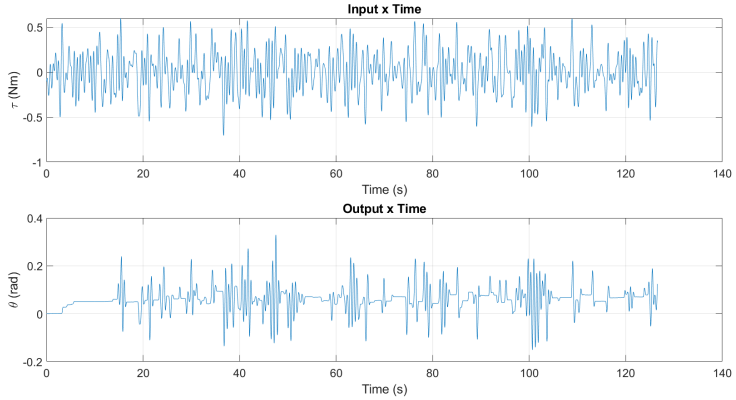

(a) Subject 3 NB input and output.

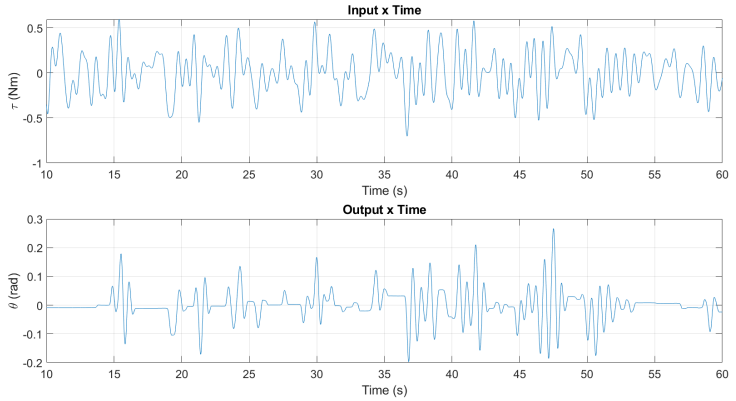

(b) Subject 3 NB `detrended` input and output, for the chosen time window.

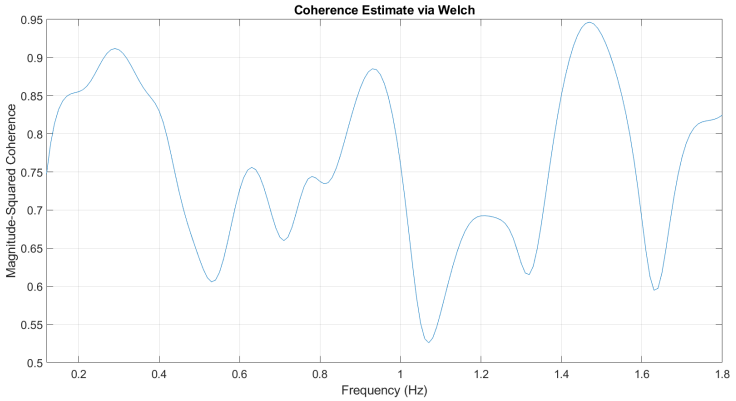

(c) Subject 3 NB Coherence.

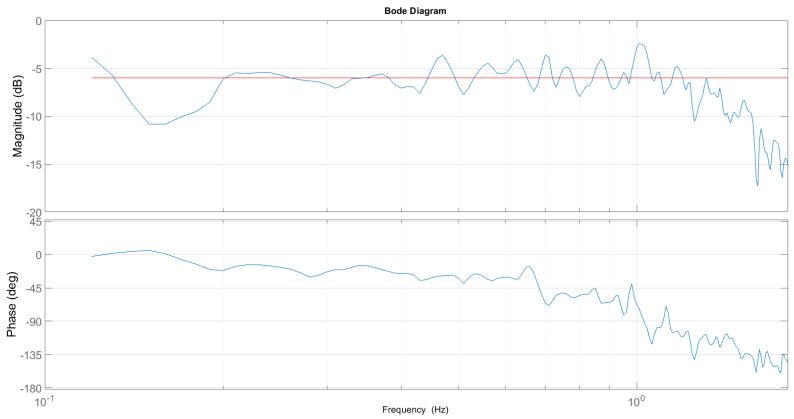

(d) Subject 3 NB FRF and respective gain mean (horizontal line) for the chosen time window.

Figure 4.23: NB results for subject 3.

The normalized EMG for both electrodes for subject 3 are presented in Figure 4.24. By the end of the results section, Table 4.2 presents the mean and standard deviation for the normalized EMG. Data for the non-normalized EMG and Accelerometer are presented in Figure 6.17 and Table 6.4 in the Appendix.

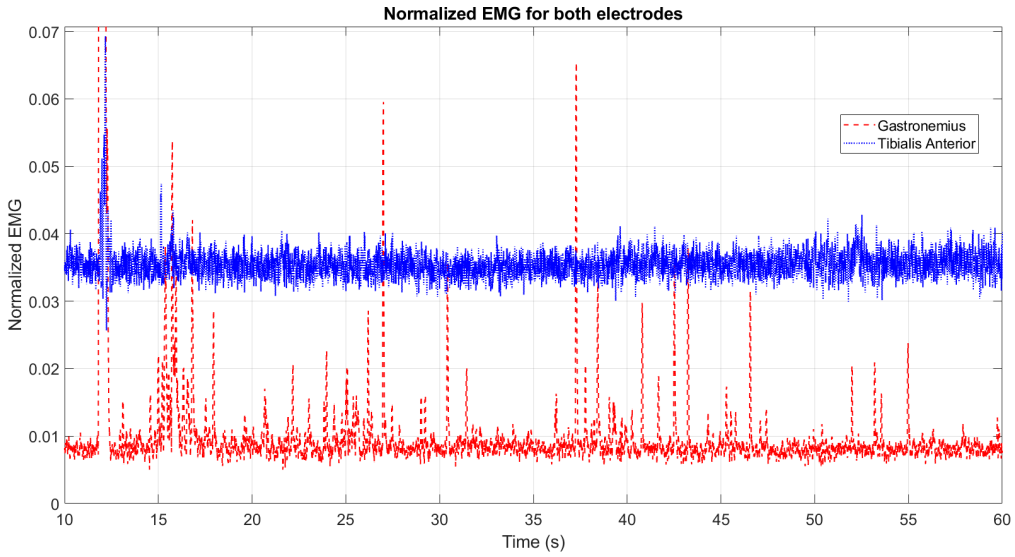

Figure 4.24: Normalized EMG NB trial for the gastronemius and tibialis anterior muscles for subject 4.

4.1.4.3 Wide band

The chosen time window for the signal was [60 120]s, it can be seen in Figure 4.25 (b). The output's statistical parameter for The chosen time window (without `detrend`) are in Table 4.1. In Figure 4.25 (d) the resulting FRF is presented for the WB trial. This FRF resembles a second order system. The TF can be represented by Equation 4.5 and it has the following parameterization: 2 poles and 0 zeros. The percentage of the FRF fit is 83.96%.

$$\mathrm{TF}_{3,\mathrm{WB(s)}} = \frac{79.12}{s^2 + 4.499s + 94.23} \tag{4.5}$$

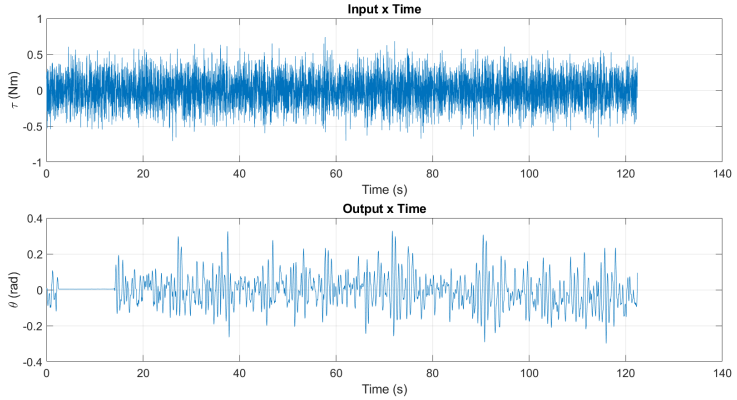

(a) Subject 3 WB input and output.

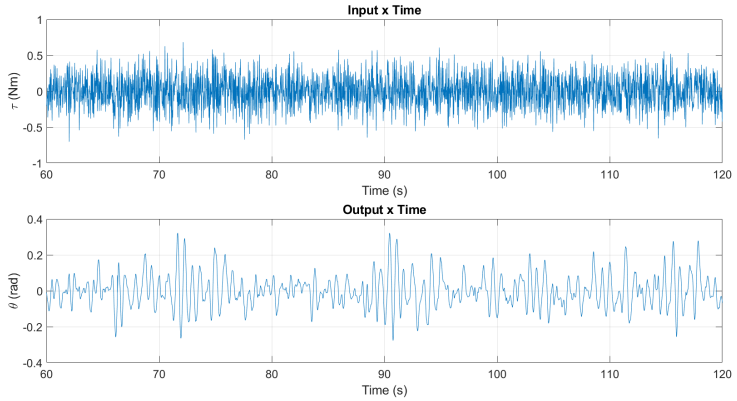

(b) Subject 3 WB `detrended` input and output, for the chosen time window.

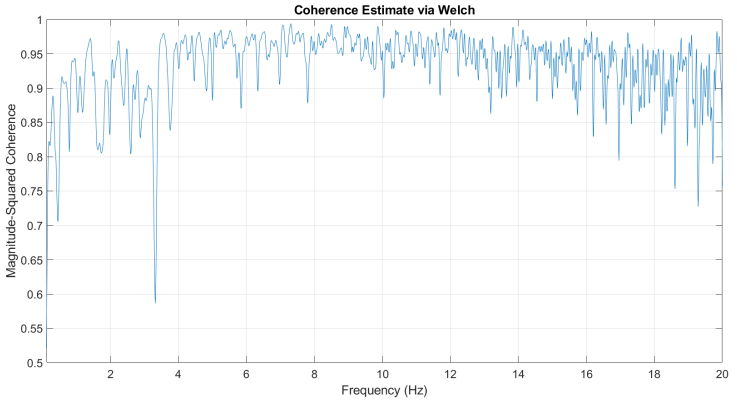

(c) Subject 3 WB Coherence.

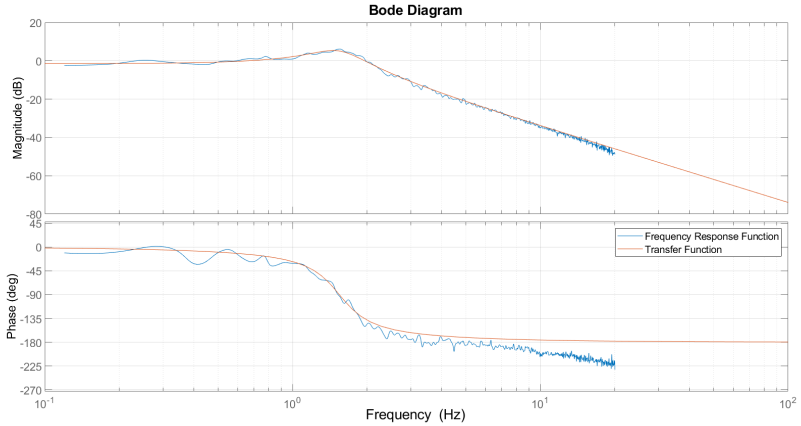

(d) Subject 3 WB fit.

Figure 4.25: WB results for subject 3.

The resulting impedance for this test was derived of the subtraction of the system total impedance and the motor impedance: $Z_{a,WB3} = Z_{am} - Z_m = \frac{s^2+4.505s+94.22}{79.21} - \frac{s^2+5.778s+45.73}{19.92} = \frac{-59.29s^2-367.9s-1745}{1578}$. By inverting the impedance the admittance is obtained: $Y_{a,WB3} = \frac{1}{Z_{a,WB3}} = \frac{-1578}{59.29s^2+367.9s+1745}$. The system's cutoff frequency is $\omega_{c,WB3} = 1.0299$ Hz and the damping ratio is $\zeta_{WB3} = 0.2883$. The damping ratio is between 0 and 1. Hence, this is an underdamped system.

The normalized EMG for both electrodes for subject 3 are presented in Figure 4.26. By the end of the results section, Table 4.2 presents the mean and standard deviation for the normalized EMG. Data for the non-normalized EMG and Accelerometer are presented in Figure 6.18 and Table 6.4 in the Appendix.

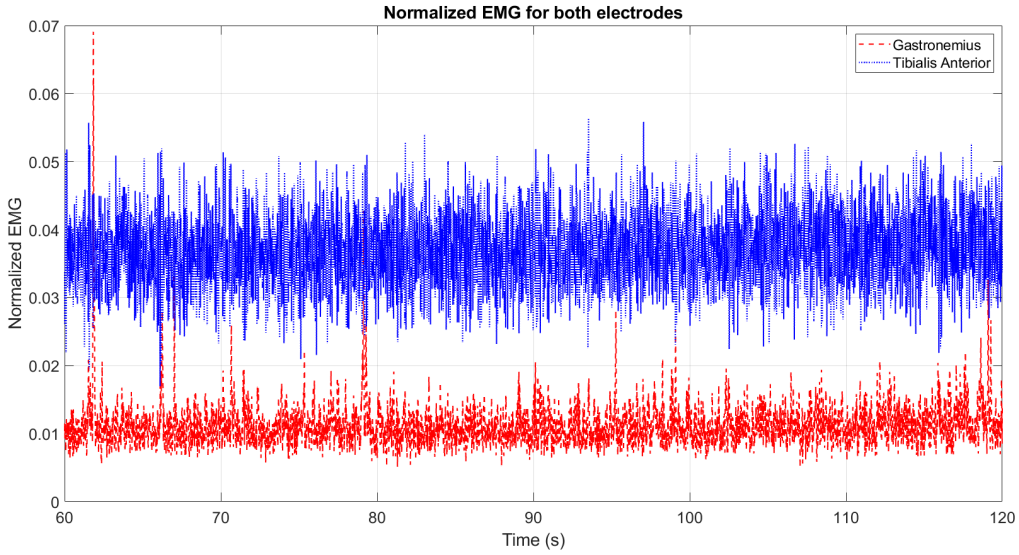

Figure 4.26: Normalized EMG NB trial for the gastronemius and tibialis anterior muscles for subject 3.

4.1.4.4 FRFs comparison between NB and WB

The FRFs comparison is presented in Figure 4.27. The difference between the WB and NB stiffness for the ankle isolated dynamics is 6.7081 *Nm/rad*.

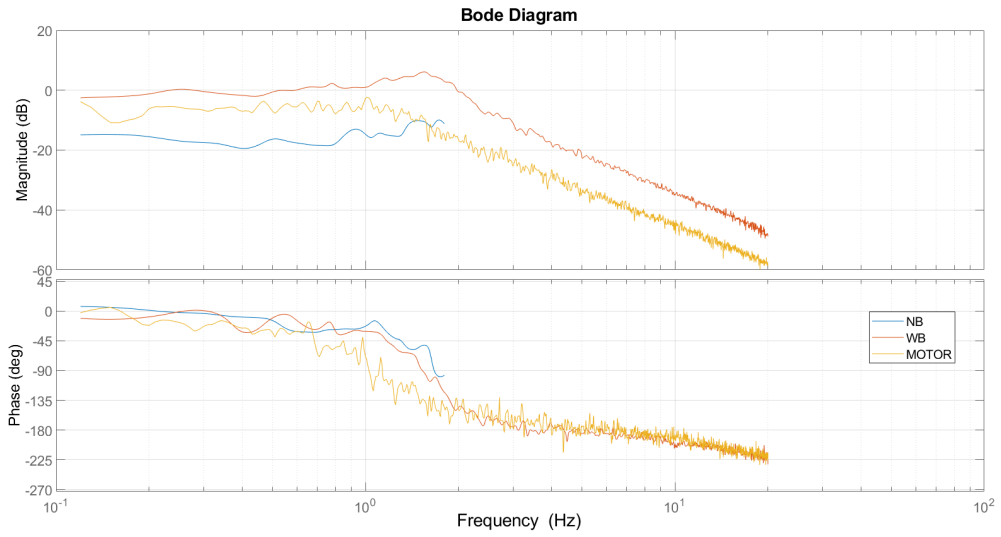

Figure 4.27: FRF overlap of the motor and NB, WB results for subject 3.

4.1.5 Subject 4

Results from the fifth experiment carried out with subject 4 are represented on this section. Firstly, Figure 4.28 constitutes results from the MVC trial. Then, NB (Figures 4.29 and 4.30) and WB (Figures 4.31 and 4.32) results are introduced. The power/frequency spectrum is presented in the Appendix in Figures 6.9 and 6.10. Lastly, FRF comparison results (Figure 4.34) are presented. The summary of the impedance and stiffness acquired is presented in Table 4.3 by the end of the Trials section.

4.1.5.1 Maximum Voluntary Contraction

In order to normalize EMG data, the MVC data presented below was collected for subject 4.

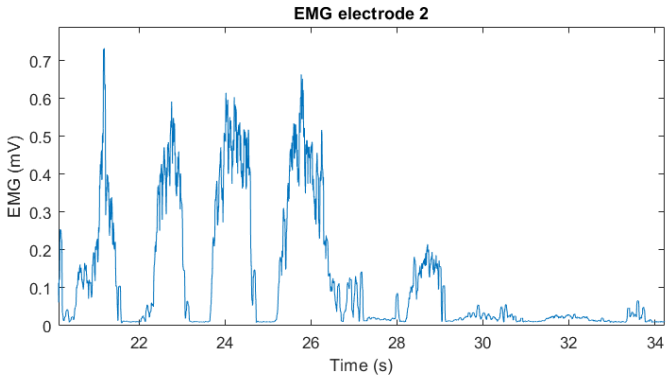

(a) Subject 4 MVC results for electrode 1 (gastronemius muscle).

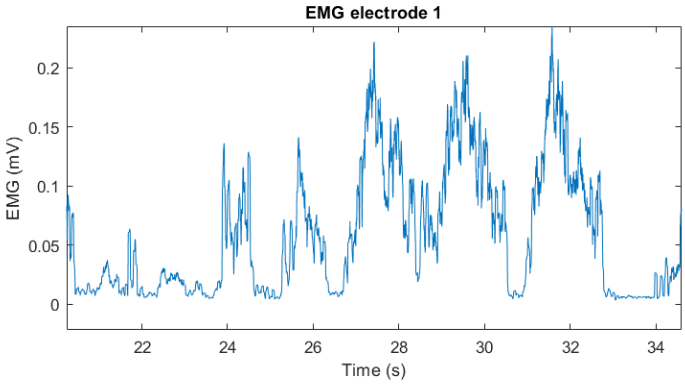

(b) Subject 4 MVC results for electrode 2 (tibialis anterior muscle).

Figure 4.28: MVC EMG results for subject 4.

4.1.5.2 Narrow band

The chosen time window for the signal was [50 150]s, it can be seen in Figure 4.29 (b). The output's statistical parameter for The chosen time window (without `detrend`) are in Table 4.1. In Figure 4.29 (d) the resulting FRF is presented for the NB trial. The red constant horizontal graphic represents the mean for this trial's gain at the chosen time window, which is the inverse of the stiffness.

From Figure 4.11 (d), it is possible to see the stiffness part of this trial. It ends close to the cutoff frequency, and for this trial this value is $\omega_{c,NB4} = 1.658$ Hz. By inverting the compliance, the system's stiffness is obtained. Once the motor's stiffness is subtracted, the resultant ankle's stiffness is: $k_{a,NB4} = 2.1139$ *Nm/rad*.

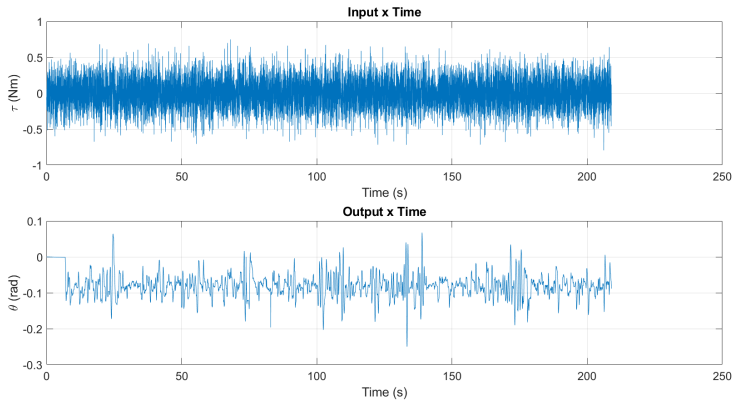

(a) Subject 4 NB input and output.

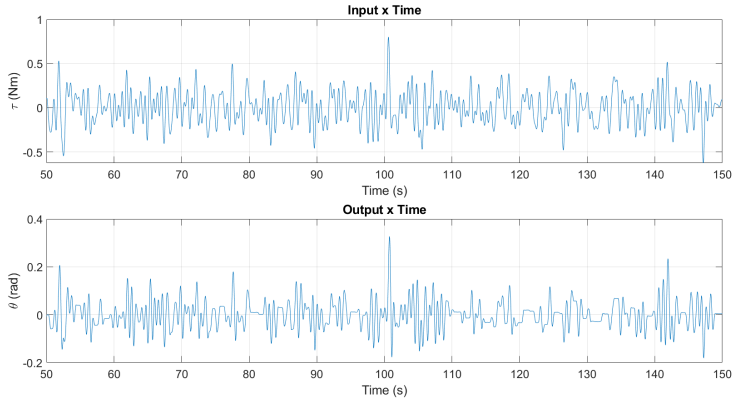

(b) Subject 4 NB `detrended` input and output, for the chosen time window.

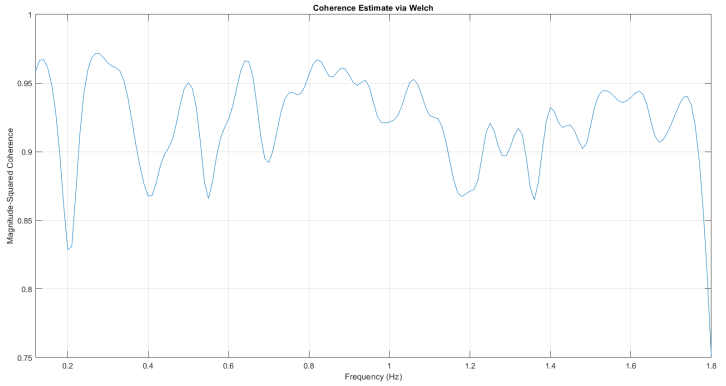

(c) Subject 4 NB Coherence.

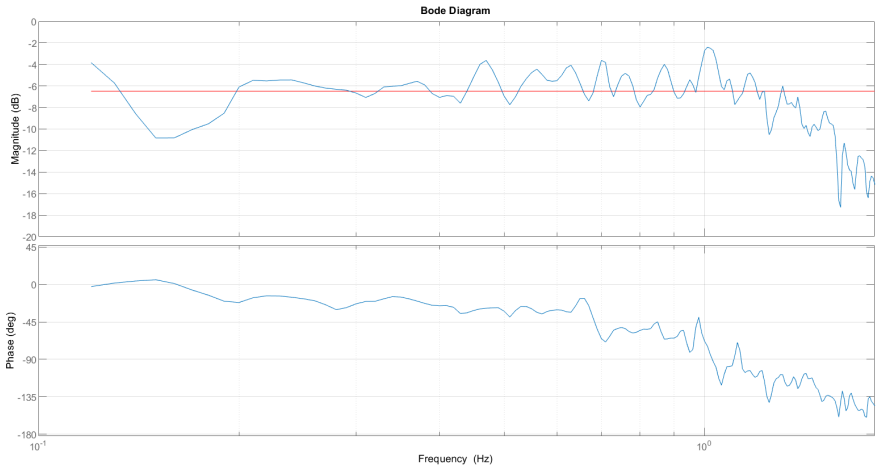

(d) Subject 4 NB FRF and respective gain mean (horizontal line) for the chosen time window.

Figure 4.29: NB results for subject 4.

The normalized EMG for both electrodes for subject 4 are presented in Figure 4.30. By the end of the results section, Table 4.2 presents the mean and standard deviation for the normalized EMG. Data for the non-normalized EMG and Accelerometer are presented in Figure 6.19 and Table 6.5 in the Appendix.

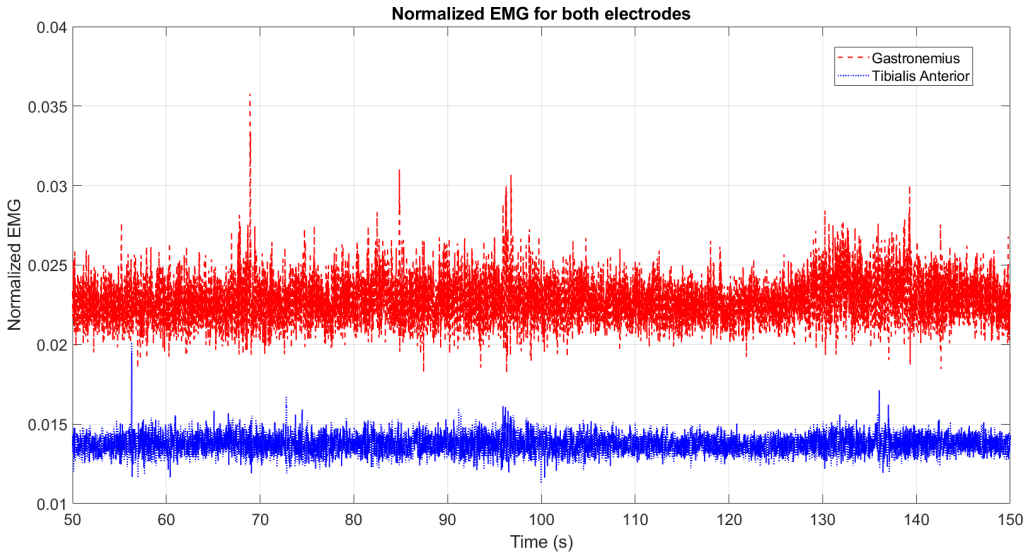

Figure 4.30: Normalized EMG NB trial for the gastronemius and tibialis anterior muscles for subject 4.

4.1.5.3 Wide band

The chosen time window for the signal was for it to start at 80s, it can be seen in Figure 4.31 (b). The output's statistical parameter for The chosen time window (without `detrend`) are in Table 4.1. In Figure 4.31 (d) the resulting FRF is presented for the WB trial. This FRF resembles a second order system. The TF can be represented by Equation 4.6 and it has the following parameterization: 2 poles and 0 zeros. The percentage of the FRF fit is 83.14%.

$$\mathrm{TF}_{4,\mathrm{WB}}(s) = \frac{36.65}{s^2 + 8.814s + 204.5} \tag{4.6}$$

The resulting impedance for this test was derived of the subtraction of the system total impedance and the motor impedance: $Z_{a,WB4} = Z_{am} - Z_m = \frac{s^2+8.814s+204.5}{36.65} - \frac{s^2+5.778s+45.73}{19.92} = \frac{-16.72s^2-36.14s+2398}{730.2}$. By inverting the impedance the admittance is obtained: $Y_{a,WB4} = \frac{1}{Z_{a,WB4}} = \frac{-730.2}{16.72s^2+36.14s-2398}$. The system's cutoff frequency is $\omega_{c,WB4} = 1.4606$ Hz and the damping ratio is $\zeta_{WB4} = 0.3366$. The damping ratio is between 0 and 1. Hence, this is an underdamped system.

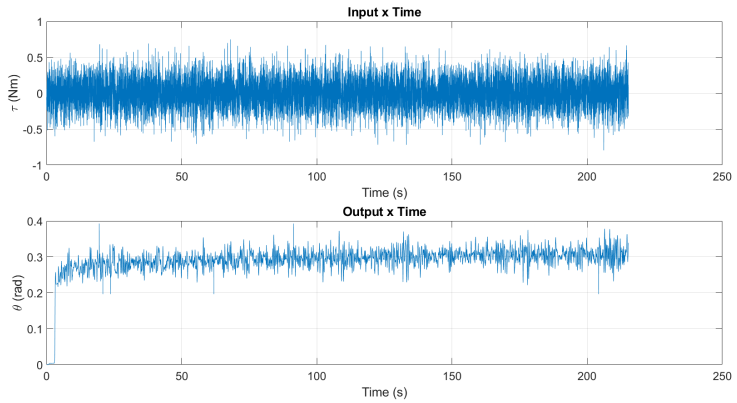

(a) Subject 4 WB input and output.

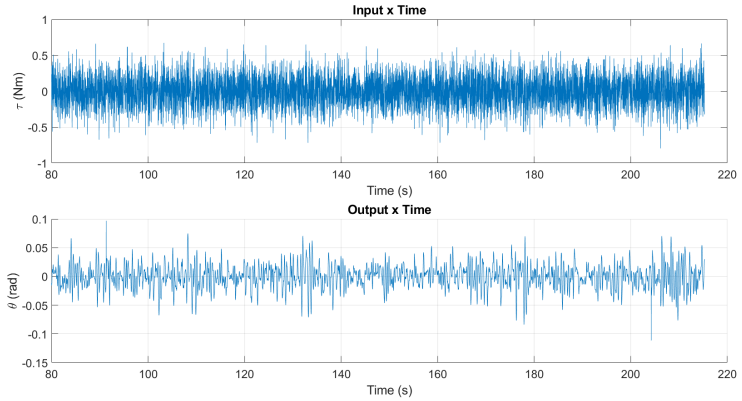

(b) Subject 4 WB `detrended` input and output, for the chosen time window.

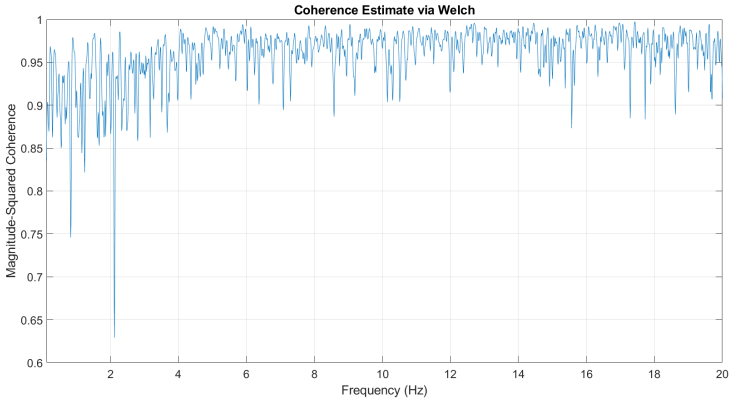

(c) Subject 4 WB Coherence.

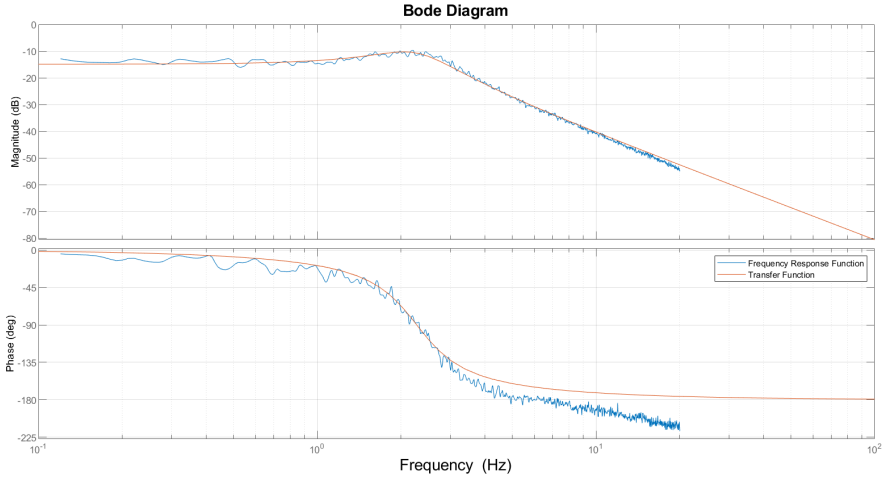

(d) Subject 4 WB fit.

Figure 4.31: WB results for subject 4.

The normalized EMG for both electrodes for subject 1 are presented in Figure 4.32. By the end of the results section, Table 4.2 presents the mean and standard deviation for the normalized EMG. Data for the non-normalized EMG and Accelerometer are presented in Figure 6.20 and Table 6.5 in the Appendix.

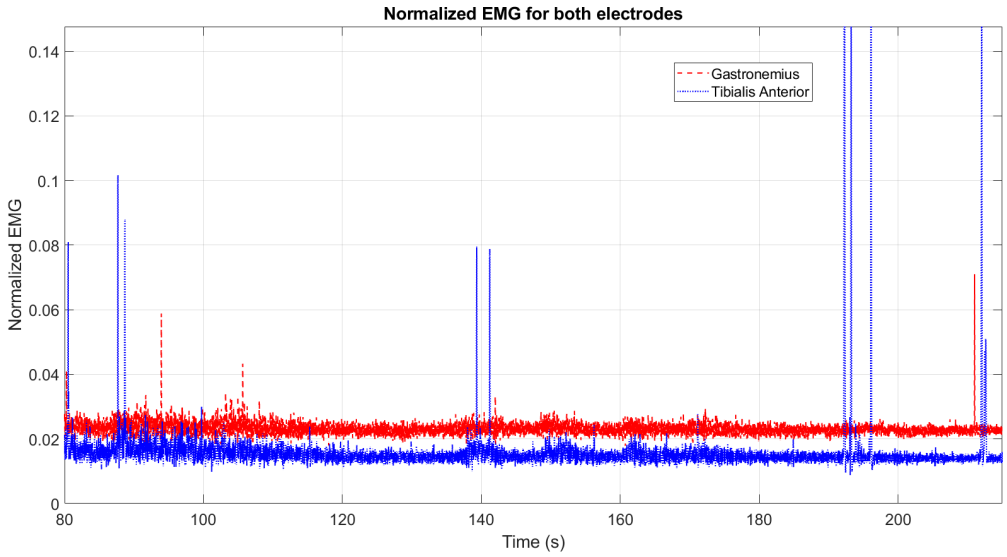

Figure 4.32: Normalized EMG WB trial for the gastronemius and tibialis anterior muscles for subject 4.

4.1.5.4 FRFs comparison between NB and WB

The FRFs comparison is presented in Figure 4.9. The difference between the WB and NB stiffness for the ankle isolated dynamics is -0.5102 *Nm/rad*.

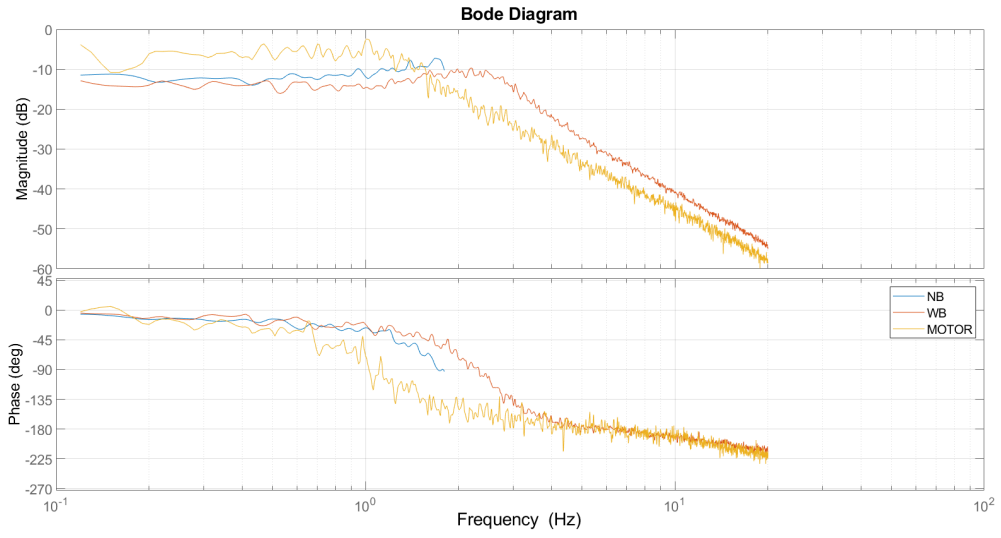

Figure 4.33: FRF overlap of the motor and NB, WB results for subject 4.

4.1.6 Results Summary

4.1.6.1 Input and Output

The mean and respective standard deviation results for NB and WB are presented in Table 4.1.

Table 4.1: NB and WB input and output mean, and respective standard erros, results for all of the subjects.

	Narrow Band		Wide Band	
	Input (*Nm*)	Output (*rad*)	Input (*Nm*)	Output (*rad*)
Subject 1	-0.0013 ± 0.2169	0.1784 ± 0.1183	$-1.1768 \times 10^{-4} \pm 0.1694$	0.2255 ± 0.0675
Subject 2 Trial 1	$7.3486 \times 10^{-4} \pm 0.2143$	0.1038 ± 0.0738	$-7.1076 \times 10^{-4} \pm 0.1871$	0.1402 ± 0.0425
Subject 2 Trial 2	$-9.7601 \times 10^{-5} \pm 0.1946$	-0.0810 ± 0.0314	$-4.9869 \times 10^{-4} \pm 0.1738$	-0.0824 ± 0.0189
Subject 3	-0.0029 ± 0.2278	0.0617 ± 0.0526	$-6.1896 \times 10^{-4} \pm 0.1942$	-0.0141 ± 0.0928
Subject 4	$-8.9200 \times 10^{-4} \pm 0.1820$	0.2846 ± 0.0569	$4.2642 \times 10^{-4} \pm 0.1947$	0.3018 ± 0.0204

4.1.6.2 EMG

The EMG (electrode 1: Gastronemius; electrode 2: Tibialis Anterior) results for NB and WB are presented in Table 4.2.

Table 4.2: NB and WB EMG normalized results for all of the subjects for each electrode (Gastronemius and Tibialis Anterior muscles).

	Narrow Band		Wide Band	
	Gastronemius	T. Anterior	Gastronemius	T. Anterior
Subject 1	$0.0044 \pm 7.9693 \times 10^{-4}$	$0.0114 \pm 6.0979 \times 10^{-4}$	$0.0044 \pm 7.3835 \times 10^{-4}$	$0.0117 \pm 5.9315 \times 10^{-4}$
Subject 2 Trial 1	0.0092 ± 0.0017	0.0425 ± 0.0033	0.0109 ± 0.0023	0.0433 ± 0.0063
Subject 2 Trial 2	0.0151 ± 0.0017	0.0404 ± 0.0015	0.0298 ± 0.0110	0.0562 ± 0.0231
Subject 3	0.0340 ± 0.3661	0.0356 ± 0.0020	0.0114 ± 0.0032	0.0374 ± 0.0049
Subject 4	0.0229 ± 0.0013	$0.0138 \pm 5.1624 \times 10^{-4}$	0.0233 ± 0.0019	0.0161 ± 0.0105

4.1.6.3 Impedance and Stiffness

The frequency response function results, impedance and stiffness, for NB and WB are presented in Table 4.3.

Table 4.3: NB and WB stiffness and impedance results for all of the subjects.

	NB Stiffness (*Nm/rad*)		WB Impedance		$\Delta k = \mathrm{k}_{NB} - k_{WB}$ (*Nm/rad*)
	Ankle + Motor	Ankle	Ankle + Motor	Ankle	
Subject 1	2.8266	0.5309	$\frac{s^2+5.156s+148}{102.2}$	$-\frac{82.27s^2+487.7s+1724}{2036}$	1.3784
Subject 2 Trial 1	4.3167	2.0210	$\frac{s^2+7.507s+99.89}{47.22}$	$-\frac{27.3s^2+123.3s+169.1}{940.9}$	2.2013
Subject 2 Trial 2	5.5702	3.2745	$\frac{s^2+10.18s+152.9}{34.46}$	$\frac{-14.53s^2+3.652s+1470}{686.6}$	1.1332
Subject 3	7.8976	5.6019	$\frac{s^2+4.505s+94.22}{79.21}$	$-\frac{59.29s^2+367.9s+1745}{1578}$	6.7081
Subject 4	5.0696	2.1139	$\frac{s^2+8.814s+204.5}{36.65}$	$-\frac{16.72s^2+36.14s-2398}{730.2}$	-0.5102

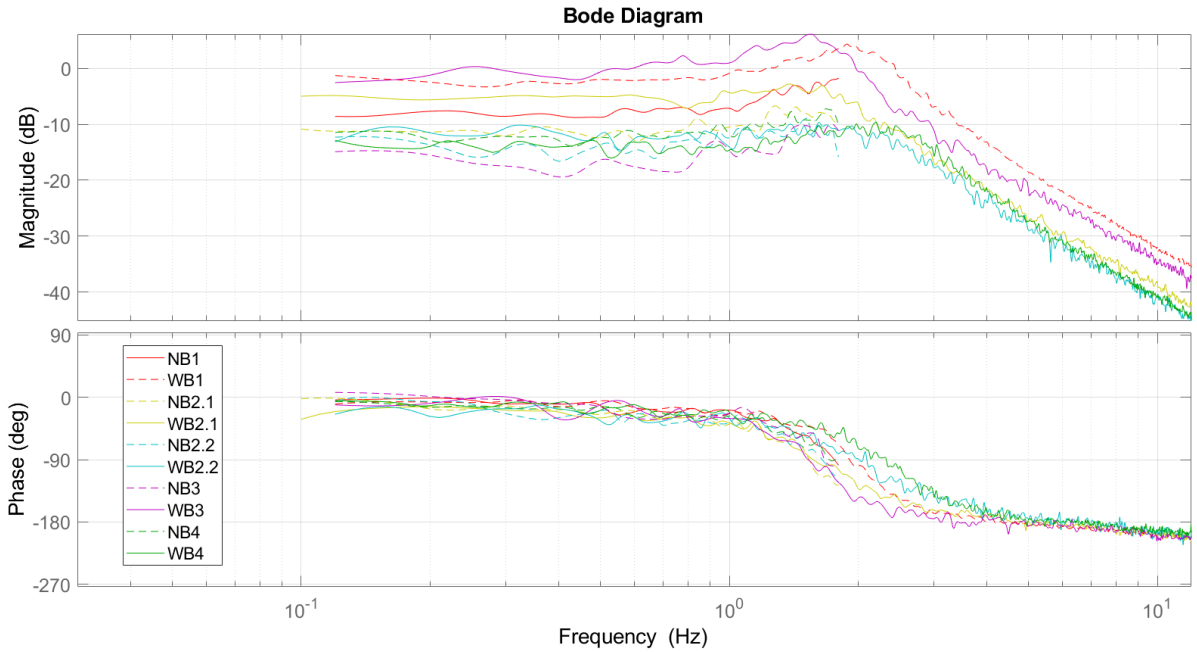

Figure 4.34: FRF overlap of all of the NB and WB results for all subjects.

4.2 Analysis

Firstly, the motor's dynamics was studied. The selected window was to eliminate the first 10s to erase that constant value registered initially in the output signal (Figure 4.1 (a) and (b)). The coherence obtained (Figure 4.1 (c)) has low values at a low frequency range but then stabilizes to values extremely close to 1. This means an existence of a good linear relation between the input and output (Figure 4.1 (d)). Visually, a second order system is a good approximation for the motor's dynamics. The high percentage fit confirms that (74.67%). The motor's obtained cutoff WB frequency was $\omega_c = 1.075$ Hz. From that value on, the signal will be filtered, which means that the amplitude is attenuated, enabling a comparison to a low pass filter dynamics. By inverting the FRF, the impedance for the WB trial is obtained. From that, it was possible to isolate the ankle's dynamics from the total system's (ankle+motor) for all of the following WB trials.

For the NB trials, a FRF was estimated using the same trial as the WB but only considering the stiffness factor. Figure 4.2 results showed that the motor's dynamics does not vary from the NB to the WB frequency range, so it is confirmed that the same trial can be used for both of the bandwidths. The peak between [0.5 0.9] Hz is the part where NB and WB show the most difference for this motor trial. This difference is not significant and it can be concluded that the NB and WB results for this trial are mostly the same. Nonetheless, the NB trial values are the most reliable, since this trial had a higher coherence (Figure 4.3).

With the previous conclusion, it was confirmed that the motor's stiffness could be obtained by considering $s = 0$ in the WB trial. From that result, it was possible to isolate the ankle's stiffness from the total's stiffness (ankle+motor) for all of the following NB trials.

4.2.1 Frequency Response

In general, the obtained signals were very satisfactory for this study. Before moving forward with any comparison it is important to check if the results were even comparable. The mean was acquired for the input and output signals for both the NB and WB trials. The results showed that the mean was similar for the different bandwidths (Table 4.1).

The NB results showed lower coherences when compared to the WB trials. However, the difference is not that substantial and the coherence values are not considerably low. In some cases it was obtained a lower coherence at the beginning (Figure 4.5 (c)), middle (Figure 4.23 (c)) or at the end of the frequency range (Figure 4.29 (c)). This could be due to: transient behavior (initial signal fluctuations or sudden changes can cause low coherence) or signal processing artifacts (pre-processing or filtering can introduce errors in the initial signal). Nevertheless, for most of the frequency range, the signals have an elevated coherence (close to 1).

The power/frequency spectrum is very similar for all of the NB trials. Frequencies with significant power are predominantly at the spectrum's extremities for the input. Nevertheless, the inputs' spectra are mostly flat, varying between an amplitude of [-26 -16] dB/Hz. For the outputs, it seems that the power is lower, it varies between [-38 -26] dB/Hz. Power/frequency spectra are presented in the Appendix.

As explained many times during this dissertation, it does not make sense to do a fit in the NB FRFs. The resulting FRFs for the NB trials are similar to each other. The mean gain seems to be similar for most of the trials. It varies between [-8 -6] dB. For trial 2 of subject 2, the mean is -14 dB, which outlies from all of the others FRF. This could simply mean that this subject's stiffness varies differently from the other's.

Stiffness results varied between [0.5309 5.6019] *Nm/rad*. Results for subject 1 and subject 3 have a significant difference from the others. In the case of subject 1, the stiffness is too low, which means that his stiffness is too close from the motor's stiffness. Therefore, subject 1 seem to have a low stiffness value. As a result, less motor units present synchronized firing and, consequently, the reflex gain is smaller. This could just be a natural subject's characteristic. However, it could also be a result of muscle weakness, neuromuscular condition, medications, previous injuries, among other possibilities. Subject 3 presents the highest stiffness result. This subject might naturally have a higher baseline muscle tone and reflex gains. Nonetheless, when the stiffness value are too high, it might indicate a pathology.

The cutoff frequency for the NB trials varied between [1.448 2.094] Hz. From this results it is possible to say that the cutoff frequencies are very similar for the NB trials since they did not varied much from each other.

As mentioned before, coherences seem to be higher for the WB trials. For most cases, coherence is a little bit lower at the beginning and at the end of the frequency range. But overall, the coherence is mostly close to 1. The power/frequency spectrum are pretty much identical for all of the WB trials. For the inputs, it seems that the power is constant through the frequency range for all of the subjects, its amplitude varies between [-40 -24] dB/Hz. Frequencies with significant power are predominantly at the beginning of the output's spectrum, since the curve is descending. Values vary between [-90 -20] dB/Hz. Power/frequency spectra are presented in the Appendix.

The WB FRF approximation to a second order system is considerably good, since the FRF fit results have a high percentage. The lowest percentage is 79.86% (subject 2, trial 2) and the highest is 87.78% (subject 1). Visually, the WB FRFs look almost identically to a second order system. After isolating the ankle's dynamics from the motor's, the resulting cutoff frequency showed to be of the same order of magnitude to all of the WB trials. This value is an important parameter as it provides information

about the system's ability to respond to different frequencies of perturbations. A high cutoff frequency implies that the system can respond effectively to a wide range of frequencies. It can accurately capture and represent rapid changes in the input signal or perturbations, including high-frequency variations. Conversely, a low cutoff frequency means that the system's response is limited to lower frequencies, and it may not capture rapid changes or high-frequency components in the input signal. It tends to smooth out or attenuate higher-frequency details. Considering that the wide band interval is approximately [0.12 20] Hz, the cutoff frequencies for the WB trials are low, which fits in the last conclusion and it also permits to conclude that this system can be compared to a low pass filter.

The damping ratio results vary between [0.1226 0.3604]. Since they vary between 0 and 1, it leads to the conclusion that all of the trials relate to an underdamped system. Having an underdamped system means that they are not heavily damped, and oscillations occur as a system's response. For the ankle, it might indicate a healthy neuromuscular system capable of producing oscillatory reflex responses (stretch reflex). (Zhang et al., 2013)

Literature suggested that stretch reflex dynamics are primarily governed by muscle spindles, particularly at lower frequencies near their resonance, enhancing reflex mechanisms. Higher frequencies, conversely, dampen reflex responses, with synchronous firing of spindle sensory fibers leading to reflex initiation (Kearney, Stein, et al., 1997). As perturbation frequency increases, synchronous firing likelihood diminishes. Since the stretch reflex is highly associated with the stiffness, as many studies have showed, a higher stretch reflex indicate a higher the muscle stiffness. It is expected from the frequency response study for the narrow frequency bandwidth to present higher stiffness values. (Helm et al., 2002)

Hence, it is expected for the stretch reflex to predominate at lower frequencies. As a consequence, the stiffness will also be prominent at lower frequencies. In this study, the lower frequencies are represented by the narrow band range of frequency. The FRFs WB and NB comparison represented by their bode diagrams overlap are mostly consistent. For most of the subjects, the gain is higher for the WB trial, which means a higher stiffness for the NB trials. This means a higher stretch reflex activity as well.

Nonetheless, for the last trial (Figure 4.34), subject 4 presented a slightly higher gain for the NB trial. This means that the NB's stiffness is lower than the WB's, as it can also be confirmed by the negative Δk in Table 4.3. This was not expected and can indicate that the subject have an unique reflex response and neuromuscular specific characteristics. Even so, the NB and WB are almost overlapping, so the difference is not that significant.

Another unexpected result is for the motor to have a higher impedance than the trials with motor+ankle for the WB results. This result leads to an ankle's negative impedance. This results was already anticipated from the FRF overlapping plot of NB, WB and the motor, for each subject. In this overlap, the motor gain was always higher than the NB gain and lower than the WB gain. As a consequence, the motor has lower stiffness than NB trials and higher impedance than the WB trial. This result can be attributed to the characteristics of the motor and how it interacts with the ankle. This outcome may indicate that, in specific conditions or frequency ranges, the motor's dynamics are more prominent or influential than those of the ankle. Additional testing may be necessary to reach further conclusions.

4.2.2 Electromiography

From the normalized EMG, the mean was obtained. The mean is used to compare the EMG amplitudes between NB and WB, and also between subjects. From that, it is possible to ascertain for whether the amplitude is higher for the NB or for the WB trial. From the literature, it is expected to obtain differences between the EMG results (Kearney and Hunter, 1984; Schouten et al., 2008a). The amplitude

should be higher for the NB results, where the stiffness is the principal factor, this was confirmed in the FRFs results of this study. As explained before, the stiffness is related to the stretch reflex. A system where the stiffness is more prominent should result in a raised stretch reflex rate as well. Which should result in a augmentation of the EMG results.

From Table 4.2, the EMG response can be evaluated in a dimensionless way in a scale from 0 to 1. Zero means no contraction and one means maximum contraction. The results obtained showed little to no discrepancies between NB and WB results for all of the subjects. Most of the results are also closer to 0 than to 1, which means that low amplitude contractions were detected.

Hence, from the EMG data acquired, it was not possible to have any conclusion for whether the reflexes are more accentuated in the narrow band or in the wide band frequency range. Sometimes, the difference can be a bit significant. For example, in subject 2 (trial 2) or subject 3, the gastronemius muscle shows more activity for the narrow band frequency range. However, this could be due to a voluntary contraction, since it is not a consistency in the results for the other subjects.

As mentioned before, in this dissertation experimental work, subjects were relaxed and did not tried to oppose the input perturbations, whilst in other studies subjects were asked to contract the muscles. Which means, this was uncharted territories and a tentative to shed light on an unknown facet of ankle reflex dynamics. Additional testing would be necessary to confirm that the results are not affected by other factors that are non-reflex related.

Chapter 5

Conclusion

In the pursuit of understanding the intricate mechanisms governing human locomotion and neuromuscular control, this dissertation delved into the fascinating realm of ankle reflex dynamics. The human ankle, a pivotal joint in maintaining stability and facilitating movement, relies heavily on reflex responses to external perturbations. This study focused on the examination of these reflex dynamics through the manipulation of the frequency bandwidth (narrow band and wide band), with torque as the input stimulus and displacement angle as the resultant output. The fundamental premise of this investigation revolves around the manipulation of the frequency bandwidth, employing both narrow and wide frequency bands to perturb the ankle system. Torque was the perturbation input and the displacement angle was the resultant output.

The underlying hypothesis that steered the course of this investigation proposes a perspective wherein the frequency characteristics inherent in the applied stimulus transcend mere subtleties; rather, they emerge as indispensable factors that significantly shape the response of the ankle reflex. This proposition asserts that the alterations in the frequency bandwidths are not inconsequential nuances but, in fact, pivotal determinants that give rise to discernible variations in reflex gains. This, in turn, provides an insightful lens through which we can glean a distinctive understanding of the adaptability and sensitivity intrinsic to the ankle reflex system.

The findings of the study, when it comes to the frequency response results, validate the expected outcomes as documented in the existing body of literature. These anticipated results align with the prevailing understanding that within the spectrum of frequency ranges, the reflex dynamics exhibit a more pronounced influence in the context of a narrow bandwidth. In contrast, the wider band frequency range appears to exhibit relatively less significant reflex dynamics. This confirmation not only substantiates the previously established knowledge but also provides a nuanced perspective on the distinctive characteristics associated with reflex behaviors across varying frequency ranges.

Unfortunately, an analogous outcome could not be attained through electromyography analysis, as the results obtained from both wide band and narrow band assessments exhibited a near-identical amplitude. This lack of differentiation in the EMG outcomes could potentially be attributed to a variety of contributing factors. These factors encompass a spectrum ranging from the specific conditions under which the experiment was conducted, the positioning of the electrodes utilized in the measurement process, to the varied responses exhibited by the muscles of the subjects involved. Additionally, the semblance in amplitudes observed in the filtered EMG signals may be a consequence of identical filtering settings applied to both narrow band and wide band signals, among various other plausible considerations. The complexity and multifaceted nature of these factors underline the intricacies inherent in interpreting EMG data, emphasizing the need for a comprehensive and nuanced approach to discerning

the intricacies of muscle responses within the experimental context.

In the comprehensive analysis of this dissertation's objectives, it is affirmatively established that the set goals have been successfully realized, culminating in the confirmation of the primary hypothesis through the elucidation provided by the frequency response function results. These findings not only signify the attainment of the overarching research objectives but also serve as a substantive response to the fundamental inquiry encapsulated in the dissertation's central question: "How does the manipulation of stimulus frequency impacting the ankle system influence the intricate dynamics of the ankle reflex?" Revisiting this pivotal question, the response surfaces once more, elucidating that the ankle system exhibits discernible variations in its response patterns in direct correlation with alterations in the frequency bandwidth. This underscores the significance of frequency modulation in influencing the dynamics of the ankle reflex.

However, it is imperative to note that the electromyography outcomes presented a less straightforward interpretation, warranting a nuanced examination of the methodological approaches employed. The results suggest the potential necessity for refining and fine-tuning the procedures associated with electromyographic measurements, indicating that procedural adjustments may be requisite for achieving significant outcomes within the specific context of this study. This acknowledgment emphasizes the ongoing iterative nature of scientific inquiry, encouraging future investigations to delve deeper into the intricacies of EMG methodologies to glean more robust and conclusive insights in the realm of ankle reflex dynamics.

5.1 Future Work

This dissertation explored the ankle's reflexes, investigating their behavior across different bandwidths and shedding light on the complex interplay between sensory input and motor responses in the human ankle reflex system. While offering valuable insights, the study sparks curiosity for further exploration. Through result analysis, promising avenues emerge for advancing our understanding of ankle reflexes in clinical and physiological contexts, with potential implications for medical diagnostics, rehabilitation strategies, and neurophysiological studies.

Firstly, it was concluded that mechanical differences could be identified but not neurological. Other studies EMG's results showed a reflex dynamics variation for different bandwidths. To address potential electrode positioning impact, altering the electrode placement is recommended in future research.

The results may stem from reflex arch amplitude, potentially amplified by altering input type. Instead of a random signals mix, future research could explore the impact of abrupt signals such as step functions, impulse functions, or rectangular pulses. In Dias, 2022, Dias also made experiments using chirp signals as input. This could be done to check if the input signal has any influence under the conclusions. Kearney et al. used displacement angle as input and torque as output, resulting in a signal with less noise. This approach could also be applied in future studies.

The obtained results could be specific for the bandwidths used, so in future work, it could be used a range of NB and WB bandwidths, to eliminate this hypothesis.

In this dissertation, FRFs were approximated to a second-order mass-spring-damper system. Future exploration could consider alternative system approximations, like the Hill-type muscle model commonly used in biomechanical and physiological studies.

Lastly, assuming relaxation during experiments solely produces reflex outcomes may be overstated, even with equal voluntary contribution in both bandwidths. Future studies could refine this by isolating the reflex component through a specific algorithm, as previously done by Kearney and others.

Bibliography

Aeyels, D. and J. Willems (1995). *Digital Control Systems Implementation Techniques*. New York: Academic Press, pp. 353–378.

Allum, J. and K. Mauritz (1984). "Compensation for intrinsic muscle stiffness by short-latency reflexes in human triceps surae muscles". In: *J Neurophysiol* 52.5, pp. 797–818.

Burdet, E., D. Franklin, and T. Milner (2013). *Human Robotics: Neuromechanics and Motor Control*. England: The MIT Press.

Caires, N. (2022). "Impedance Controlled Planar Flexible Robot for Identification of Human Ankle Dynamics". Instituto Superior Técnico da Universidade de Lisboa.

Carr, J. (2000). *Chapter 6 - Filtering Electronic Circuits*. Woburn: Newnes.

Carter, R., P. Crago, and P. Gorman (1993). "Nonlinear stretch reflex interaction during cocontraction". In: *Biol Cybern* 69.3, pp. 943–952.

Carter, R., P. Crago, and M. Keith (1990). "Stiffness regulation by reflex action in the normal human hand". In: *J Neurophysiol* 64.1, pp. 105–118.

Carvalho, N. et al. (2008). "Multisine Signals for Wireless System Test and Design [Application Notes]". In: *IEEE Microwave Magazine* 9.3, pp. 122–138.

CENTRAL HEALTH: physiotherapy (2023). *Ankle & Foot Pain*. [Online]. URL: `https://www.central-health.com/ankle-foot-pain/`.

Coelho, R. (2021). "Characterization of Gait and Ankle Impedance Towards Rehabilitation". PhD thesis. Instituto Superior Técnico da Universidade de Lisboa.

Crago, P. E., J. C. Houk, and Z. Hasan (1976). "Regulatory actions of human stretch reflex". In: *Journal of neurophysiology* 39.5, pp. 925–935.

Delsys (2023). *Delsys*. [Online]. URL: `https://delsys.com/`.

DeLuca, C. et al. (1982). "Behaviour of human motor units in different muscles during linearly varying contractions". In: *J Physiol* 329.28.

Derderian, C., K. Shumway, and P. Tadi (2023). "Physiology, Withdrawal Response". In: *National Library of Medicine*.

Dias, V. (2022). "Frequency Domain Identification of the Human Ankle Dynamics". Instituto Superior Técnico da Universidade de Lisboa.

Eccles, J. and R. Granit (1929). "Crossed extensor reflexes and their interaction". In: *Journal of Neuroscience Methods* 67.1, pp. 97–118.

Gordon, A., A. Huxley, and F. Julian (2004). "The variation in isometric tension with sarcomere length in vertebrate muscle fibres". In: *Philosophical transactions of the Royal Society of London, Series B, Biological sciences* 184.1, pp. 170–192.

Helm, F. van der et al. (2002). "Identification of Intrinsic and Reflexive Components of Human Arm Dynamics During Postural Control". In: *Journal of Neuroscience Methods* 119.1, pp. 1–14.

Henneman, E. et al. (1974). "Rank order of motoneurons within a pool: law of combination". In: *Journal of neurophysiology* 37.6, pp. 1338–1349.

Hoffer, J. and S. Andreassen (1981). "Regulation of soleus muscle stiffness in premammillary cats: Intrinsic and reflex components". In: *Journal of neurophysiology* 45, pp. 267–85.

Horak, F., D. Wrisley, and J. Frank (1993). "The Balance Evaluation Systems Test (BESTest) to differentiate balance deficits". In: *Acta Neurol Scand* 89.5, pp. 484–498.

Houk, J. (1979). "Regulation of stiffness by skeletomotor reflexes". In: *Annual review of physiology* 41, pp. 99–114.

Housed Direct Drive Rotary (DDR) Motors: Selection Guide (2017). Kollmorgen. North America.

Huxley, A. and H. Huxley (1957). "Muscle structure and theories of contraction. Progress in biophysics and biophysical chemistry". In: *Acta Neurol Scand* 7, pp. 255–318.

Kearney, R. and W. Hunter (1984). "System Identification of Human Stretch Reflex Dynamics: Tibialis Anterior". In: *Experimental Brain Research* 56, pp. 40–49.

Kearney, R., R. Stein, and L. Parameswaran (1997). "Identification of Intrinsic and Reflex Contributions to Human Ankle Stiffness Dynamics". In: *IEEE Transactions on Biomedical Engineering* 44.6, pp. 493–504.

Lacquaniti, F., F. Licata, and J. Soechting (1982). "The mechanical behavior of the human forearm in response to transient perturbations". In: *Biol Cybern* 44.1, pp. 35–46.

Lee, H., H. Krebs, and N. Hogan (2014). "Multivariable dynamic ankle mechanical impedance with relaxed muscles". In: *IEEE Transactions on Neural Systems and Rehabilitation Engineering* 22.6, pp. 1104–14.

Leonard, T., M. DuVall, and W. Herzog (2010). "Force enhancement following stretch in a single sarcomere". In: *American journal of physiology* 299.6, pp. 1398–1401.

Ljung, L. (1999). *System Identification: Theory for the User*. Upper Saddle River, NJ: Prentice Hall.

Lyle, M. and T. Nichols (2019). "J Physiol." In: *Journal of Neuroscience Methods* 597.17, pp. 4627–4642.

McMahon, T. (1984). *Muscles, Reflexes, and Locomotion*. Lauflabor: Institut für Sportwissenschaft Friedrich-Schiller-Universität Jena.

Mendez-Rebolledo, G. et al. (2021). "Contribution of the peroneus longus neuromuscular compartments to eversion and plantarflexion of the ankle". In: *PLoS One* 16.4, pp. 267–85.

Michael-Titus, A., P. Revest, and P Shortland (2010). *The Nervous System: Systems of the Body Series*. London, England: Elsevier Health Sciences.

Milner-Brown, H., R. Stein, and R. Lee (1975). "Synchronization of human motor units: possible roles of exercise and supraspinal reflexes". In: *Electroencephalography and clinical neurophysiology* 38.3, pp. 245–254.

Nicholas, S., D. Doxey-Gasway, and W. Paloski (1998). "A link-segment model of upright human posture for analysis of head-trunk coordination". In: *Journal of vestibular research : equilibrium orientation* 8.3, pp. 187–200.

Nyitrai, M. and M. Geeves (2004). "Adenosine diphosphate and strain sensitivity in myosin motors". In: *Philosophical transactions of the Royal Society of London, Series B, Biological sciences* 359, pp. 1867–1877.

Ogata, K. (1970). *Modern Control Engineering*. Saddle River, NJ, United States: Prentice Hall PTRUpper.

Partridge, L. (1965). "Stretch reflex interactions studied with the aid of simulation". In: *Am J Phys Med*.

Purves, D., G. Augustine, and D. Fitzpatrick (2001). *Neuroscience: The Motor Unit*. Sunderland: Sinauer Associates.

Schouten, A., E. de Vlugt, and F. van der Helm (May 2008a). "Design of Perturbation Signals for the Estimation of Proprioceptive Reflexes". In: *IEEE Transactions on Biomedical Engineering* 55.5, pp. 1612–1619.

Schouten, A., E. Vlugt, and F. van der Helm (2008b). "Design of Perturbation Signals for the Estimation of Proprioceptive Reflexes". In: *IEEE Transactions on Biomedical Engineering* 55.5, pp. 1612–1619.

Sinkjaer, T. and R. Hayashi (1989). "Regulation of wrist stiffness by the stretch reflex". In: *J Biomech* 22.11, pp. 1133–1140.

Stein, R. and R. Kearney (1995). "Nonlinear behavior of muscle reflexes at the human ankle joint". In: *J Neurophysiol* 73.1, pp. 65–72.

Toft, E. and T. Sinkjaer (1993). "H-reflex changes during contractions of the ankle extensors in spastic patients". In: *Acta Neurol Scand* 88.5, pp. 327–333.

Toft, E., T. Sinkjaer, et al. (1988). "Muscle stiffness in human ankle dorsiflexors: intrinsic and reflex components". In: *J Neurophysiol* 60.3, pp. 1110–1121.

Tynelius, G., L. Bondemark, and E. Lilja-Karlander (2010). "Evaluation of orthodontic treatment after 1 year of retention–a randomized controlled trial". In: *European journal of orthodontics* 32.5, pp. 542–547.

Walsh, L. et al. (2011). "Proprioceptive signals contribute to the sense of body ownership". In: *The Journal of physiology* 589.12, pp. 3009–3021.

Winter, D. (2009). *BIOMECHANICS AND MOTOR CONTROL OF HUMAN MOVEMENT*. Waterloo, Ontario, Canada: JOHN WILEY SONS, INC.

Zajac, Felix (1989). "Muscle and tendon: properties, models, scaling, and application to biomechanics and motor control". In: *Critical reviews in biomedical engineering* 17.4, pp. 359–411.

Zhang, Li-Qun et al. (May 2013). "Simultaneous Characterizations of Reflex and nonreflex, dynamic and static changes in spastic hemiparesis." In: *Journal of neurophysiology* 110. DOI: 10.1152/jn.00573.2012.

Chapter 6

Appendix

Power/frequency spectra

This part of the appendix is referred to the power/frequency spectra results of each trial. Firstly for the NB trial and then for the WB trial.

Subject 1

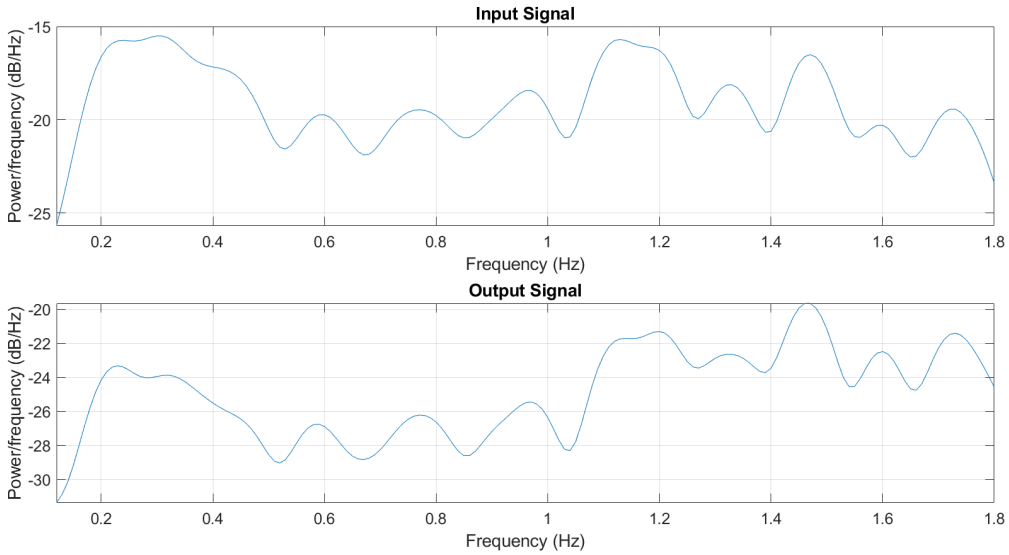

Figure 6.1: Subject 1 NB power/frequency spectrum.

6. APPENDIX

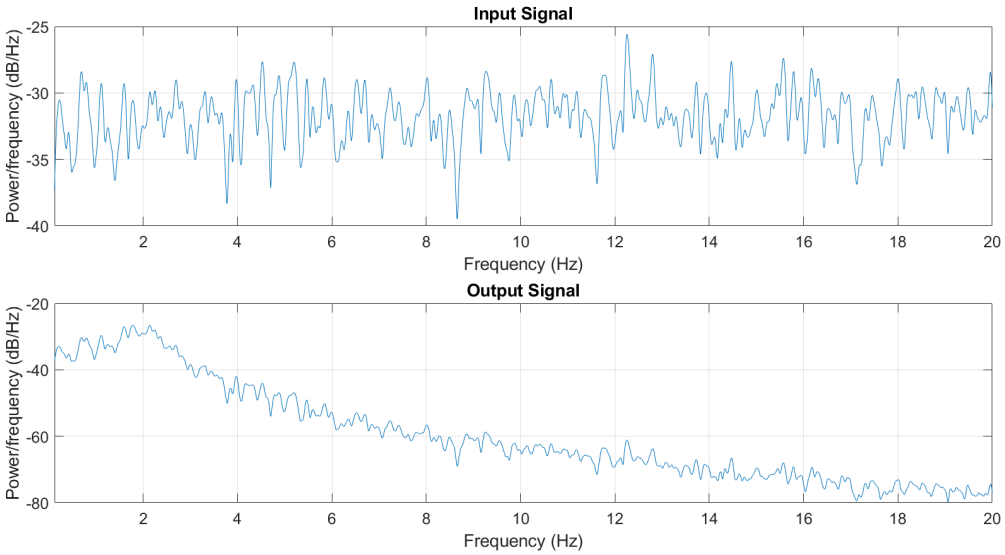

Figure 6.2: Subject 1 WB power/frequency spectrum.

Subject 2

Trial 1

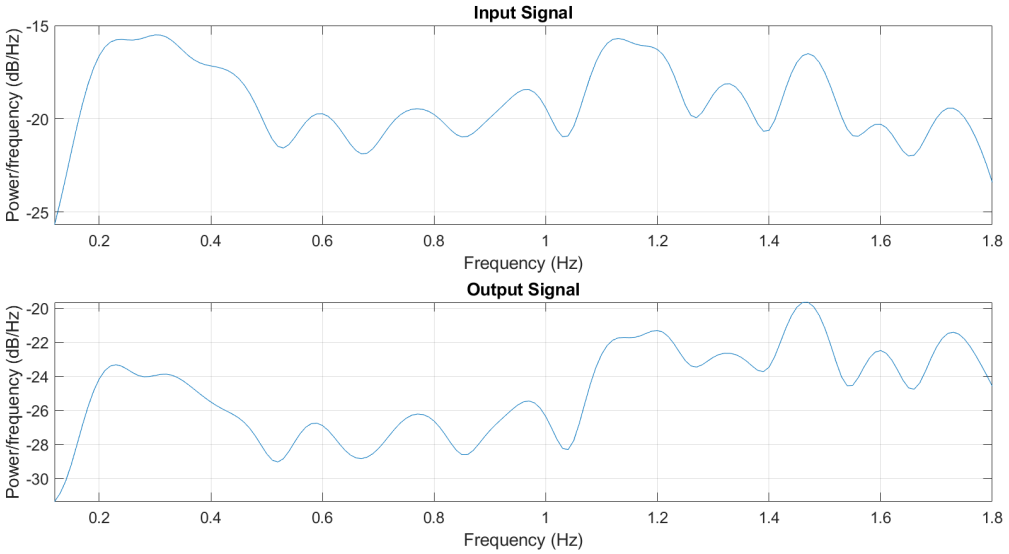

Figure 6.3: Subject 2, trial 1, NB power/frequency spectrum.

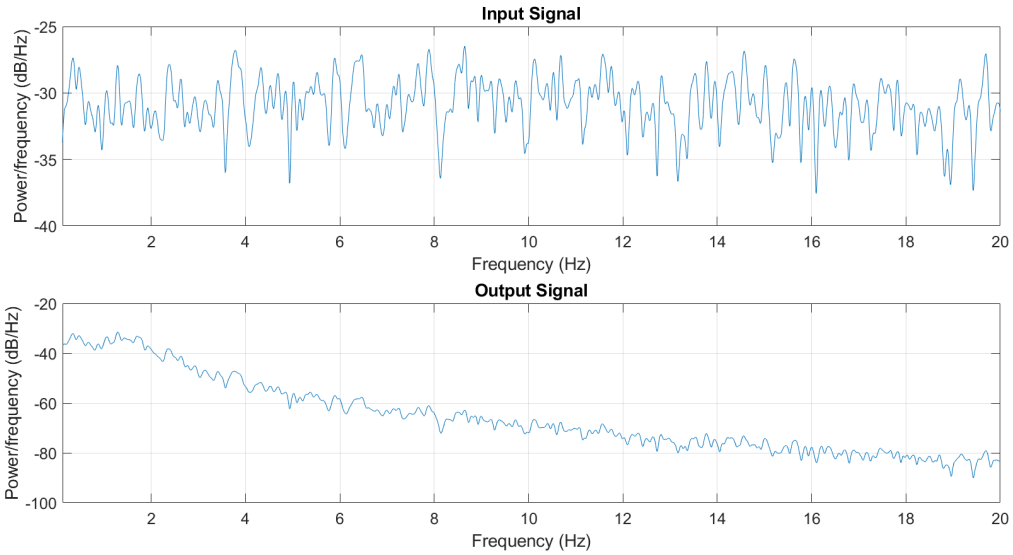

Figure 6.4: Subject 2, trial 1, WB power/frequency spectrum.

Trial 2

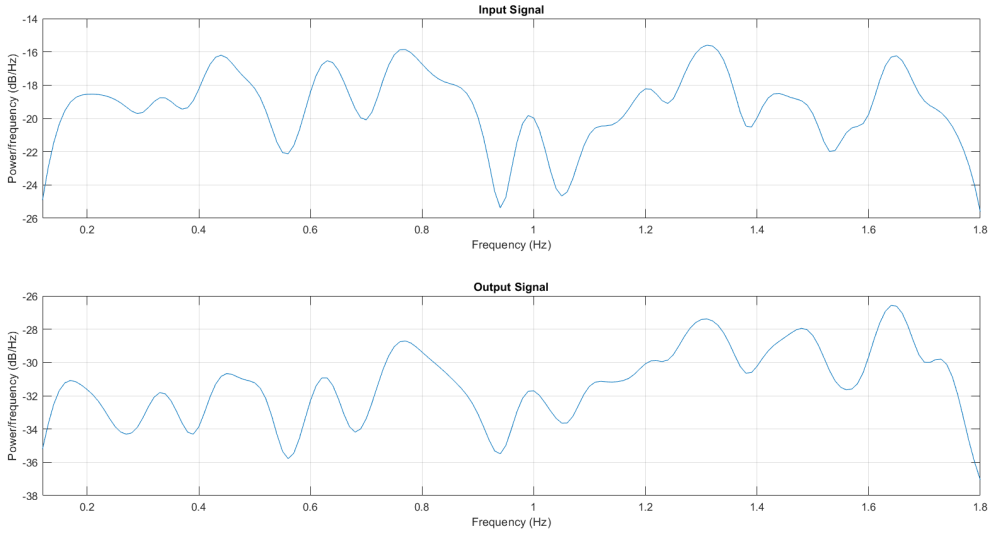

Figure 6.5: Subject 2, trial 2,NB power/frequency spectrum.

6. APPENDIX

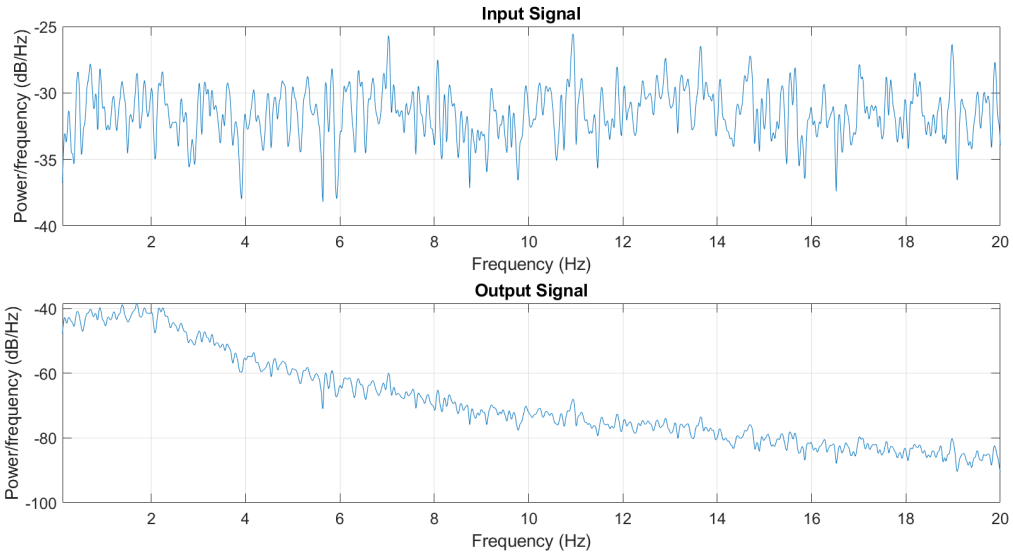

Figure 6.6: Subject 2, trial 2, WB power/frequency spectrum.

Subject 3

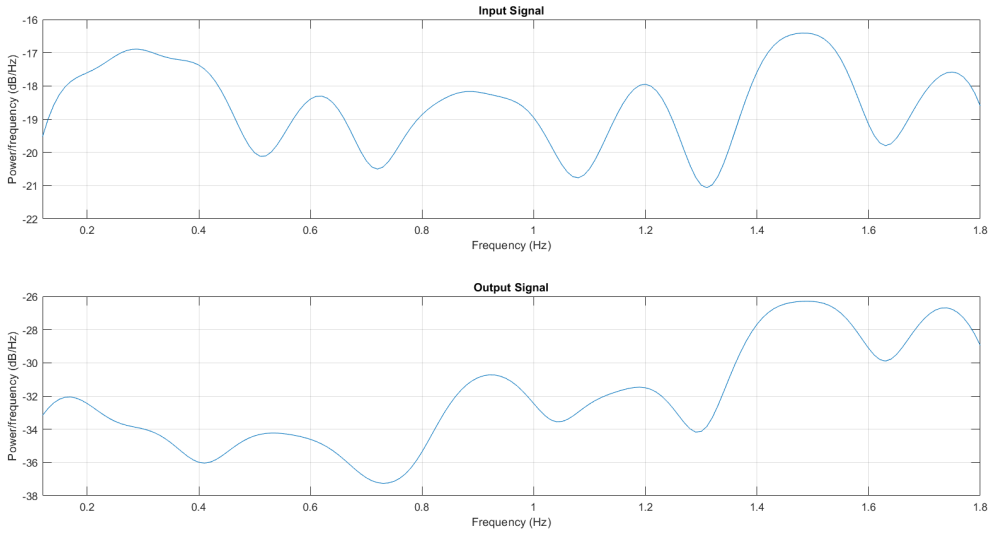

Figure 6.7: Subject 3 NB power/frequency spectrum.

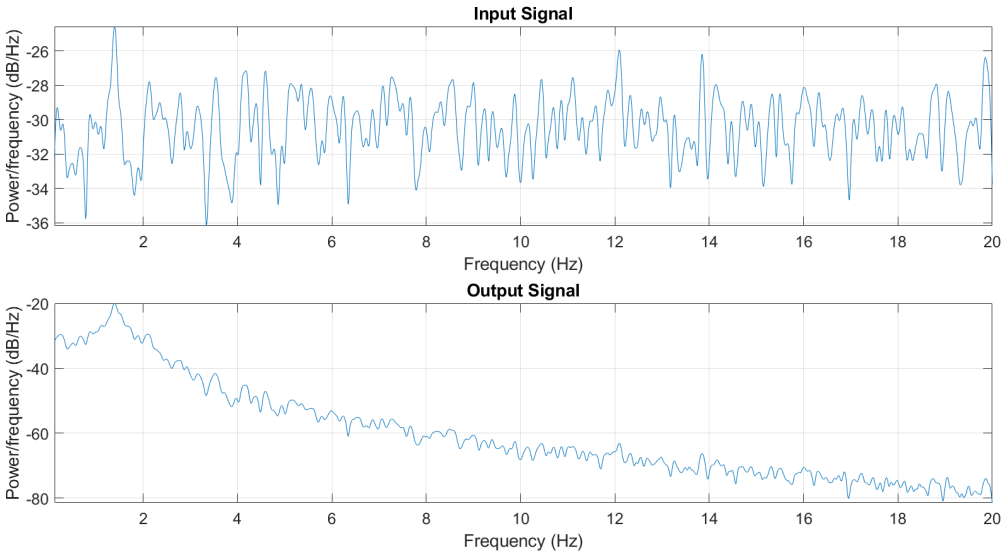

Figure 6.8: Subject 3 WB power/frequency spectrum.

Subject 4

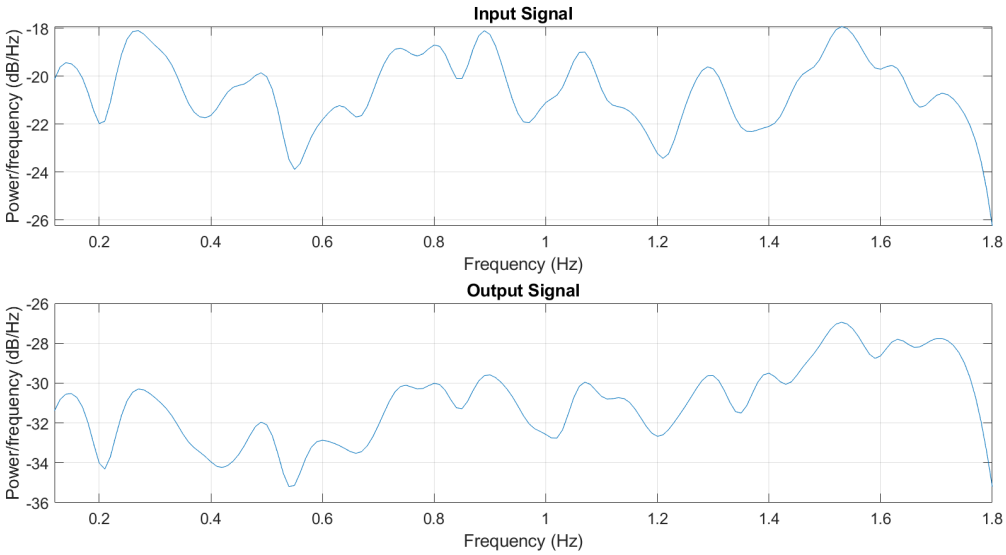

Figure 6.9: Subject 4 NB power/frequency spectrum.

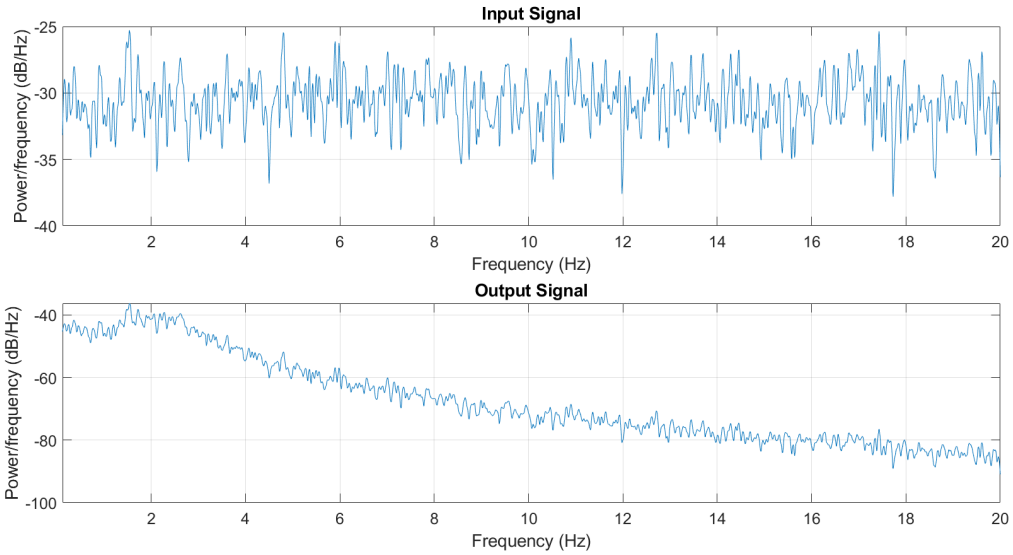

Figure 6.10: Subject 4 WB power/frequency spectrum.

6.1 Non-normalized EMG and Accelerometer data

The non-normalized EMG and Accelerometer data is presented in this section for each subject. First NB results are showed and then WB results are presented. By the end of each subject section there is a table presenting the mean and the respective standard deviation for each subject and trial.

6.1.1 Subject 1

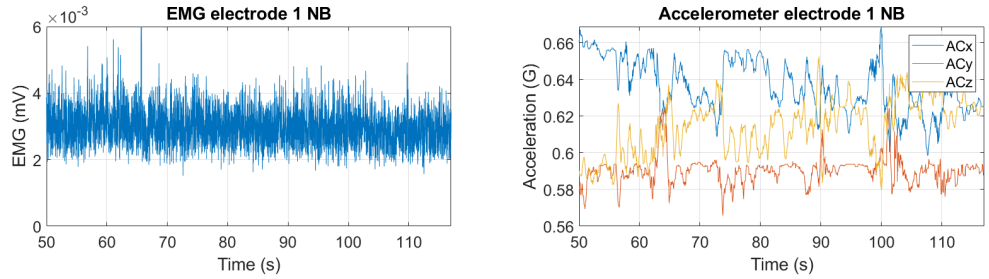

(a) Subject 1 NB EMG and Accelerometer results for electrode 1 (gastronemius muscle).

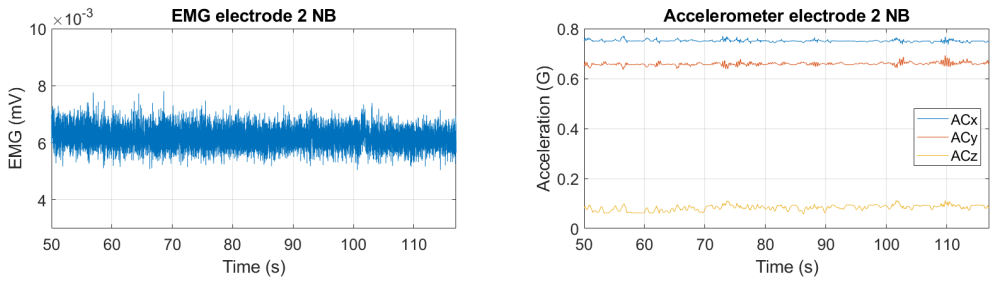

(b) Subject 1 NB EMG and Accelerometer results for electrode 2 (tibialis anterior muscle).

Figure 6.11: NB EMG and Accelerometer results for subject 1.

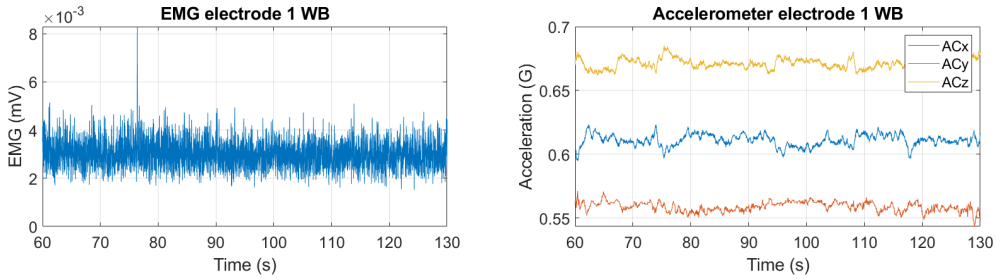

(a) Subject 1 WB EMG and Accelerometer results for electrode 1 (gastronemius muscle).

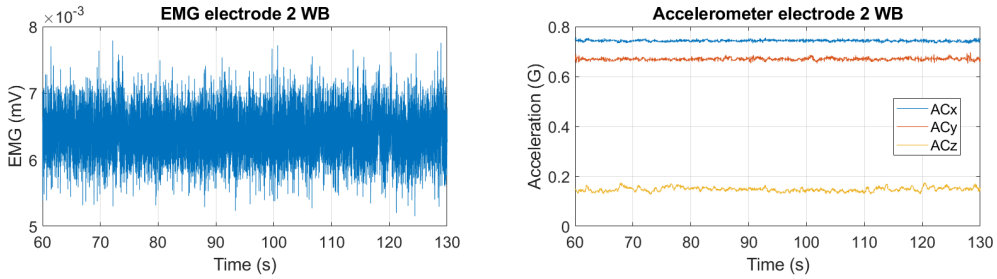

(b) Subject 1 WB EMG and Accelerometer results for electrode 2 (tibialis anterior muscle).

Figure 6.12: WB EMG and Accelerometer results for subject 1.

Table 6.1: NB and WB EMG statistical parameters for subject 1.

Mean (mV)	NB	WB
Electrode 1	$0.0030 \pm 5.5753 \times 10^{-4}$	$0.0031 \pm 5.1655 \times 10^{-4}$
Electrode 2	$0.0062 \pm 3.3368 \times 10^{-4}$	$0.0062 \pm 3.2457 \times 10^{-4}$

6.1.2 Subject 2

6.1.2.1 Trial 1

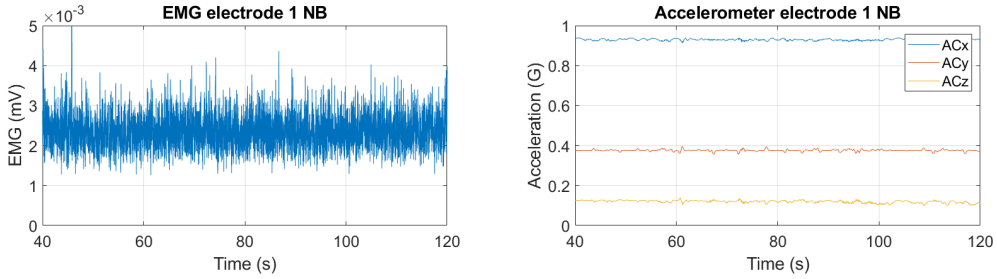

(a) Subject 2, trial 1, NB EMG and Accelerometer results for electrode 1 (gastronemius muscle).

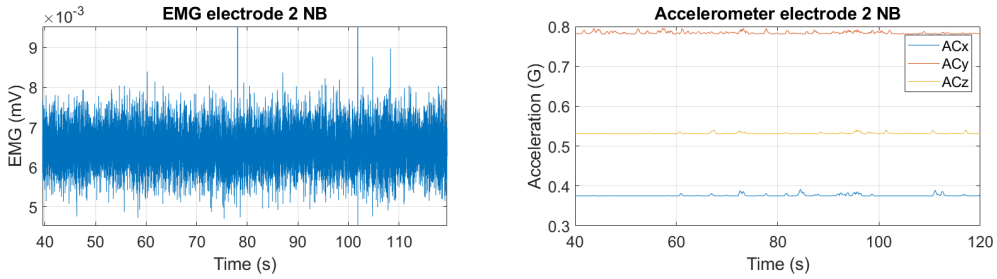

(b) Subject 2, trial 1, NB EMG and Accelerometer results for electrode 2 (tibialis anterior muscle).

Figure 6.13: NB EMG and Accelerometer results for subject 2, trial 1.

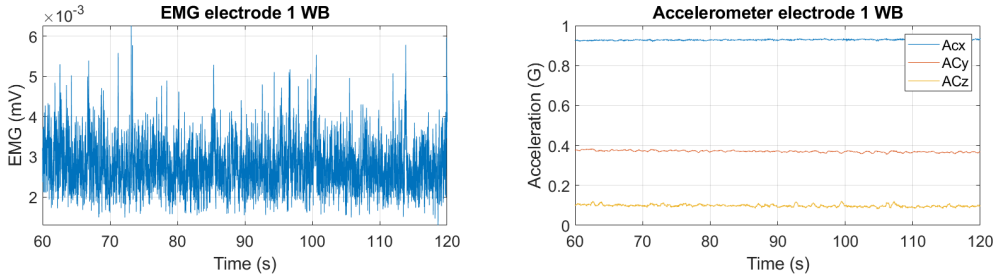

(a) Subject 2, trial 1, WB EMG and Accelerometer results for electrode 1 (gastronemius muscle).

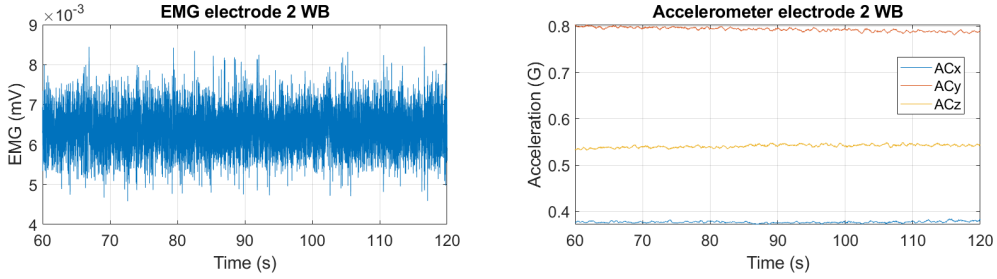

(b) Subject 2, trial 1, WB EMG and Accelerometer results for electrode 2 (tibialis anterior muscle).

Figure 6.14: WB EMG and Accelerometer results for subject 2, trial 1.

Table 6.2: NB and WB EMG statistical parameters for subject 2, trial 1.

Mean (mV)	NB	WB
Electrode 1	$0.0024 \pm 4.4635 \times 10^{-4}$	$0.0029 \pm 6.0337 \times 10^{-4}$
Electrode 2	$0.0065 \pm 5.1331 \times 10^{-4}$	$0.0067 \pm 9.7307 \times 10^{-4}$

6.1.2.2 Trial 2

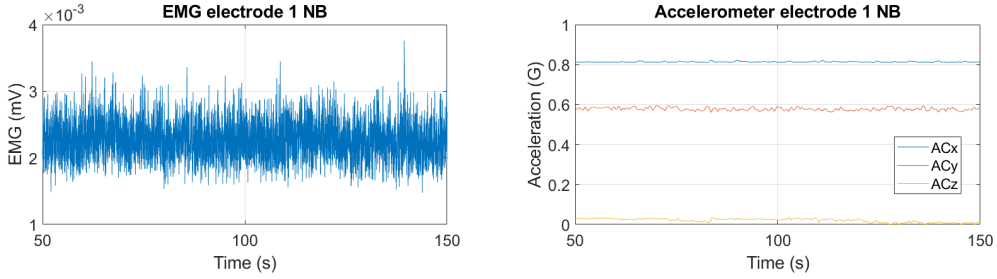

(a) Subject 2, trial 2,NB EMG and Accelerometer results for electrode 1 (gastronemius muscle).

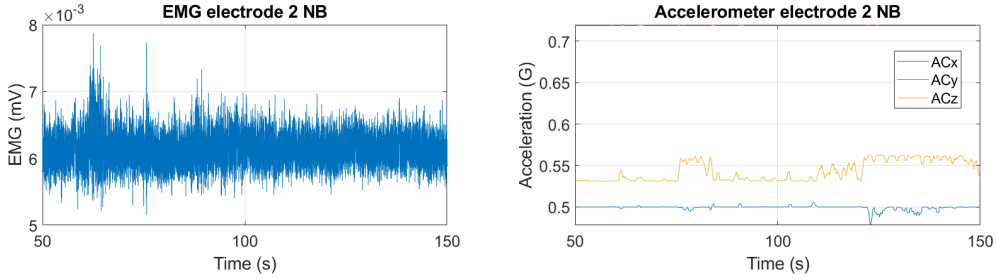

(b) Subject 2, trial 2,NB EMG and Accelerometer results for electrode 2 (tibialis anterior muscle).

Figure 6.15: NB EMG and Accelerometer results for subject 2, trial 2.

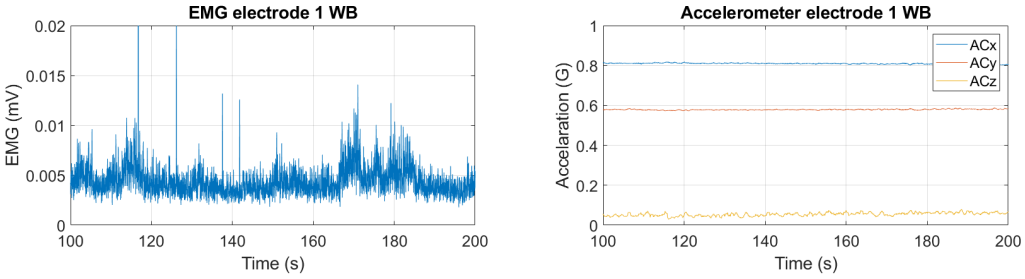

(a) Subject 2, trial 2, WB EMG and Accelerometer results for electrode 1 (gastronemius muscle).

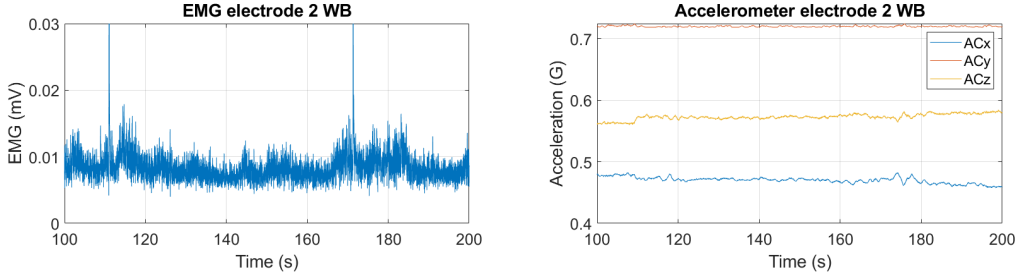

(b) Subject 2, trial 2, WB EMG and Accelerometer results for electrode 2 (tibialis anterior muscle).

Figure 6.16: WB EMG and Accelerometer results for subject 2, trial 2.

Table 6.3: NB and WB EMG statistical parameters for subject 2, trial 2.

Mean (mV)	NB	WB
Electrode 1	$0.0023 \pm 2.5625 \times 10^{-4}$	0.0045 ± 0.0017
Electrode 2	$0.0062 \pm 2.2966 \times 10^{-4}$	0.0086 ± 0.0035

6.1.3 Subject 3

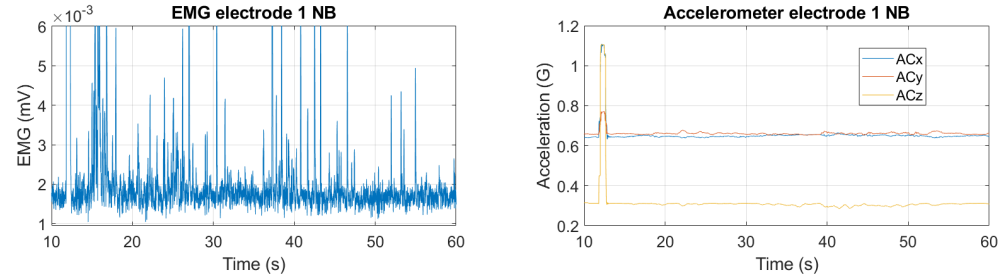

(a) Subject 3 NB EMG and Accelerometer results for electrode 1 (gastronemius muscle).

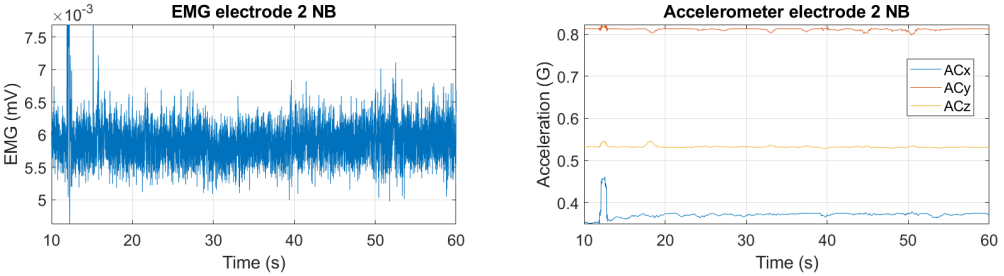

(b) Subject 3 NB EMG and Accelerometer results for electrode 2 (tibialis anterior muscle).

Figure 6.17: NB EMG and Accelerometer results for subject 3.

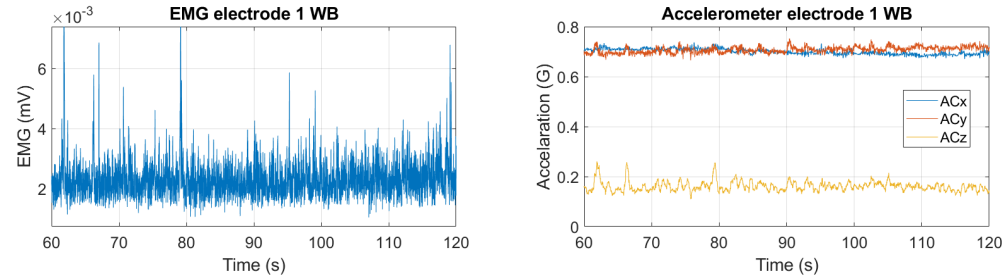

(a) Subject 3 WB EMG and Accelerometer results for electrode 1 (gastronemius muscle).

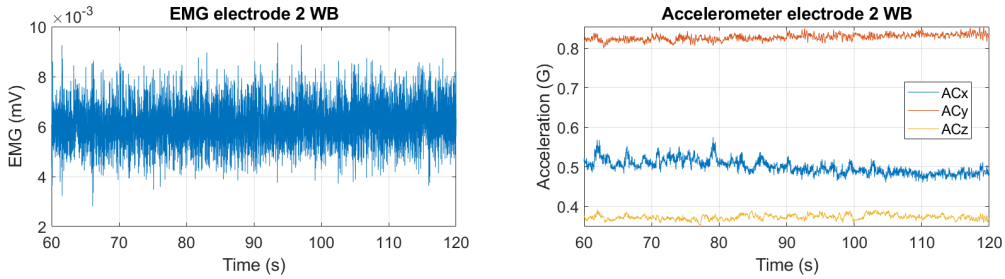

(b) Subject 3 WB EMG and Accelerometer results for electrode 2 (tibialis anterior muscle).

Figure 6.18: WB EMG and Accelerometer results for subject 3.

Table 6.4: NB and WB EMG statistical parameters for subject 3.

Mean (mV)	NB	WB
Electrode 1	$0.0024 \pm 6.6166 \times 10^{-4}$	0.0071 ± 0.0761
Electrode 2	$0.0062 \pm 8.0932 \times 10^{-4}$	$0.0059 \pm 3.3246 \times 10^{-4}$

6.1.4 Subject 4

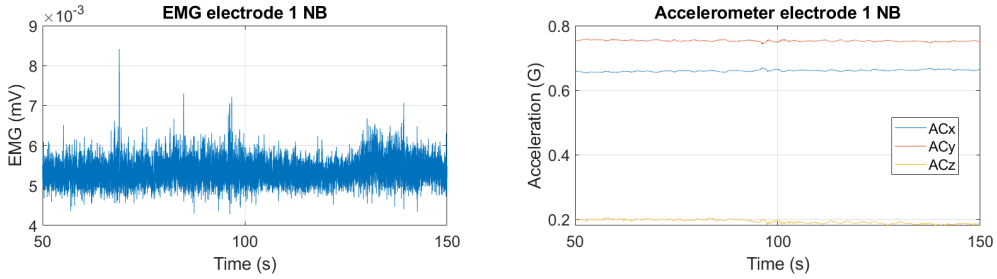

(a) Subject 4 NB EMG and Accelerometer results for electrode 1 (gastronemius muscle).

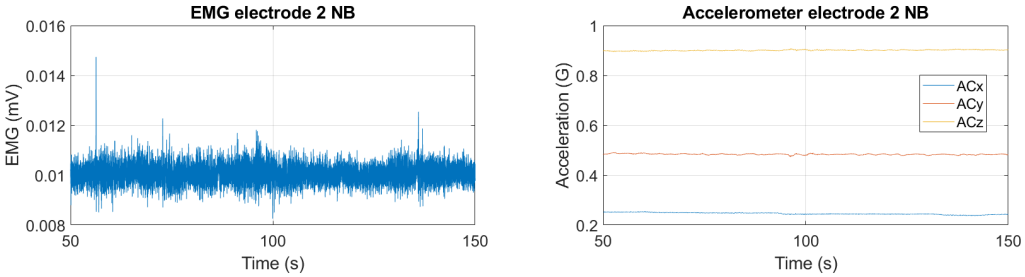

(b) Subject 4 NB EMG and Accelerometer results for electrode 2 (tibialis anterior muscle).

Figure 6.19: NB EMG and Accelerometer results for subject 4.

6. APPENDIX

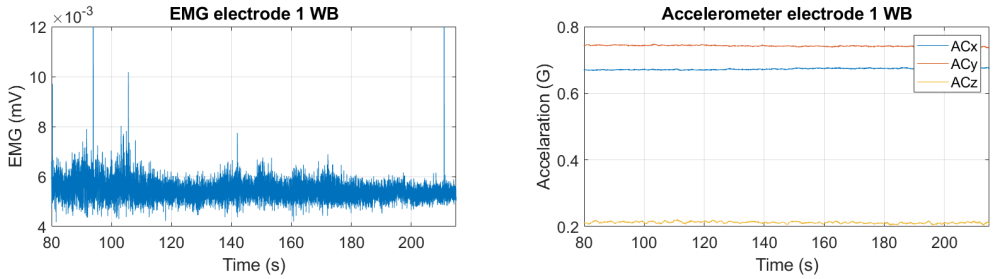

(a) Subject 4 WB EMG and Accelerometer results for electrode 1 (gastronemius muscle).

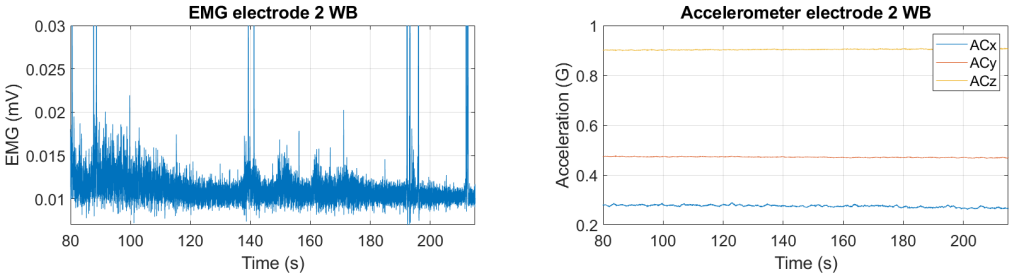

(b) Subject 4 WB EMG and Accelerometer results for electrode 2 (tibialis anterior muscle).

Figure 6.20: WB EMG and Accelerometer results for subject 4.

Table 6.5: NB and WB EMG statistical parameters for subject 4.

Mean (mV)	NB	WB
Electrode 1	$0.0054 \pm 2.9404 \times 10^{-4}$	$0.0055 \pm 4.5603 \times 10^{-4}$
Electrode 2	$0.0101 \pm 3.7794 \times 10^{-4}$	0.0118 ± 0.0077